European Journal of Medicinal Chemistry 190 (2020) 112090

Contents lists available at ScienceDirect

European Journal of Medicinal Chemistry

journal homepage: http://www.elsevier.com/locate/ejmech

Research paper

Tuning melatonin receptor subtype selectivity in oxadiazolone-based analogues: Discovery of QR2 ligands and NRF2 activators with neurogenic properties

Clara Herrera-Arozamena [a], Martín Estrada-Valencia [a], Concepción Pérez [a], Laura Lagartera [a], José A. Morales-García [b, c, d], Ana Pérez-Castillo [b, c], Juan Felipe Franco-Gonzalez [e], Patrycja Michalska [e], Pablo Duarte [e], Rafael León [e, f], Manuela G. López [e], Alberto Mills [g], Federico Gago [g], Ángel Juan García-Yagüe [b, c, h], Raquel Fernández-Ginés [b, c, h], Antonio Cuadrado [b, c, h], María Isabel Rodríguez-Franco [a, *]

[a] *Instituto de Química Médica, Consejo Superior de Investigaciones Científicas (IQM-CSIC), C/ Juan de La Cierva 3, E-28006, Madrid, Spain*
[b] *Instituto de Investigaciones Biomédicas (CSIC-UAM), C/ Arturo Duperier, 4, E-28029, Madrid, Spain*
[c] *Centro de Investigación Biomédica en Red Sobre Enfermedades Neurodegenerativas (CIBERNED), C/ Valderrebollo, 5, E-28031, Madrid, Spain*
[d] *Departamento de Biología Celular, Facultad de Medicina, Universidad Complutense de Madrid, Avda. Complutense S/n, E-28040, Madrid, Spain*
[e] *Instituto Teófilo Hernando de I+D Del Medicamento, Departamento de Farmacología y Terapéutica, Facultad de Medicina, Universidad Autónoma de Madrid, E-28029, Madrid, Spain*
[f] *Instituto de Investigación Sanitaria, Servicio de Farmacología Clínica, Hospital Universitario de La Princesa, E-28006, Madrid, Spain*
[g] *Area de Farmacología, Departamento de Ciencias Biomédicas & "Unidad Asociada IQM-CSIC", Facultad de Medicina y CC. Salud, Universidad de Alcalá, E-28805, Alcalá de Henares, Madrid, Spain*
[h] *Universidad Autónoma de Madrid (UAM), Departamento de Bioquímica, Facultad de Medicina, E-28029, Madrid, Spain*

ARTICLE INFO

Article history:
Received 27 November 2019
Received in revised form
20 January 2020
Accepted 21 January 2020
Available online 25 January 2020

Keywords:
Indole or naphthalene – oxadiazolones
Melatonin receptors (MT_1R and MT_2R)
Quinone reductase-2 (QR2)
Nuclear erythroid 2-related factor (NRF2)
Kelch-like ECH associated protein 1 (KEAP1)

ABSTRACT

New multi-target indole and naphthalene derivatives containing the oxadiazolone scaffold as a bioisostere of the melatonin acetamido group have been developed. The novel compounds were characterized at melatonin receptors MT_1R and MT_2R, quinone reductase 2 (QR2), lipoxygenase-5 (LOX-5), and monoamine oxidases (MAO-A and MAO-B), and also as radical scavengers. We found that selectivity within the oxadiazolone series can be modulated by modifying the side chain functionality and coplanarity with the indole or naphthalene ring. In phenotypic assays, several oxadiazolone-based derivatives induced signalling mediated by the transcription factor NRF2 and promoted the maturation of neural stem-cells into a neuronal phenotype. Activation of NRF2 could be due to the binding of indole derivatives to KEAP1, as deduced from surface plasmon resonance (SPR) experiments. Molecular modelling studies using the crystal structures of QR2 and the KEAP1 Kelch-domain, as well as the

Abbreviations: AD, Alzheimer's disease; AREs, antioxidant response elements; Aβ, amyloid-β peptide; COSY, homonuclear correlation spectroscopy; GPCR, G-protein-coupled receptor; HMBC, heteronuclear multiple bond correlation; HSQC, heteronuclear single quantum correlation; KEAP1, Kelch-like ECH associated protein 1; LOX-5, lipoxygenase-5; MAO-A and MAO-B, monoamine oxidases; MAP-2, microtubule-associated protein 2 marker; MMGBSA, molecular mechanics generalized born surface area approach; MT_1R and MT_2R, GPCRs of melatonin; MTDL, multi-target directed ligand; MW, microwaves; ND, neurodegenerative disease; NDGA, nordihydroguaiaretic acid; NRF2, nuclear erythroid 2-related factor; NSC, neural stem cells; ORAC, oxygen radical absorbance capacity assay; PAMPA-BBB, parallel artificial membrane permeability assay for the blood–brain barrier; PDB, protein data bank; QR2, quinone reductase 2; ROS and RNS, reactive oxygen and nitrogen species; SGZ, subgranular zone; SPR, surface plasmon resonance assay; SVZ, subventricular zone; TuJ-1, β_{III}-tubulin marker; uMD, unrestrained molecular dynamics; XFEL, X-ray free-electron laser.

* Corresponding author.
E-mail address: isabelrguez@iqm.csic.es (M.I. Rodríguez-Franco).

https://doi.org/10.1016/j.ejmech.2020.112090
0223-5234/© 2020 The Authors. Published by Elsevier Masson SAS. This is an open access article under the CC BY license (http://creativecommons.org/licenses/by/4.0/).

Monoamine oxidases (MAO-A and MAO-B)
Lipoxygenase-5 (LOX-5)
Neurogenic activity

recently described X-ray free-electron laser (XFEL) structures of chimeric MT_1R and MT_2R, provided a rationale for the experimental data and afforded valuable insights for future drug design endeavours.
© 2020 The Authors. Published by Elsevier Masson SAS. This is an open access article under the CC BY license (http://creativecommons.org/licenses/by/4.0/).

1. Introduction

Alzheimer's disease (AD) is the most common age-associated neurodegenerative disorder (ND), whose main hallmarks are the extracellular deposits of the misfolded amyloid-β peptide (Aβ), the intracellular accumulation of the hyperphosphorylated microtubule-associated tau protein and a massive neuronal loss [1]. AD aetiology is not completely understood, although different causative factors have been postulated, such as oxidative stress and neuroinflammation [2].

Oxidative stress is the consequence of the progressive failure of the antioxidant defence systems, particularly noticeable in the brains of AD-patients, where the increased levels of oxidized biomolecules correlate to disease progression [3]. Thereby, the control of transcription factors involved in the regulation of antioxidant genes and the inhibition of the main enzymes that produce reactive oxygen and nitrogen species (ROS and RNS) would be a valuable strategy to combat AD [4].

The nuclear erythroid 2-related factor (NRF2) is a transcriptional protein that regulates the expression of antioxidant and anti-inflammatory enzymes [5]. In non-stressed conditions, NRF2 is mainly located in the cytosol bound to the Kelch-like ECH associated protein 1 (KEAP1), which favours its proteasome degradation. Under pathological conditions (oxidative stress, toxic insults, etc.), KEAP1 changes its conformation and NRF2 is released and translocated to the nucleus, where it binds to the DNA antioxidant response elements (AREs), inducing the expression of antioxidant enzymes such as NAD(P)H quinone oxidoreductase and heme oxygenase-1 [6,7].

Monoamine oxidases (MAO-A and MAO-B) are outer mitochondrial membrane-bound flavoproteins, whose levels are increased in the brain of patients suffering NDs, such as AD and Parkinson's disease. Both enzymes catalyse the oxidative deamination of biogenic amines, including several neurotransmitters, what it produces hydrogen peroxide, ROS, and accordingly oxidative stress [8]. Besides, overexpression of MAO-B increases the formation of aberrant Aβ [9]. In this regard, MAO inhibition could provide neuroprotection against AD, by regulating neurotransmitters' levels, ameliorating oxidative pathologies and stopping the deposition of amyloid plaques.

Neuroinflammation is another important player in AD that generates cytokines and neurotoxins, leading to neuronal damage and death [10]. The iron-containing enzyme lipoxygenase-5 (LOX-5, EC 1.13.11.34) catalyses two early steps of the oxidation of the arachidonic acid, producing finally pro-inflammatory leukotrienes [11]. LOX-5 is present in the CNS particularly in the hippocampus, where its levels appear to increase in AD [12]. Several works have demonstrated that blockade of LOX-5 in transgenic mice diminishes cytokines levels and both Aβ and tau pathologies [13,14]. Therefore, LOX-5 inhibitors could be valuable therapeutic agents, as they could reduce neuroinflammation and aberrant protein aggregation.

In mammals, melatonin is secreted in nanomolar concentrations from the pineal gland to the blood, when it transmits the circadian rhythm to the peripheral organs by interacting with two G-protein-coupled receptors (GPCRs), called MT_1 and MT_2 (MT_1R and MT_2R) [15]. Melatonin also interacts with a third binding site, MT_3, which has been identified as the flavin adenine dinucleotide (FAD)-dependent enzyme quinone reductase-2 (QR2, EC 1.10.99.2) [16,17]. Melatonin activates MT_1R and MT_2R at sub-nanomolar concentrations (K_d ~ 0.1 nM), whereas its affinity as a QR2 inhibitor is about 100-fold lower [16].

QR2 catalyses the two-electron reduction of quinones into unstable hydroquinones, which are excreted through conjugation or reconverted to quinones in the presence of oxygen while producing ROS [18]. Given that QR2 levels are increased in the hippocampus of AD patients, inhibitors of this enzyme are promising therapeutic agents to fight neurodegeneration by reducing the oxidative stress [19–21].

Adult neurogenesis is a matter of intense research, although its scope and function remain debatable [22,23]. Restricted to small regions, namely the subventricular zone (SVZ) of the lateral ventricle and the subgranular zone (SGZ) of the hippocampus, the adult mammalian brain retains neural stem cells (NSC) niches that could develop and integrate new cells in the neuronal circuitry. Therefore, a neurogenic drug would induce the differentiation of NSCs into mature neurons capable of replacing those lost by neurodegeneration, allowing the brain to recover its own self-renewal capacity [24].

In recent years, numerous molecular targets and signalling cascades involved in neurogenesis have been identified and, as a consequence, different types of drugs have been evaluated in neuronal regeneration. For example, neurogenic properties have been found in MTRs' ligands, NRF2 activators, antioxidants and anti-inflammatory agents [25].

Melatonin modulates hippocampal neurogenesis by increasing both cellular precursor proliferation and survival in the hippocampi of aged mice [26]. Given these outstanding properties, many research groups (including ours) have devoted great efforts aimed to the identification of new MTR ligands and their molecular interaction pathways [27–30]. In this context, our melatonin analogue IQM316 was recently found to be capable of inducing hippocampal neurogenesis in mice at a healthy and sustainable rate, thus helping to preserve previous memories [31,32]. We have also described the bioisosteric replacement of the acetamido group of melatonin by a series of reversed amides and azoles [29]. Among these azole derivatives, 5-[2-(5-methoxy-1*H*-indol-3-yl)ethyl]-1,3,4-oxadiazol-2(3*H*)-one (**1**) was the most potent partial agonist at the human MTRs, displaying the highest affinity for both human MTRs (K_i = 35 and 4 nM for hMT$_1$R and hMT$_2$R, respectively). Moreover, this compound also showed potent neurogenic properties *in vitro*, better than melatonin itself, but it was predicted that it would not enter the CNS in view of the unfavourable results in *in vitro* blood-brain barrier (BBB) permeability assays.

Given the complex nature of AD, the multi-target directed ligand (MTDL) strategy has emerged as a valid alternative to fight different pathological cascades involved in this disease. To achieve maximum efficiency, MTDLs should promote endogenous defensive and/or regenerative pathways and be directed towards biomolecular targets located upstream in the neurotoxic cascades [2,33].

With these ideas in mind, in this work we planned to develop new melatonin-based MTDLs that could improve the CNS permeability of **1** and also incorporate additional activities on targets related to oxidative stress and neuroinflammation. For this purpose, we modified each part of the starting molecule by: (i) addition

of different substituents to the oxadiazolone nitrogen; (ii) replacement of the oxadiazolone ring by an oxadiazolamine; (iii) insertion of a double bond in the linker; and (iv) replacement of the indole by a dihydronaphthalene or naphthalene ring (Figure 1).

2. Results and discussion

2.1. Chemistry. Synthesis of new indole- and naphthalene-based compounds

The microwave (MW)-assisted reaction (120 °C, 10 min) of **1** with the corresponding alkyl halide in basic media (K_2CO_3) using acetone as solvent gave derivatives **2**–**15**, in moderate to excellent yields (49–92%) (Scheme 1).

Moreover, the treatment of **1** with methyl- or ethylamine in the presence of (benzotriazol-1-yloxy)tris(dimethylamino)phosphonium hexafluorophosphate (BOP) and triethylamine (TEA) in DMF, yielded 1,3,4-oxadiazol-2-amines (**16** and **17**) in low yields (18 and 6%, respectively).

Modifications in the linker were performed using the commercially available 5-methoxy-1*H*-indole-3-carbaldehyde (**18**) as starting material. The introduction of a methyl group in the *beta*-

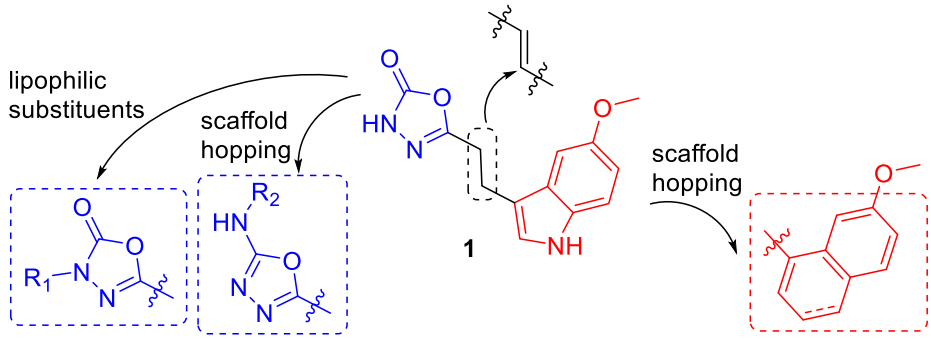

Fig. 1. Design strategy for the novel melatonin-based MTDLs.

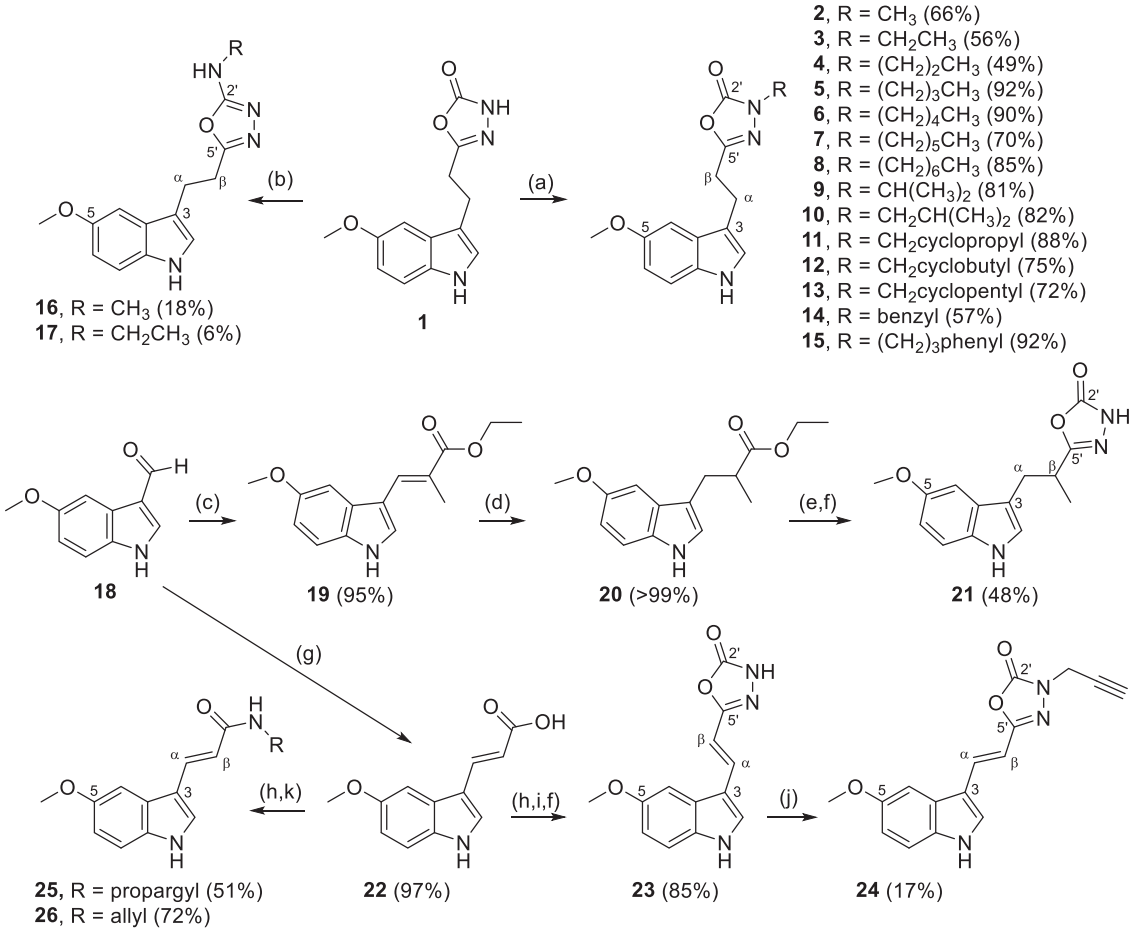

Scheme 1. Reagents and conditions: (a) RX, K_2CO_3, acetone, MW, 120 °C, 10 min; (b) RNH_2, BOP, TEA, DMF, rt, overnight; (c) $Ph_3P{=}CH{-}CO_2Et$, DCM, reflux, overnight; (d) H_2/Pd–C (5%), EtOH, rt, overnight; (e) $N_2H_4{\cdot}H_2O$, MW, 150 °C, 45 min; (f) CDI, DMF, MW, 120 °C, 25 min; (g) Malonic acid, piperidine, pyridine, 70 °C, overnight; (h) HOBt, EDC·HCl, DMAP, ACN, rt, 3 h; (i) $N_2H_4{\cdot}H_2O$, rt; (j) Propargyl bromide, K_2CO_3, acetone, MW, 120 °C, 10 min; (k) Propargylamine or allylamine, rt.

position with respect to the indole ring was carried out from **18** and (carbethoxyethylidene)triphenylphosphorane by a *Wittig* reaction, giving the corresponding α,β-unsaturated ester **19** in high yields (95%). Then, **19** was reduced by catalytic hydrogenation to the saturated ester **20**, followed by its transformation to the corresponding hydrazide and further MW-assisted cyclization in the presence of 1,1-carbonildiimidazole (CDI) to give the 1,3,4-oxadiazol-2(3*H*)-one derivative **21** in 48% yield.

The conjugated double bond in the linker was introduced by the treatment of **18** with malonic acid in basic media that generate the α,β-unsaturated acid **22**, in almost quantitative yield by a *Knoevenagel-Doebner* reaction. Activation of **22** with hydroxybenzotriazole (HOBt) and *N*-(3-dimethylaminopropyl)-*N*′-ethylcarbodiimide hydrochloride (EDC·HCl) as coupling agents, and a catalytic amount of 4-dimethylaminopyridine (DMAP) at rt during 3 h, followed by the addition of hydrazine hydrate, yielded the corresponding hydrazide in quantitative yield. It is worth-mentioning that the order of addition of the reagents is crucial for obtaining high yields. Once the hydrazide is formed, its MW-assisted cyclization with CDI afforded the indole−*NH*-oxadiazolone derivative **23** in good yield (85%). The treatment of **23** with propargyl bromide in basic media (K_2CO_3) and acetone in an MW-oven at 120 °C during 10 min afforded the corresponding *N*-propargyl-oxadiazolone **24** (Scheme 1). Bioisosteric replacement of the oxadiazolone ring by an amide group was carried out from the α,β-unsaturated acid **22** by condensation with propargyl or allyl amine in acetonitrile at rt during 3 h, in the presence of EDC·HCl, HOBt, and DMAP, giving the corresponding propargyl (**25**) or allyl derivative (**26**) in moderate to good yields (Scheme 1).

Indole scaffold replacement by either a dihydronaphthalene or a naphthalene ring was carried out from commercial 7-methoxy-1-tetralone (**27**) by two different synthetic routes. Reaction of **27** with a solution of methyl magnesium iodide in ether at rt for 3 h afforded the corresponding alcohol (non-isolated intermediate), which was treated with HCl to yield the 1-methyl dihydronaphthalene **28** in quantitative yield [34]. Oxidation of the above methyl group with selenium dioxide gave aldehyde **29**, in low yield due to the easy aromatization of the dihydronaphthalene ring. In spite of the mild oxidative conditions used, a mixture of dihydronaphthalene **29** and naphthalene **30** [35] was obtained, in 25% and 20% yield respectively (Scheme 2).

Then, we planned to transform the dihydronaphthalene derivative **29** into the unsaturated acid **31** by the treatment with malonic acid in *Knoevenagel-Doebner* conditions, obtaining unexpected ^1H and ^{13}C NMR data for the isolated product. A deeper NMR analysis (COSY, HSQC, and HMBC) demonstrated that this structure corresponded to lactone **32**, formed under basic conditions by an intramolecular cyclization (Scheme 2). Probably, the carboxylate group attacked the intracyclic double bond forming the intermediate enol, which could develop to lactone **32**. Nevertheless, given that in solution this cyclization is an equilibrium, acid activation was possible after treatment with coupling reagents (EDC·HCl, HOBt). Further treatment with $N_2H_4 \cdot H_2O$ and CDI, led to the desired dihydronaphthalene-based *NH*-oxadiazolone **33**, although in low yield (15%), probably due to the easy aromatization that could also give the corresponding naphthalene (non-isolated).

Aiming to improve the yield of the oxadiazolone derivative with a dihydronaphthalene core **33**, another alternative synthetic route was explored. 7-Methoxy-1-tetralone (**27**) was reacted with trifluoromethanesulfonic anhydride (Tf_2O) and 2-chloropyridine as base to yield the vinyl triflate **34** in good yield (78%) [36] (Scheme 2).

Then, the introduction of an α,β-unsaturated ester was carried out by olefination of vinyl triflates under palladium-catalysed conditions (*Heck* reaction), using ethyl acrylate as reactant and TEA as base. Since first attempts to obtain **35** in good yields failed, different experimental conditions in a MW oven were probed, modifying the palladium-based catalyst [$Pd(OAc)_2$+PPh_3 or $Pd(PPh_3)_2Cl_2$], temperature (100−140 °C) and reaction time (10−40 min). Optimized conditions for the synthesis of **35** resulted from the use of $Pd(PPh_3)_2Cl_2$ as catalyst and MW irradiation at 105 °C for 15 min, obtaining the desired ester derivative in 87% yield.

Then, the ester **35** was hydrolysed under basic condition with lithium hydroxide (LiOH) followed by acid treatment with HCl to obtain the corresponding acid. This acid was not isolated but transformed into the corresponding hydrazide, followed by cyclization with CDI to afford the desired dihydronaphthalene-based oxadiazolone **33** in low yields (21%) due to its easy aromatization. In fact, the aromatic analogue was detected by HPLC-MS, although

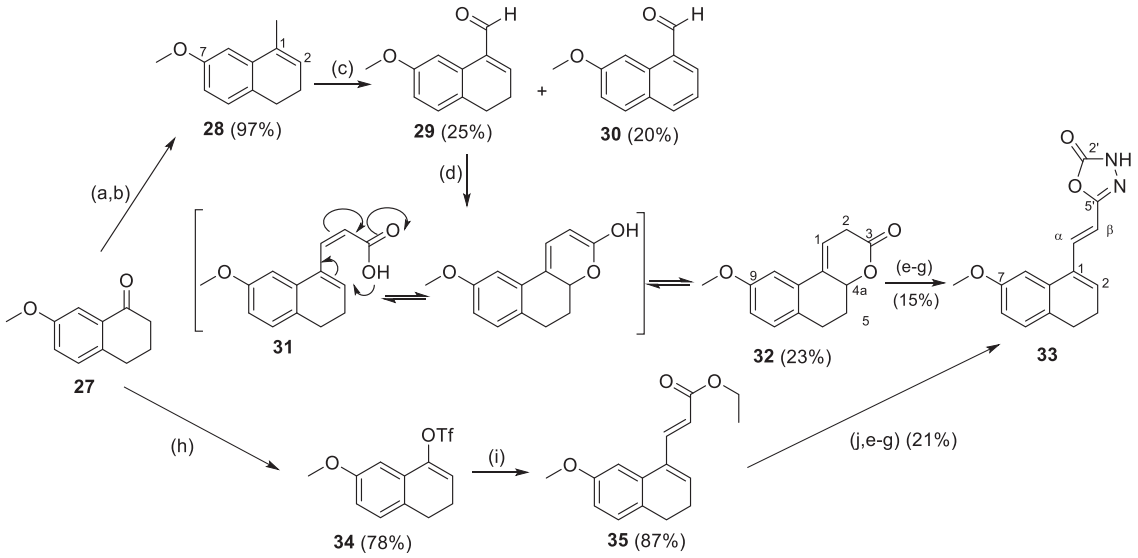

Scheme 2. Reagents and conditions: (a) CH_3MgI, Et_2O, rt, 3 h; (b) 2 M HCl, 40 °C, 3 h; (c) SeO_2, EtOH:H_2O (10:1), reflux, overnight; (d) Malonic acid, piperidine, pyridine, 70 °C, overnight; (e) EDC·HCl, HOBt, DMAP, ACN, rt, 3 h; (f) $N_2H_4 \cdot H_2O$, rt; (g) CDI, DMF, MW, 120 °C, 25 min; (h) Tf_2O, 2-chloropyridine, DCM, 2 h, rt; (i) Ethyl acrylate, $Pd(PPh_3)_2Cl_2$, TEA, MW, 105 °C, 15 min; (j) LiOH, THF:H_2O (1:1), rt, overnight.

it was not isolated (Scheme 2).

Given that the best yields were achieved using the *Heck* reaction in triflate derivatives, this strategy was applied for obtaining naphthalene derivatives. The conditions previously used in the synthesis of the vinyl triflate **34** (Scheme 2) were extended to the dimethoxylated derivative (Scheme 3). However, derivative **37** was obtained in low yields due to the formation of several by-products, probably due to the lesser electrophilic character of the carbonyl group. Aromatization of triflates **34** and **37** with 2,3-dichloro-5,6-dicyano-1,4-benzoquinone (DDQ) at rt, led naphthalenes **38** and **39**, respectively (Scheme 3). Then, the ethyl acrylic moiety was introduced by a *Heck* reaction, treating the corresponding triflate derivative with ethyl acrylate in the presence of $Pd(OAc)_2$, 1,10-phenanthroline and TEA, to yield naphthalene esters **40** and **41** in high yields (90 and 81%, respectively). These esters were hydrolysed under basic conditions, obtaining acids **42** and **43** in quantitative yields. Finally, these acids were transformed into the corresponding hydrazides, followed by cyclization with CDI to afford naphthalene–*NH*-oxadiazolones **44** and **45** in good yields (91 and 85%, respectively).

All new compounds were isolated and purified using flash column chromatography (automatic IsoleraOne-Biotage equip), preparative thin-layer plates (TLC) or semipreparative HPLC (Waters Autopurification system). Purity (>95%) was evaluated by HPLC-MS and chemical structure was characterized by their spectroscopic data (^{1}H NMR, ^{13}C NMR). Complete NMR assignments were made by two-dimensional NMR experiments, mainly COSY (homonuclear correlation spectroscopy), HSQC (heteronuclear single quantum correlation) and HMBC (heteronuclear multiple bond correlation).

2.2. Characterization in melatonin receptors

Experiments on human MT_1R and MT_2R were performed in Chinese hamster ovary cells, where these receptors were stably transfected. The QR2 binding assays were carried out using membrane homogenates of hamster brains. In all cases, displacement of the radioligand 2-[^{125}I]iodomelatonin was measured in the absence or presence of the tested compound and nonspecific binding was determined with melatonin, following described protocols [37–39].

Firstly, radioligand displacements were measured at a fixed concentration of compound (100 or 10,000 nM) in each receptor subtype. Then, binding constants (K_i) were calculated only for compounds with a radioligand displacement above 80%, using a range of 5 different concentrations of tested compound in 3 independent experiments. Melatonin was assayed for comparative purposes and results are gathered in Table 1.

The indole–*NH*-oxadiazolone **1** showed high binding affinities for *h*MT_1R and *h*MT_2R (K_i = 35 and 4 nM, respectively) [29]. In contrast, it did not show a substantial affinity toward QR2, as it only displaced 5% of the radioligand at 100 nM (Table 1). The introduction of substituents in the *NH* group of the oxadiazolone ring to give derivatives **2**–**15** caused a great decrease in the affinity for all melatonin receptors, reaching in some cases the total loss of activity. Only compounds with longer chains namely, **7** [R = $(CH_2)_5CH_3$], **8** [R = $(CH_2)_6CH_3$], **12** (R = CH_2cyclobutyl), **13** (R = CH_2cyclopentyl), and **15** [R = $(CH_2)_3$phenyl] showed a slight selectivity for *h*MT_2R over *h*MT_1R, with binding constants around 10^{-7} M in the case of *h*MT_2R. This affinity drop could be due to a possible hydrogen bond between the *NH* group of the oxadiazolone ring of **1** and the receptors, which is lost when it is substituted. The evaluation of derivative **4** in QR2 gave only a 68% displacement at 10 μM, so its K_i was not calculated and the rest of the indole-oxadiazolones were not evaluated in QR2.

The replacement of the oxadiazolone ring by a 1,3,4-oxadiazol-2-amine to give **16** provided binding constants in the hundred-nanomolar range for the three melatonin targets (K_i = 550, 110, and 330 nM, for *h*MT_1R, *h*MT_2R and QR2, respectively). Thus, this change maintained the binding constants for *h*MT_1R and *h*MT_2R and improved the affinity for QR2, compared to some *N*-substituted oxadiazolone derivatives (e.g., **12** and **15**).

The addition of a methyl group in the aliphatic linker of **1** to give the *beta*-methyl derivative **21**, resulted in the complete loss of affinity for *h*MT_1R, a similar binding for *h*MT_2R (K_i = 12 nM) and

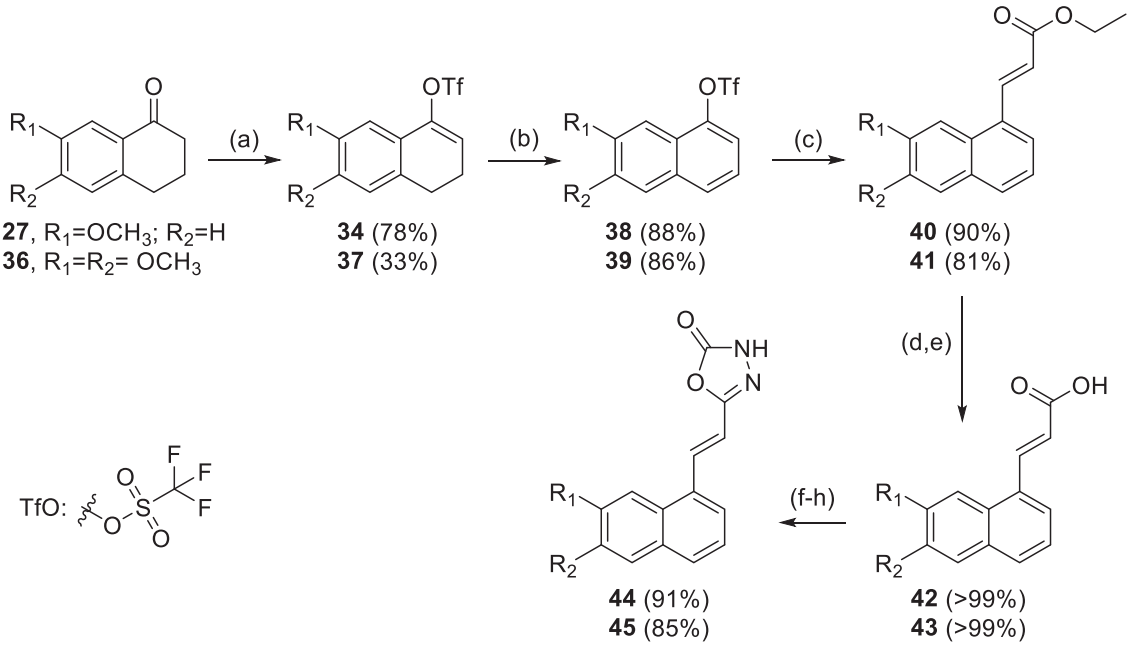

Scheme 3. Reagents and conditions: (a) Tf_2O, 2-chloropyridine, DCM, rt, 2 h; (b) DDQ, DCM, rt, 10 min; (c) Ethyl acrylate, $Pd(OAc)_2$, 1,10-phenanthroline, DMF, MW, 150 °C, 1 h; (d) LiOH, THF:H_2O 1:1, rt, overnight; (e) 1 M HCl; (f) EDC·HCl, HOBt, DMAP, ACN, rt; (g) $N_2H_4 \cdot H_2O$, rt; (h) CDI, DMF, MW, 130 °C, 25 min.

Table 1
Binding constants at hMT$_1$R, hMT$_2$R and QR2 (K_i, nM), or percentage of radioligand displacement at the specified concentration (in brackets), antioxidant properties (ORAC, trolox equiv.) and NRF2 induction capability (CD, μM) of new indole and naphthalene derivatives.

Compd.	K_i (nM)[a]			ORAC (Trolox equiv)[b]	NRF2 (CD, μM)[c]
	hMT$_1$R	hMT$_2$R	QR2		
1	35 ± 1[d]	4.0 ± 0.5[d]	>10^2 (5%)	2.7 ± 0.3	n.d.
4	>10^4	>10^4	~10^4 (68%)	3.0 ± 0.2	>30
7	>10^4	530 ± 40	n.d.	2.1 ± 0.2	n.d.
8	>10^4	300 ± 30	n.d.	2.2 ± 0.1	n.d.
12	550 ± 40	230 ± 20	n.d.	2.8 ± 0.2	n.d.
13	>10^4	390 ± 30	n.d.	2.7 ± 0.2	n.d.
15	690 ± 60	320 ± 20	n.d.	1.8 ± 0.2	n.d.
16	550 ± 40	110 ± 20	330 ± 30	2.3 ± 0.1	n.d.
21	>10^2 (37%)	12 ± 0.9	220 ± 20	2.3 ± 0.1	>60
23	>10^2 (8%)	>10^2 (17%)	6.6 ± 0.4	2.4 ± 0.1	15.1 ± 0.9
24	>10^2 (0%)	>10^2 (0%)	3.2 ± 0.2	1.8 ± 0.1	1.76 ± 0.20
25	>10^2 (13%)	~10^2 (58%)	9.3 ± 0.5	1.3 ± 0.1	27.4 ± 1.5
26	>10^2 (34%)	~10^2 (78%)	110 ± 10	1.8 ± 0.1	>30
33	~10^4 (46%)	260 ± 20	250 ± 20	0.4 ± 0.04	n.d.
44	260 ± 20	5.1 ± 0.4	270 ± 20	<0.1	>30
45	~10^4 (63%)	69 ± 6	35 ± 2	<0.1	>30
Melatonin	0.27 ± 0.03	0.13 ± 0.02	77 ± 1	2.3 ± 0.1	n.d.
Sulforaphane	n.d.	n.d.	n.d.	n.d.	0.54 ± 0.07[e]

n.d., not determined.
[a] Results are the mean ± SEM of three independent experiments (n = 3).
[b] Results are the mean ± SD of three independent experiments (n = 3).
[c] Values are expressed as the mean ± SEM of four independent experiments in duplicate.
[d] Value from Ref. [29].
[e] Value from Ref. [40].

better affinity for QR2 (K_i = 230 nM) than the starting molecule **1**.

Introduction of a double bond in the linker of the indole series provided interesting effects on the behaviour of these unsaturated oxadiazolones (**23** and **24**) and amides (**25** and **26**). These four derivatives lost their affinities toward hMT$_1$R and hMT$_2$R (K_is > 100 nM), while drastically improved their binding to QR2. Unsaturated indole-oxadiazolone compounds **23** and **24**, and the propargyl amide derivative **25** showed K_is between 3.2 and 9.3 nM in QR2, one order of magnitude better than melatonin itself (K_i = 77 nM).

According to previously published results [41], we also found that the *NH*-indole fragment was not indispensable for activity on melatonin targets. In fact, the 7-methoxy-3,4-dihydronaphthalene **33** showed affinities toward hMT$_2$R and QR2 in the 10^{-7} M range (K_i = 410 and 260 nM, respectively), although resulted poor active in hMT$_1$R. Ring aromatization to give the naphthalene counterpart greatly modified its profile, as **44** recovered a moderated affinity for hMT$_1$R (K_i = 260 nM), maintained a similar affinity for QR2 (K_i = 270 nM), and interestingly, displayed a potent binding constant in hMT$_2$R in the low-nanomolar range (K_i = 5.1 nM). The introduction of a second methoxy group in position 6 of the naphthalene ring was partially detrimental for affinity, since **45** was inactive in hMT$_1$R, not as active as **44** in hMT$_2$R (K_i = 69 nM), although **45** was one order of magnitude more active in QR2 (K_i = 35 nM).

5-(2-(7-Methoxynaphthalen-1-yl)vinyl)-1,3,4-oxadiazol-2(3*H*)-one (**44**), which displayed the highest affinity for hMT$_2$R, was also functionally characterized by measuring its effects on cAMP modulation, according to a described HTRF-detection protocol [38,42]. Compound **44** was found to be a potent agonist in hMT$_2$R with a half maximal effective concentration in the low-nanomolar range (EC_{50} = 1.2 ± 0.1 nM) and a maximum activity of 85% with respect to melatonin.

2.3. Evaluation of the oxygen radical absorbance capacity (ORAC)

As a measure of antioxidant properties, we tested new indole- and naphthalene-based compounds in the ORAC assay, following described protocols [43–46]. (±)-6-Hydroxy-2,5,7,8-tetramethylchromane-2-carboxylic acid (trolox), the aromatic part of vitamin E responsible for its scavenging properties, was used as the internal standard with the arbitrary value of ORAC = 1.0. Results are expressed as trolox equivalents (trolox mmol/tested compd. mmol) in a comparative scale that indicates if a compound is a better (ORAC > 1.0 trolox equiv) or a worse oxygen radical scavenger (ORAC < 1.0 trolox equiv) than vitamin E. Melatonin was also evaluated for comparative purposes, giving an ORAC value 2.3-fold higher than trolox. This activity fully agrees with the ORAC value previously described by Sofic et al. (2.0 trolox equiv) [47], thus supporting the reliability of our experiments.

As shown in Table 1, all indole derivatives displayed ORAC values ranging from 1.3 to 3.0 trolox equiv., independently of the nature of the substituent attached to position 3 of the heterocycle. Consequently, they could be considered as excellent antioxidant agents. Surprisingly, the unsaturated derivative **23** did not show a substantial difference in the ORAC value (2.4 trolox equiv) compared to its saturated analogue **1** (2.7 trolox equiv), despite the view that an increase of the conjugation between the indole and oxadiazolone rings would bring about augmented radical scavenger properties.

Replacement of indole by a dihydronaphthalene or naphthalene core was detrimental to the antioxidant activity in the ORAC assay. Dihydronaphthalene **33** displayed a reduced ORAC value (0.4 trolox equiv) and naphthalenes **44** and **45** were inactive at the maximum concentration tested (10 μM). In summary, it can be inferred that in these compounds the radical absorbance capacity was mainly due to the presence of the indole ring, rather than other structural motifs.

2.4. Induction of the transcription factor NRF2 pathway in the AREc32 cell line

The ability to activate NRF2 was evaluated using an NRF2-dependent luciferase reporter assay in the AREc32 cell line [40,48]. Cells were cultured for 24 h and then treated with

increasing concentrations of the corresponding compound (0.3, 3, 10 and 30 μM). A selection of new derivatives, covering different structural features, was tested as inducers of NRF2 signalling and the results are gathered in Table 1. Sulforaphane was used as reference compound and data are expressed as the concentration needed to duplicate the specific activity of the luciferase reporter (CD).

In general, saturated indole-oxadiazolone derivatives (e.g., **4**) did not show activity at the maximum concentration tested (30 μM). On the contrary, the unsaturated indole-oxadiazolone **23** and its *N*-propargylic counterpart **24** were able to increase luciferase activity, with CD values of 15.1 and 1.8 μM, respectively (Table 1). Removal of the oxadiazolone ring in **24** to give the propargylic amide **25** caused a decrease by one order of magnitude in NRF2 activation (CD = 27.4 μM). When the propargyl moiety was replaced by an allyl fragment (**26**) the activity *vs.* NRF2 was lost. Dihydronaphthalene and naphthalene analogues were inactive. The above results indicated the importance of the presence of the indole core and a double bond in the linker to achieve good induction of NRF2.

2.5. Binding studies by surface plasmon resonance (SPR) assay

As explained in the introduction, activation of NRF2 could be due to conformational changes in KEAP1 that preclude the union between both proteins and stimulate the expression of antioxidant enzymes by NRF2. To evaluate the ability of our molecules to interact with the Kealch domain of KEAP1, a surface plasmon resonance (SPR) experiment was carried out. The Kelch domain was obtained from *Escherichia coli* transformed with pET15b-6xHIS-Kelch plasmid and induced by adding isopropyl-1-thio-β-D-galactopyranoside (IPTG). 6xHIS-Kelch was purified using the ProBond Purification System (Invitrogen). The Kelch domain of KEAP1 was immobilized on a carboxymethyl cellulose sensor chip (CM5) and a solution of the corresponding molecule (100 μM) was then fluxed over the sensor chip in order to detect a change in the SPR signal, resulting from the interaction between the compounds and the Kelch domain. The well-known KEAP1 binder ML334 was used as internal reference [49], which produced a change in the SPR signal of 10 resonance units (Fig. 2).

As shown in Fig. 2, SPR responses of compounds **23**–**25** were equal to, or greater than ML334, while the rest of the compounds tested (**4**, **21**, **26**, and **45**) gave fewer values. Importantly, the most active compounds in the phenotypic assay based on AREc32 cells showed a better binding to KEAP1 than the less active derivatives. Therefore, we can tentatively think that the activation of NRF2 by compounds **23**–**25** in the cellular assay could be due to the binding of these molecules to KEAP1.

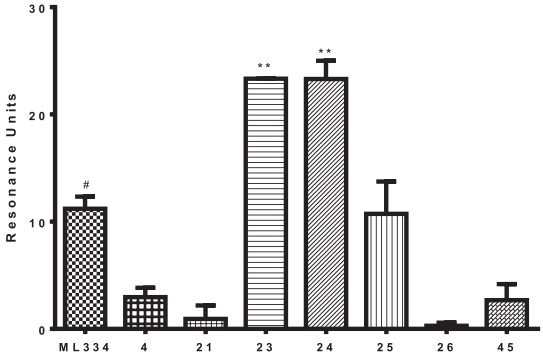

Fig. 2. Binding of selected compounds (**4**, **21**, **23**–**26** and **45**) to immobilized KEAP1 Kelch domain protein in comparison with ML334, determined by SPR spectroscopy. Mean ± SD (n = 3), one-way ANOVA plus Dunnett's test compared to ML334 (#). **P < 0.05.

2.6. Inhibition of human MAO and LOX-5

All compounds were evaluated as inhibitors of human MAO-A, MAO-B and LOX-5 and the results of the most representative compounds are collected in Table 2. For the sake of clarity, data of inactive compounds in the three enzymes are omitted. The *h*MAO-A/B inhibition was determined by the production of oxygen peroxide from a common substrate for both isoenzymes (*p*-tyramine) and quantified by the Amplex Red MAO assay kit [50]. (*R*)-Deprenyl, iproniazid and moclobemide were also tested for comparative purposes. The inhibition of *h*LOX-5 was performed following the fluorescence-based method described by Pufahl et al. [51], using the two well-known inhibitors zileuton and nordihydroguaiaretic acid (NDGA) as internal references.

In general, saturated indole–oxadiazolone derivatives did not show any appreciable inhibition of *h*MAOs or *h*LOX-5 (IC_{50} > 50 μM), with the exception of **12** and **13** which displayed a modest inhibition of *h*LOX-5 (IC_{50} = 74.2 and 22.5 μM, respectively). The 5-methoxyindole-oxadiazolamine **16** inhibited both *h*MAO-B and *h*LOX-5 (IC_{50} = 37.0 and 60.6 μM, respectively). Introduction of a double bond in the linker changed this profile, as the 5-methoxyindole-oxadiazole **23** displayed moderate inhibition of MAO-A and MAO-B (IC_{50} = 53.0 and 68.3 μM, respectively) although it was inactive in LOX-5 (IC_{50} > 100 μM). This positive effect of the double bond in the linker was not valid for the indole-amide and the naphthalene-oxadiazole series, because **25**, **26**, **44**, and **45** were inactive in the three enzymatic assays. Surprisingly, the introduction of a propargyl substituent in the oxadiazolone ring of the MAO-A/B inhibitor **23** to give **24** led to a total lack of activity on these enzymes (data not shown). Contrariwise, the dihydronaphthalene-oxadiazolone **33** inhibited *h*MAO-A, *h*MAO-B and *h*LOX-5 with IC_{50} values of 40.6, 35.7 and 12.5 μM, respectively (Table 2).

2.7. In vitro blood–brain barrier permeation assay (PAMPA-BBB)

In order to determine the capability of the new compounds to cross the BBB and reach their CNS targets, we evaluated them in the *in vitro* parallel artificial membrane permeability assay for the BBB (PAMPA-BBB) described by Di et al. [52], and modified by our group for testing molecules with limited water solubility [44–46,53,54]. The passive CNS permeation of new compounds through a lipid

Table 2
Inhibition (IC_{50}, μM)[a] of human monoamine oxidases (*h*MAO-A and *h*MAO-B) and human lipoxygenase-5 (*h*LOX-5) of indole and naphthalene derivatives[b].

Compd.	*h*MAO-A	*h*MAO-B	*h*LOX-5
12	>50	>50	74.2 ± 2.2
13	>50	>50	22.5 ± 1.8
16	>50	37.0 ± 0.7	60.6 ± 2.6
23	53.0 ± 3.5	68.3 ± 4.6	>100
33	40.6 ± 1.1	35.7 ± 3.3	12.5 ± 0.3
(*R*)-Deprenyl	68.7 ± 4.2	0.017 ± 0.002	n.d.
Iproniazid	6.7 ± 0.8	7.5 ± 0.4	n.d.
Moclobemide	161.4 ± 19.4	>100	n.d.
(*R*,*S*)-Zileuton	n.d.	n.d.	0.15 ± 0.03
NDGA	n.d.	n.d.	0.097 ± 0.019

[a] Data are the mean ± SD of three independent experiments performed in triplicate.
[b] Data of inactive compounds in the three enzymes are not shown.

extract of porcine brain was measured at room temperature. In each experiment, 11 commercial drugs of known brain permeability were also tested, and their permeability values were normalized to the reported PAMPA-BBB data. As previously established in the literature [52], compounds with $P_e > 4.0 \cdot 10^{-6}$ cm s^{-1} would be able to cross the BBB (cns+), whereas those displaying $P_e < 2.0 \cdot 10^{-6}$ cm s^{-1} would not reach the CNS (cns-). Between these values, the predicted CNS permeability remains uncertain (cns +/−).

In the melatonin-based family, the indole−*NH*-oxadiazolone **1** and its *beta*-methyl analogue **21** (both bearing a saturated linker) were predicted as not CNS-permeable ($P_e < 2 \cdot 10^{-6}$ cm s^{-1}). In contrast, all indole−*N*-substituted oxadiazolone derivatives (**2**–**15**), showed permeability values exceeding 4.0 10^{-6} cm s^{-1} and thus, they were predicted to be CNS-permeable. The indole−oxadiazolamine **16** displayed negative CNS permeation, whereas the indole−*NH*-oxadiazolone **23**, which is the unsaturated analogue of **1**, displayed a permeability value in the ambiguous range ($P_e = 3.2 \cdot 10^{-6}$ cm s^{-1}). The attachment of a propargylic moiety onto the oxadiazolone ring nitrogen of **23** gave **24**, which -as expected-was found to be CNS-permeable. Unsaturated amides **25** and **26** showed negative CNS permeability.

The exchange of the indole heterocycle by a dihydronaphthalene (**33**) or a naphthalene (**44** and **45**) generated compounds with good CNS permeability values (P_e = 9.0, 9.8 and 4.5 10^{-6} cm s^{-1}, respectively), even when the *NH*-unsubstituted oxadiazolone ring was retained. From these experiments we can conclude that, in general, the new indole and naphthalene derivatives with a single *NH*-unsubstituted motif are expected to be CNS-penetrating, whereas compounds with two *NH* groups would experience more difficulties to reach the CNS.

2.8. Drug-like calculations

To choose the best candidates for neurogenic assays, we studied the medicinal chemistry alerts of new indole- or naphthalene-oxadiazolones in two free databases, namely ZINC15 (http://zinc15.docking.org/) [55] and Aggregator Advisor (http://advisor.bkslab.org/) [56] (Table S2 in the Supplementary Information). None of the new compounds was highlighted as a pan assay interference compound (PAINS), according to the ZINC15 database. However, the Aggregator Advisor website identified compounds **13** and **15** with a fairly high calculated LogP in the range reported for other aggregators. Thus, these compounds were discarded for further biological assays.

Moreover, we calculated several physicochemical and ADME properties (log P, solubility, pK_a and Lipinski rule) of selected compounds (**23**, **24** and **44**) in comparison with melatonin (Table S3 in the Supplementary Information). According to the Swiss Institute of Bioinformatics (http://www.swissadme.ch/) [57], these compounds showed a good drug-like profile and thus, they are good candidates for further pharmacological studies.

2.9. Neurogenic studies

We investigated the capacity of a selection of the new compounds, covering different structural features, to promote cell differentiation into neurons. To this end, hippocampal-derived neurospheres adhered to a substrate and cultured under differentiation conditions in the presence of compounds were used [27,58]. The neurogenic potential of each compound was determined using fluorescence confocal microscopy, by direct observation of the expression of two immunofluorescent dyes linked to two well-known neuronal markers, β_{III}-tubulin (TuJ-1 clone) shown in green and microtubule-associated protein 2 (MAP-2) in red. TuJ-1 is expressed in new born neurons in early stages of their differentiation, whereas the expression of MAP-2 indicates a consolidated neuronal stage [59]. Vehicle-treated cultures (considered as basal) showed only a few scattered positive TuJ-1 or MAP-2 cells. In contrast, treatment with the compounds resulted in an increase in the number of TuJ-1 and MAP-2-positive cells compared to basal levels.

In the melatonin-based family several compounds promoted the expression of TuJ-1 and MAP-2, indicating positive neurogenic activities (Fig. 3). Comparing derivatives with a dimethylene liker, the indole−oxadiazolone **4** displayed good neurogenic properties, whereas its indole−oxadiazolamine counterpart **16** was inactive. This result points out the importance of the presence of an oxadiazolone ring for successful neurogenesis.

Among indole compounds bearing a double bond in the linker, the indole−*N*-propargyloxadiazolone **24** was one of the most active derivatives, as it greatly increased the expression of both TuJ-1 and MAP-2. Conversely, its indole−*NH*-oxadiazolone analogue **23** was inactive, suggesting that the *N*-propargyl group is beneficial for activity.

Both naphthalene−*NH*-oxadiazolone derivatives **44** and **45** showed positive effects in the expression of TuJ-1 and MAP-2. In contrast, the dihydronaphthalene analogue **33** was inactive, suggesting that the naphthalene core is more useful for biasing the compounds towards neurogenesis.

2.10. Theoretical studies. Conformational analysis of indole and naphthalene derivatives *23* and *44*

As explained above, the indole−*NH*-oxadiazolone derivative **23** showed marked selectivity towards QR2 (K_i = 6.6 nM), in comparison with hMT$_1$R and hMT$_2$R (K_i > 100 nM). In contrast, substitution of a naphthalene ring for the indole heterocycle gave **44**, which was a potent and selective agonist at hMT$_2$R (EC_{50} = 1.1 nM), compared to hMT$_1$R and QR2 (K_i = 260 and 270 nM, respectively) (Table 1).

With the aim of explaining this distinct behaviour in *NH*-oxadiazolone derivatives that only differ in the nature of the fused heterocycle, we performed a conformational analysis of **23** and **44** using quantum mechanics (Fig. 4).

The conformational analysis revealed higher energy barriers (~2 kcal mol^{-1}) for rotation about the C2−C3 bond and a preferred flat conformation in the indole−*NH*-oxadiazolone **23** (Fig. 4). This co-planar arrangement of the ring systems is prevented in the naphthalene derivative **44** due to steric clash as a consequence of the decreased C1−C2−C3 angle. These results seemed to indicate that the flat conformation of **23** might favour the stacking interaction with the isoalloxazine ring of FAD in QR2, whereas the slight non-planarity of **44** (dihedral angle of ~40°) would be preferred for its agonist activity on hMT$_2$R. On the other hand, the energy barriers for rotation about the C4−C5 bond are of similar magnitude in both molecules.

2.11. Molecular dynamics simulations on hQR2, hMT_1R and hMT_2R

To test the previous hypotheses, we undertook some molecular dynamics studies. In agreement with the previous statement, our modelled complexes of hQR2 (Fig. 5) and hMT$_2$R (Fig. 6) with **23** and **44**, respectively, show that the proposed stacking of the flat **23** molecule on FAD is reminiscent of that described for resveratrol [60], with the indole nitrogen establishing a hydrogen bond to the

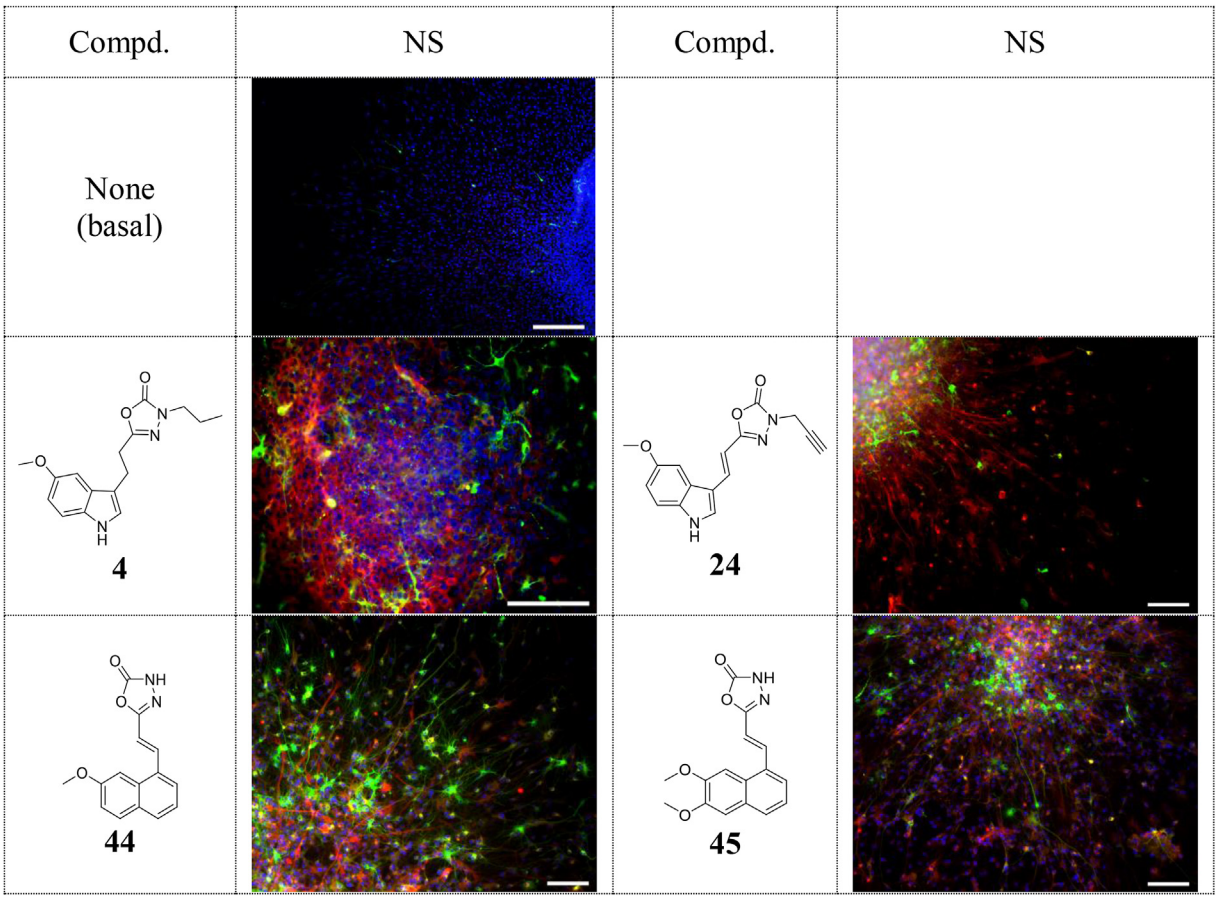

Fig. 3. Melatonin-based compounds promote neuronal differentiation on SGZ-derived neurospheres. Neurospheres were cultured in the presence of compounds (10 μM) for 7 days and later adhered for 3 days to allow differentiation in the presence of compounds. Confocal images show the expression of the neuronal markers TuJ clone (early neurogenesis) in green and MAP-2 (mature neurons) in red. DAPI was used for nuclear staining. Fluorescent representative images from four independent experiments were displayed. Scale bar = 100 μm (images of inactive compounds are not shown). (For interpretation of the references to color in this figure legend, the reader is referred to the Web version of this article.)

carbonyl oxygen of Gly174 that is similar to that observed for one of the resorcinol hydroxyls of this naturally occurring polyphenol. It can also be seen that the oxadiazolone nitrogen is engaged in hydrogen bonds to water molecules, which would be displaced when the attached hydrogen is replaced with a short substituent, as is the case for the propargyl group present in **24** (Fig. S1, Supporting Information).

In contrast, for the less coplanar naphthalene derivatives, the variety of binding orientations we found is commensurate with that observed in X-ray crystal structures of QR2 in complex with melatonin and derivatives [61]. Nonetheless, the out-of-plane conformation of **44** is ideally suited to mimic the bound conformation of melatonin that has been observed in the XFEL structures of chimeric MT_1R and MT_2R constructs, very recently described by Stauch et al. [62] and Johansson et al. [63], respectively. At this location in our modelled MT_2R, binding of **44** is largely stabilized by the phenyl ring of Phe192^{ECL2}, additional hydrophobic interactions with neighbouring residues (including the highly conserved Trp264$^{6.48}$ that was replaced by Phe in the experimental constructs) and a number of direct and water-mediated hydrogen bonds with the polar side chains of Gln194^{ECL2}, Asn162$^{4.60}$, and Asn268$^{6.52}$. The most important difference relative to MT_1R is the orientation of Tyr200$^{5.38}$, which is close to the side chains of Val178 ^{ECL2} and Ser180 ^{ECL2} and whose phenolic group hydrogen bonds to the carbonyl oxygen of Ala171$^{4.56}$. In MT_1R, the equivalent residues are Ala165 ^{ECL2} and Thr167 ^{ECL2} so that the side chain of Tyr187$^{5.38}$ points towards the membrane [62,63] and slightly different interactions are observed (Fig. S2, Supporting Information).

2.12. Molecular docking studies and molecular dynamics simulations on KEAP1

Molecular docking studies of **23** and **24** were performed on four different crystal structures of the KEAP1 Kelch domain (PDB entries 4XMB, 5CGJ, 5FNU and 4IFL) to consider, at least partially, protein flexibility. At physiologic pH, compound **23** exists as two different species, as deduced from its experimental pK_a of 7.45 ± 0.09 (Fig. S3, Supporting Information). No substantial differences in the average binding energy values were observed in both species, named **23-0** and **23-1**. On the other hand, the higher affinity score obtained for **24** correlated with the experimental NRF2 induction value in the AREc32 cell line (Table S1, Supporting Information).

The most stable molecular docking poses found for **23** and **24** on the four 3D-structures of the KEAP1 Kelch domain (Figs. S4 and S5, Supporting Information) were used as the starting structures for uMD simulations, which after 200 ns of production run showed some drifting of the bound ligand towards a new ligand-protein interface (Fig. 7). The binding site residues involved in the NRF2-KEAP1 interaction are very well known and have been reported by several authors [64]. It has been shown that residues Arg380,415,483; Ser363,508,555,602; and Tyr525,572,334 on KEAP1 are essential to interact with NRF2. Our uMD simulations

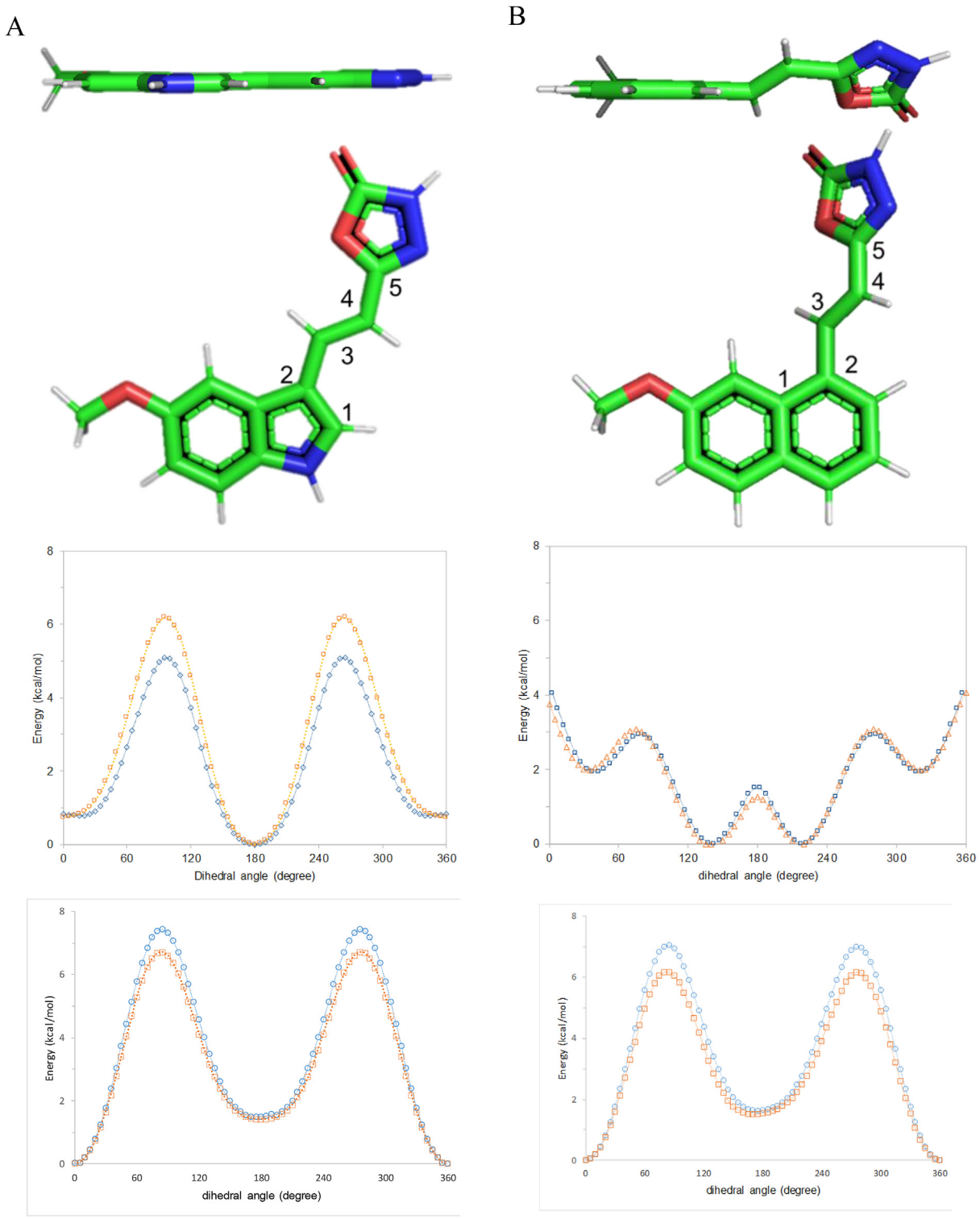

Fig. 4. Global energy conformations of indole–*NH*-oxadiazolone **23** (A) and naphthalene–*NH*-oxadiazolone **44** representative molecules (B), together with the rotational barriers (*in vacuum*, blue; using an implicit solvent model for water, orange) upon rotation about the bonds connecting atoms labelled 2 and 3 (top) and 4 and 5 (bottom). (For interpretation of the references to color in this figure legend, the reader is referred to the Web version of this article.)

show that **23** and **24** do interact with some of these residues (Fig. 7) and also **23** experiences greater fluctuations within the binding pocket in KEAP1. This difference mostly arises from the fact that **24** interacts with hydrophobic residues Phe577 and Ala556 whereas **23** does not.

Finally, thermodynamic calculations over the last 10 ns of the production run, using the Molecular Mechanics Generalized Born Surface Area approach (MMGBSA) [65], revealed a noticeably higher affinity for **24** relative to **23** that is in consonance with the experimental finding that **24** leads to a larger activation and expression of NRF2 in AREc32 cells (Table 1).

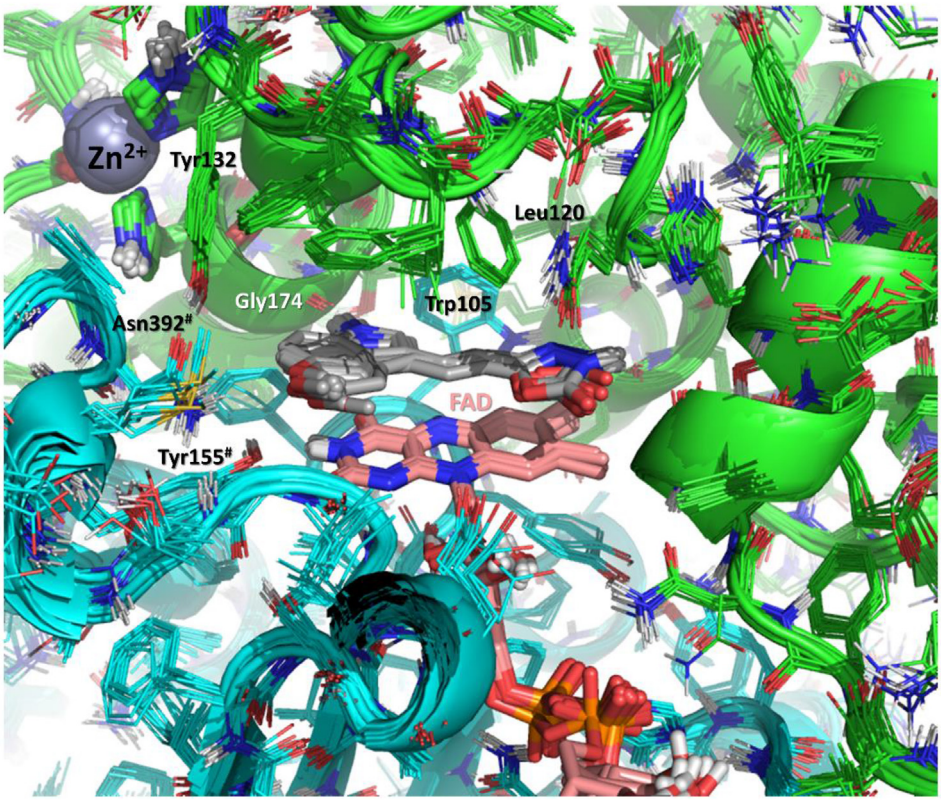

Fig. 5. Representative models of *h*QR2 in complex with indole − *NH*-oxadiazolone derivative **23** (sticks with C atoms coloured in grey) obtained after the simulated annealing procedure following molecular dynamics simulations. The starting reference structure was PDB entry 1SG0.

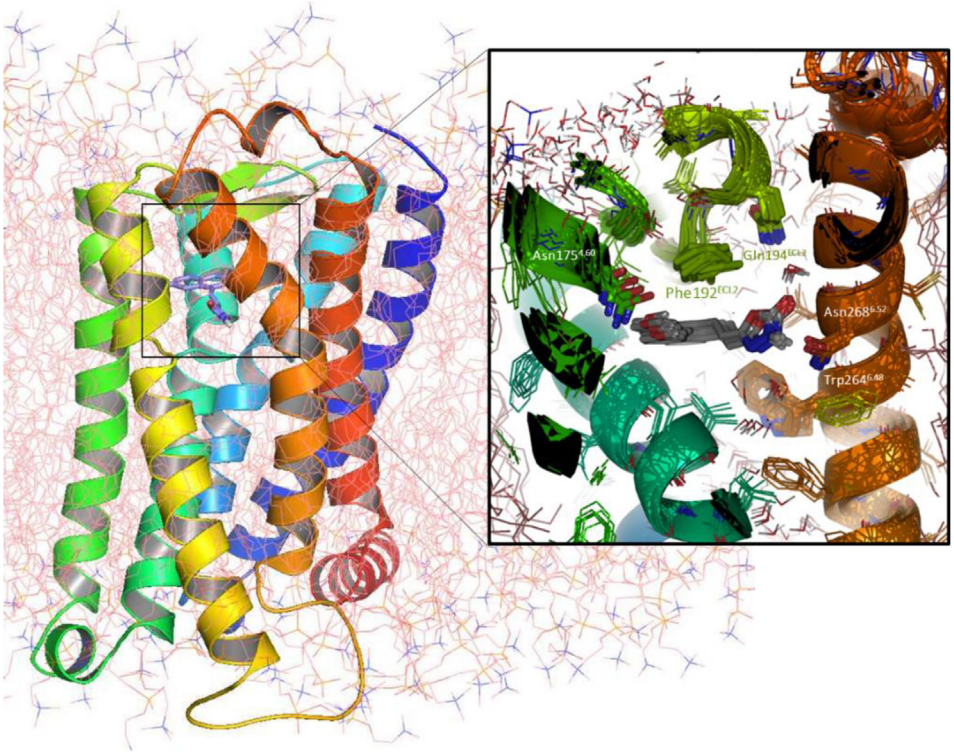

Fig. 6. Model of a membrane-embedded $h\mathrm{MT_2R}$ (rainbow coloured) in complex with naphthalene−*NH*-oxadiazolone derivative **44** (sticks with C atoms coloured in grey). The enlarged region in the box shows the superposition of eight cooled and energy-minimized snapshots from the last 170–200 ns of unrestrained molecular dynamics (uMD) simulation. The starting reference structure was PDB entry 6ME8.

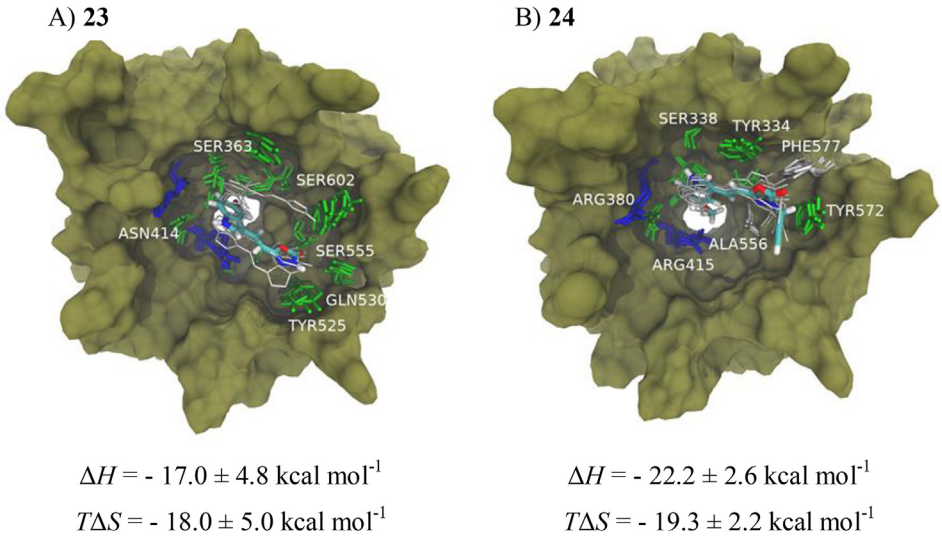

Fig. 7. Dynamic conformation of KEAP1-ligand complexes. A) KEAP1-**23** complex. B) KEAP1-**24** complex. Water molecules and ions are not depicted for clarity. KEAP1 is represented as a brown molecular surface [66]. Residues involved into protein-ligand interaction are represented as sticks by colour type: green are polar residues, blue are positive charged residues and white are hydrophobic residues. Ligands are represented as sticks with grey carbon atoms, blue nitrogen atoms, red oxygen atoms and white hydrogen atoms. Thinner white sticks correspond to the ligand conformations during the last 10ns of the MD production. These images were made with VMD software support [67]. The most stable molecular docking poses found for **23** and **24** on the 3D-structures of the KEAP1 Kelch domain with pdbcode 4XMB were used as the starting reference structure. (For interpretation of the references to color in this figure legend, the reader is referred to the Web version of this article.)

3. Conclusions

By structural modifications of our described *h*MT_1R and *h*MT_2R nanomolar ligand 5-[2-(5-methoxy-1*H*-indol-3-yl)ethyl]-1,3,4-oxadiazol-2(3*H*)-one (**1**), new indole– and naphthalene–oxadiazolone MTDLs have been obtained and evaluated on targets related to oxidative stress and neuroinflammation. Introduction of lipophilic substituents on the nitrogen of the oxadiazolone ring improved their *in vitro* CNS permeation but was detrimental for their affinity for the GPCRs *h*MT_1R and *h*MT_2R. The addition of a methyl group in the aliphatic linker of **1** or the replacement of the oxadiazolone ring by a 1,3,4-oxadiazol-2-amine scaffold yielded compounds with K_is in the hundred-nanomolar range in melatonin targets, but they were predicted as not CNS-permeable.

Introduction of a double bond in the linker provided interesting effects on the behaviour of these less flexible indole- and naphthalene-oxadiazolone compounds. The 5-methoxyindole derivatives **23** and **24** displayed remarkable selectivity towards QR2 (K_i = 6.6 and 3.2 nM, respectively) in reference to *h*MT_1R and *h*MT_2R (K_is > 100 nM). In contrast, when the 5-methoxyindole of **23** was replaced by a 7-methoxynaphthalene the selectivity changed drastically, since **44** was preferably bound to *h*MT_2R (K_i = 5.1 nM) compared to *h*MT_1R and QR2 (K_i = 260 and 270 nM, respectively). Moreover, **44** was functionally characterized as a potent *h*MT_2R agonist with a maximum activity of 85% with respect to melatonin and an EC_{50} of 1.1 nM.

Conformational analyses using quantum mechanics revealed that the indole-*NH*-oxadiazolone **23** presents a co-planar arrangement of the ring systems, whereas the naphthalene-*NH*-oxadiazolone **44** shows a dihedral angle of ~40° between both heterocycles. These differences could explain the observed selectivity of **23** and **44** towards QR2 and *h*MT_2R, respectively. Molecular modelling and computer simulations, using the crystal structure of QR2 and the recently described XFEL structures of chimeric MT_1R and MT_2R, have provided a rationale for the experimental selectivity and afford valuable insight that can aid in future drug design endeavours.

In the ORAC assays, indole derivatives were found to be as good radical scavengers as melatonin, whereas naphthalene-based compounds showed worse ORAC values. Thus, the radical absorbance capacity was mainly linked to the indole ring.

In relation to NRF2 induction, best results were obtained with the indole–*NH*-oxadiazolone derivative with a double bond in the linker **23** and its *N*-propargylic counterpart **24** (CD = 15.1 and 1.8 μM, respectively). When comparing with other derivatives, we can infer the importance of the presence of the indole core and a double bond in the connector to achieve a good induction of NRF2. From the SPR experiments using the KEAP1 Kelch domain, we could infer that the cellular NRF2 induction by compounds **23** and **24** could be due to the binding of these molecules to KEAP1. Moreover, molecular dynamics simulations on the KEAP1 Kelch domain showed that **23** and **24** interact with several essential residues involved in the binding KEAP1-NRF2. Thermodynamic calculations revealed higher affinity for **24** than for **23**, according to the experimental finding that **24** leads to a larger activation and expression of NRF2 in cellular experiments.

Several saturated indole–oxadiazolone derivatives were modest *h*LOX-5 inhibitors and inactive in *h*MAOs. However, the introduction of a double bond in the linker again reversed selectivity, as the indole–*NH*-oxadiazolone **23** inhibited *h*MAOs but it is inactive in *h*LOX-5. Only the dihydronaphthalene-oxadiazolone **33** was found to inhibit the three enzymes, with IC_{50} values in the two-digit micromolar range.

In neurogenic assays, several of the new melatonin-oxadiazolone derivatives stimulated the differentiation of NSC to a consolidated neuronal stage, as they could contribute to the auto-repair processes of the CNS.

Finally, it can be emphasized that it is possible to modulate the selectivity of these new oxadiazolone-based MTDLs by modifying the side chain functionality and co-planarity with the indole or naphthalene ring.

4. Experimental section

4.1. Chemistry. General methods

High-grade reagents and solvents were purchased from

commercial suppliers and were used without further purification. Reactions were followed by thin-layer chromatography (TLC) or high-performance liquid chromatography coupled to mass spectrometry (HPLC-MS). TLC was performed using Merck silica gel 60 F254 plates and compounds were detected under UV-light (λ = 254 or 365 nm) and/or stained with 10% wt. phosphomolybdic acid, ninhydrin, or vanillin solutions in EtOH. HPLC-MS data were acquired in an Alliance Watters 2695 coupled to a quadrupole mass spectrometer (Micromass ZQ). HPLC was equipped with a SunFire C_{18} column (3.5 μm, 4.6 mm × 50 mm) and a UV−visible photodiode array detector (λ = 190−700 nm). MS were acquired in an electrospray ionization (ESI) interface working in the positive or negative-ion mode. Microwave driven reactions were performed in a Biotage Initiator 2.5 reactor. Unless otherwise stated, products were purified by automatized flash column chromatography using an IsoleraOne (Biotage) equipment, with different cartridges of silica gel Biotage ZIP KP-Sil 50 μm. Alternatively, we used preparative TLC on Merck silica gel 60 F254 plates or semipreparative HPLC on a Waters Autopurification system with UV−visible photodiode array detector (λ = 190−700 nm) coupled to a quadrupole mass spectrometer (3100 Mass Detector). Purity of all compounds (≥95%) was determined by HPLC on a Waters 2690 equipment, at a flow rate of 1.0 mL/min, with a UV−visible photodiode array detector (λ = 190−700 nm), using a SunFire C_{18} column (3.5 μm, 4.6 mm × 50 mm). The gradient of the mobile phase consisted of H_2O:ACN with formic acid (0.1%), and the gradients time (g.t.) are indicated for each compound. Melting points (mp) (uncorrected) were determined in a MP70 apparatus (Mettler Toledo). Nuclear magnetic resonance (^{1}H NMR and ^{13}C NMR) spectra were obtained in the following spectrometers: Varian INOVA-300, Varian INOVA-400, Varian Mercury-400 or Varian Unity-500. Chemical shifts (δ) are reported in parts per million (ppm) relative to internal tetramethylsilane scale, and coupling constants (*J*) are expressed in hertz (Hz). 2D NMR experiments namely, homonuclear correlation spectroscopy (H,H−COSY), heteronuclear multiple quantum correlation (HMQC) and heteronuclear multiple bond correlation (HMBC) were acquired to assign protons and carbons of new structures. High resolution mass spectra (HRMS) analyses were carried out by using an Agilent 1200 Series LC system (equipped with a binary pump, an autosampler, and a column oven) coupled to a 6520 quadrupole-time of flight (QTOF) mass spectrometer. ACN:H_2O (75:25, v:v) was used as mobile phase at 0.2 mL/min. The ionization source was an ESI interface working in the positive-ion mode. The electrospray voltage was set at 4.5 kV, the fragmentary voltage at 150 V and the drying gas temperature at 300 °C. Nitrogen (99.5% purity) was used as nebulizer (207 kPa) and drying gas (6 L/min).

4.2. General procedure for the synthesis of **2**–**15**

A mixture of **1** (1 equiv.), K_2CO_3 (1.2 equiv.) and the corresponding halide (1.2 equiv) in acetone (7 mL/mmol) was heated under MW-irradiation at 120 °C for 10 min. Solvent was evaporated under reduced pressure, EtOAc (10 mL/mmol) was added and the organic layer was washed with H_2O (x3) and brine and then, dried over $MgSO_4$, filtered, and evaporated to dryness under reduced pressure. The crude was purified by column chromatography using the appropriate eluent to afford the corresponding alkyl derivative **2**–**15**.

4.3. Characterization of compounds **2**–**45**

4.3.1. 5-[2-(5-Methoxy-1H-indol-3-yl)ethyl]-3-methyl-1,3,4-oxadiazol-2(3H)-one (**2**)

Chromatography: DCM to DCM:MeOH 95:5. White solid (66% yield) of mp 83−86 °C. ^{1}H NMR (500 MHz, $CDCl_3$) δ 7.97 (s, 1H, NH), 7.25 (d, *J* = 8.6 Hz, 1H, H_7), 7.00 (d, *J* = 2.5 Hz, 1H, H_2), 6.99 (d, *J* = 2.4 Hz, 1H, H_4), 6.87 (dd, *J* = 8.7, 2.4 Hz, 1H, H_6), 3.87 (s, 3H, OCH_3), 3.35 (s, 3H, NCH_3), 3.12 (t, *J* = 7.7 Hz, 2H, H_α), 2.92 (t, *J* = 7.7 Hz, 2H, H_β). ^{13}C NMR (126 MHz, $CDCl_3$) δ 155.9 ($C_{5'}$), 154.4 ($C_{2'}$), 154.2 (C_5), 131.5 (C_{7a}), 127.4 (C_{3a}), 122.5 (C_2), 113.6 (C_3), 112.6 (C_6), 112.2 (C_7), 100.3 (C_4), 56.1 (OCH_3), 32.5 (NCH_3), 27.4 (C_β), 21.5 (C_α). HPLC-MS (15:95- g.t.5 min) ^{t}R 3.97 min, *m/z* = 274.20 $[M+H]^+$, calcd. for $[C_{14}H_{15}N_3O_3+H]^+$ 274.29. HRMS $[ESI^+]$ *m/z* = 273.11145 $[M]^+$, calcd. for $[C_{14}H_{15}N_3O_3]^+$ 273.11134.

4.3.2. 3-Ethyl-5-[2-(5-methoxy-1H-indol-3-yl)ethyl]-1,3,4-oxadiazol-2(3H)-one (**3**)

Chromatography: DCM to DCM:MeOH 95:5. White solid (56% yield) of mp 69−72 °C. ^{1}H NMR (500 MHz, $CDCl_3$) δ 7.90 (s, 1H, NH), 7.26 (d, *J* = 8.8 Hz, 1H, H_7), 7.01 (d, *J* = 2.5 Hz, 1H, H_2), 6.99 (d, *J* = 2.3 Hz, 1H, H_4), 6.87 (dd, *J* = 8.8, 2.4 Hz, 1H, H_6), 3.87 (s, 3H, OCH_3), 3.71 (q, *J* = 7.2 Hz, 2H, CH_2CH_3), 3.15−3.11 (m, 2H, H_α), 2.95−2.90 (m, 2H, H_β), 1.28 (t, *J* = 7.2 Hz, 3H, CH_2CH_3). ^{13}C NMR (126 MHz, $CDCl_3$) δ 155.9 ($C_{5'}$), 154.3 (C_5), 154.0 ($C_{2'}$), 131.5 (C_{7a}), 127.5 (C_{3a}), 122.5 (C_2), 113.8 (C_3), 112.7 (C_6), 112.1 (C_7), 100.3 (C_4), 56.1 (OCH_3), 40.8 (CH_2CH_3), 27.6 (C_β), 21.6 (C_α), 13.5 (CH_2CH_3). HPLC-MS (15:95- g.t.5 min) ^{t}R 4.21 min, *m/z* = 288.15 $[M+H]^+$, calcd. for $[C_{15}H_{17}N_3O_3+H]^+$ 288.32. HRMS $[ESI^+]$ *m/z* = 287.1275 $[M]^+$, calcd. for $[C_{15}H_{17}N_3O_3]^+$ 287.12699.

4.3.3. 5-[2-(5-Methoxy-1H-indol-3-yl)ethyl]-3-propyl-1,3,4-oxadiazol-2(3H)-one (**4**)

Chromatography: DCM to DCM:MeOH 95:5. White solid (49% yield) of mp 95−98 °C. ^{1}H NMR (500 MHz, DMSO-d_6) δ 10.67 (s, 1H, NH), 7.21 (dd, *J* = 8.7, 0.5 Hz, 1H, H_7), 7.11 (d, *J* = 2.5 Hz, 1H, H_2), 6.97 (d, *J* = 2.4 Hz, 1H, H_4), 6.70 (dd, *J* = 8.8, 2.4 Hz, 1H, H_6), 3.75 (s, 3H, OCH_3), 3.53 (t, *J* = 6.8 Hz, 2H, NCH_2), 3.00 (t, *J* = 7.4 Hz, 2H, H_α), 2.90 (t, *J* = 7.5 Hz, 2H, H_β), 1.57 (h, *J* = 7.2 Hz, 2H, CH_2CH_3), 0.78 (t, *J* = 7.4 Hz, 3H, CH_2CH_3). ^{13}C NMR (126 MHz, DMSO-d_6) δ 155.6 ($C_{5'}$), 153.5 ($C_{2'}$), 153.0 (C_5), 131.3 (C_{7a}), 127.1 (C_{3a}), 123.3 (C_2), 112.1 (C_7), 111.9 (C_3), 111.2 (C_6), 99.7 (C_4), 55.3 (OCH_3), 46.4 (NCH_2), 26.9 (C_β), 21.0 (CH_2CH_3), 20.8 (C_α), 10.6 (CH_2CH_3). HPLC-MS (15:95- g.t.5 min) ^{t}R 4.48 min, *m/z* = 302.28 $[M+H]^+$, calcd. for $[C_{16}H_{19}N_3O_3+H]^+$ 302.35. HRMS $[ESI^+]$ *m/z* = 301.14327 $[M]^+$, calcd. for $[C_{16}H_{19}N_3O_3]^+$ 301.14264.

4.3.4. 3-Butyl-5-[2-(5-methoxy-1H-indol-3-yl)ethyl]-1,3,4-oxadiazol-2(3H)-one (**5**)

Chromatography: DCM. White solid (92% yield) of mp 64−65 °C. ^{1}H NMR (500 MHz, DMSO-d_6) δ 10.67 (s, 1H, NH), 7.21 (d, *J* = 8.7 Hz, 1H, H_7), 7.10 (d, *J* = 2.4 Hz, 1H, H_2), 6.96 (d, *J* = 2.5 Hz, 1H, H_4), 6.70 (dd, *J* = 8.7, 2.4 Hz, 1H, H_6), 3.75 (s, 3H, OCH_3), 3.55 (t, *J* = 6.9 Hz, 2H, NCH_2), 3.00 (t, *J* = 7.4 Hz, 2H, H_α), 2.91 (t, *J* = 7.5 Hz, 2H, H_β), 1.52 (p, *J* = 7.0 Hz, 2H, NCH_2CH_2), 1.17 (h, *J* = 7.4 Hz, 2H, CH_2CH_3), 0.83 (t, *J* = 7.4 Hz, 3H, CH_2CH_3). ^{13}C NMR (126 MHz, DMSO-d_6) δ 155.6 ($C_{5'}$), 153.4 ($C_{2'}$), 153.0 (C_5), 131.3 (C_{7a}), 127.1 (C_{3a}), 123.3 (C_2), 112.1 (C_7), 111.9 (C_3), 111.2 (C_6), 99.7 (C_4), 55.3 (OCH_3), 44.4 (NCH_2), 29.5 (NCH_2CH_2), 26.9 (C_β), 20.8 (C_α), 18.8 (CH_2CH_3), 13.3 (CH_2CH_3). HPLC-MS (15:95- g.t.5 min) ^{t}R 4.79 min, *m/z* = 316.11 $[M+H]^+$, calcd. for $[C_{17}H_{21}N_3O_3+H]^+$ 316.37. HRMS $[ESI^+]$ *m/z* = 315.15838 $[M]^+$, calcd. for $[C_{17}H_{21}N_3O_3]^+$ 315.15829.

4.3.5. 5-[2-(5-Methoxy-1H-indol-3-yl)ethyl]-3-pentyl-1,3,4-oxadiazol-2(3H)-one (**6**)

Chromatography: DCM. Pale yellow solid (90% yield) of mp 48−51 °C. ^{1}H NMR (500 MHz, $CDCl_3$) δ 7.90 (s, 1H, NH), 7.25 (d, *J* = 8.5 Hz, 1H, H_7), 7.01 (d, *J* = 2.5 Hz, 1H, H_2), 6.99 (d, *J* = 2.4 Hz, 1H, H_4), 6.87 (dd, *J* = 8.8, 2.5 Hz, 1H, H_6), 3.87 (s, 3H, OCH_3), 3.63 (t, *J* = 7.2 Hz, 2H, NCH_2), 3.13 (t, *J* = 7.4 Hz, 2H, H_α), 2.92 (t, *J* = 7.5 Hz,

2H, H_β), 1.67 (p, J = 7.3 Hz, 2H, NCH_2CH_2), 1.36–1.30 (m, 2H, CH_2CH_3), 1.30–1.21 (m, 2H, $N(CH_2)_2CH_2$), 0.89 (t, J = 7.2 Hz, 3H, CH_2CH_3). ^{13}C NMR (126 MHz, $CDCl_3$) δ 155.8 ($C_{5'}$), 154.3 (C_5), 154.3 ($C_{2'}$), 131.5 (C_{7a}), 127.5 (C_{3a}), 122.5 (C_2), 113.7 (C_3), 112.7 (C_6), 112.1 (C_7), 100.3 (C_4), 56.1 (OCH_3), 45.8 (NCH_2), 28.6 ($N(CH_2)_2CH_2$), 27.9 (NCH_2CH_2), 27.6 (C_β), 22.3 (CH_2CH_3), 21.6 (C_α), 14.1 (CH_2CH_3). HPLC-MS (30:95- g.t.5 min) ^{t}R 4.60 min, (50:95- g.t.5 min) ^{t}R 3.17 min, m/z = 330.13 $[M+H]^+$, calcd. for $[C_{18}H_{23}N_3O_3+H]^+$ 330.40. HRMS $[ESI^+]$ m/z = 329.17515 $[M]^+$, calcd. for $[C_{18}H_{23}N_3O_3]^+$ 329.17394.

4.3.6. 3-Hexyl-5-[2-(5-methoxy-1H-indol-3-yl)ethyl]-1,3,4-oxadiazol-2(3H)-one (**7**)

Chromatography: hexane to DCM. Colorless oil (70% yield). ^{1}H NMR (500 MHz, MeOD) δ 7.20 (d, J = 8.7 Hz, 1H, H_7), 7.03 (bs, 1H, H_2), 6.95 (d, J = 2.4 Hz, 1H, H_4), 6.74 (dd, J = 8.8, 2.4 Hz, 1H, H_6), 3.82 (s, 3H, OCH_3), 3.57 (t, J = 6.9 Hz, 2H, NCH_2), 3.11 (t, J = 7.2 Hz, 2H, H_α), 2.92 (t, J = 7.2 Hz, 2H, H_β), 1.56 (p, J = 7.0 Hz, 2H, NCH_2CH_2), 1.30–1.21 (m, 4H, $N(CH_2)_3(CH_2)_2CH_3$), 1.20–1.10 (m, 2H, $N(CH_2)_2CH_2$), 0.88 (t, J = 6.9 Hz, 3H, CH_2CH_3). ^{13}C NMR (126 MHz, MeOD) δ 157.6 ($C_{5'}$), 156.0 ($C_{2'}$), 155.1 (C_5), 133.3 (C_{7a}), 128.7 (C_{3a}), 124.1 (C_2), 113.6 (C_3), 113.0 (C_7), 112.8 (C_6), 100.7 (C_4), 56.2 (OCH_3), 46.4 (NCH_2), 32.3 ($N(CH_2)_3CH_2$), 28.9 (NCH_2CH_2), 28.7 (C_β), 26.9 ($N(CH_2)_2CH_2$), 23.5 (CH_2CH_3), 22.4 (C_α), 14.3 (CH_2CH_3). HPLC-MS (50:95- g.t.5 min) ^{t}R 3.77 min, m/z = 344.38 $[M+H]^+$, calcd. for $[C_{19}H_{25}N_3O_3+H]^+$ 344.43. HRMS $[ESI^+]$ m/z = 343.18957 $[M]^+$, calcd. for $[C_{19}H_{25}N_3O_3]^+$ 343.18959.

4.3.7. 3-Heptyl-5-[2-(5-methoxy-1H-indol-3-yl)ethyl]-1,3,4-oxadiazol-2(3H)-one (**8**)

Chromatography: hexane to DCM. Yellow oil (85% yield). ^{1}H NMR (300 MHz, $CDCl_3$) δ 7.95 (s, 1H, NH), 7.25 (d, J = 8.9 Hz, 1H, H_7), 7.02–6.95 (m, 2H, H_2, H_4), 6.86 (dd, J = 8.8, 2.4 Hz, 1H, H_6), 3.87 (s, 3H, OCH_3), 3.63 (t, J = 7.2 Hz, 2H, NCH_2), 3.13 (dd, J = 8.6, 6.3 Hz, 2H, H_α), 2.92 (dd, J = 8.6, 6.4 Hz, 2H, H_β), 1.67 (p, J = 7.3 Hz, 2H, NCH_2CH_2), 1.34–1.19 (m, 8H, $N(CH_2)_2(CH_2)_4CH_3$), 0.88 (t, J = 6.7 Hz, 3H, CH_2CH_3). ^{13}C NMR (75 MHz, $CDCl_3$) δ 155.9 ($C_{5'}$), 154.3 (C_5), 154.3 ($C_{2'}$), 131.5 (C_{7a}), 127.5 (C_{3a}), 122.5 (C_2), 113.7 (C_3), 112.6 (C_6), 112.1 (C_7), 100.3 (C_4), 56.1 (OCH_3), 45.8 (NCH_2), 31.8 ($N(CH_2)_4CH_2$), 28.9 ($N(CH_2)_3CH_2$), 28.2 (NCH_2CH_2), 27.6 (C_β), 26.4 ($N(CH_2)_2CH_2$), 22.7 (CH_2CH_3), 21.6 (C_α), 14.2 (CH_2CH_3). HPLC-MS (70:95- g.t.5 min) ^{t}R 1.56 min, m/z = 358.25 $[M+H]^+$, calcd. for $[C_{20}H_{27}N_3O_3+H]^+$ 358.45. HRMS $[ESI^+]$ m/z = 357.2056 $[M]^+$, calcd. for $[C_{20}H_{27}N_3O_3]^+$ 357.20524.

4.3.8. 5-[2-(5-Methoxy-1H-indol-3-yl)ethyl]-3-(propan-2-yl)-1,3,4-oxadiazol-2(3H)-one (**9**)

Chromatography: DCM. White solid (81% yield) of mp 130–133 °C. ^{1}H NMR (500 MHz, $CDCl_3$) δ 7.88 (bs, 1H, NH), 7.25 (d, J = 7.8 Hz, 1H, H_7), 7.01 (d, J = 2.4 Hz, 1H, H_2), 6.99 (d, J = 2.4 Hz, 1H, H_4), 6.86 (dd, J = 8.8, 2.4 Hz, 1H, H_6), 4.25–4.21 (m, 1H, $CH(CH_3)_2$), 3.87 (s, 3H, OCH_3), 3.13 (dd, J = 7.6 Hz, 2H, H_α), 2.92 (dd, J = 7.7 Hz, 2H, H_β), 1.30 (d, J = 6.7 Hz, 6H, $CH(CH_3)_2$). ^{13}C NMR (126 MHz, $CDCl_3$) δ 155.8 ($C_{5'}$), 154.3 (C_5), 153.6 ($C_{2'}$), 131.5 (C_{7a}), 127.6 (C_{3a}), 122.5 (C_2), 113.9 (C_3), 112.7 (C_6), 112.1 (C_7), 100.3 (C_4), 56.1 (OCH_3), 47.9 ($CH(CH_3)_2$), 27.7 (C_β), 21.6 (C_α), 20.8 ($CH(CH_3)_2$). HPLC-MS (15:95- g.t.5 min) ^{t}R 4.49 min, m/z = 302.35 $[M+H]^+$, calcd. for $[C_{16}H_{19}N_3O_3+H]^+$ 302.35. HRMS $[ESI^+]$ m/z = 301.14244 $[M]^+$, calcd. for $[C_{16}H_{19}N_3O_3]^+$ 301.14264.

4.3.9. 5-[2-(5-Methoxy-1H-indol-3-yl)ethyl]-3-(2-methylpropyl)-1,3,4-oxadiazol-2(3H)-one (**10**)

Chromatography: DCM. White solid (82% yield) of mp 54–56 °C. ^{1}H NMR (500 MHz, DMSO-d_6) δ 10.67 (s, 1H, NH), 7.21 (d, J = 8.7 Hz, 1H, H_7), 7.10 (d, J = 2.4 Hz, 1H, H_2), 6.97 (d, J = 2.4 Hz, 1H, H_4), 6.70 (dd, J = 8.7, 2.4 Hz, 1H, H_6), 3.75 (s, 3H, OCH_3), 3.37 (d, J = 7.1 Hz, 2H, NCH_2), 3.00 (t, J = 7.3 Hz, 2H, H_α), 2.91 (t, J = 7.2 Hz, 2H, H_β), 1.90–1.87 (m, 1H, $CH(CH_3)_2$), 0.79 (d, J = 6.7 Hz, 6H, $CH(CH_3)_2$). ^{13}C NMR (126 MHz, DMSO-d_6) δ 155.6 ($C_{5'}$), 153.7 ($C_{2'}$), 153.0 (C_5), 131.3 (C_{7a}), 127.1 (C_{3a}), 123.3 (C_2), 112.1 (C_7), 111.9 (C_3), 111.2 (C_6), 99.7 (C_4), 55.3 (OCH_3), 51.8 (NCH_2), 27.4 ($CH(CH_3)_2$), 26.9 (C_β), 20.8 (C_α), 19.4 ($CH(CH_3)_2$). HPLC-MS (15:95- g.t.5 min) ^{t}R 4.77 min, m/z = 316.34 $[M+H]^+$, calcd. for $[C_{17}H_{21}N_3O_3+H]^+$ 316.37. HRMS $[ESI^+]$ m/z = 315.15958 $[M]^+$, calcd. for $[C_{17}H_{21}N_3O_3]^+$ 315.15829.

4.3.10. 3-(Cyclopropylmethyl)-5-[2-(5-methoxy-1H-indol-3-yl)ethyl]-1,3,4-oxadiazol-2(3H)-one (**11**)

Chromatography: DCM. White solid (88% yield) of mp 94–97 °C. ^{1}H NMR (500 MHz, $CDCl_3$) δ 7.89 (s, 1H, NH), 7.26 (d, J = 8.8 Hz, 1H, H_7), 7.02 (d, J = 2.4 Hz, 1H, H_2), 7.00 (d, J = 2.7 Hz, 1H, H_4), 6.87 (dd, J = 8.8, 2.4 Hz, 1H, H_6), 3.87 (s, 3H, CH_3), 3.52 (d, J = 7.2 Hz, 2H, NCH_2), 3.13 (q, J = 7.0 Hz, 2H, H_α), 2.96–2.90 (m, 2H, H_β), 1.19–1.09 (m, 1H, $CH(CH_2)_2$), 0.57–0.51 (m, 2H, $CH(CH_2)_2$), 0.34 (dt, J = 6.2, 4.8 Hz, 2H, $CH(CH_2)_2$). ^{13}C NMR (126 MHz, $CDCl_3$) δ 155.9 ($C_{2'}$), 155.8 ($C_{5'}$), 154.3 (C_5), 131.5 (C_{7a}), 127.5 (C_{3a}), 122.5 (C_2), 113.8 (C_3), 112.7 (C_6), 112.1 (C_7), 100.3 (C_4), 56.1 (CH_3), 50.5 (NCH_2), 27.5 (C_β), 21.6 (C_α), 10.0 ($CH(CH_2)_2$), 3.6 ($CH(CH_2)_2$). HPLC-MS (15:95- g.t.5 min) ^{t}R 4.57 min, m/z = 314.03 $[M+H]^+$, calcd. for $[C_{17}H_{19}N_3O_3+H]^+$ 314.36. HRMS $[ESI^+]$ m/z = 313.14324 $[M]^+$, calcd. for $[C_{17}H_{19}N_3O_3]^+$ 313.14264.

4.3.11. 3-(Cyclobutylmethyl)-5-[2-(5-methoxy-1H-indol-3-yl)ethyl]-1,3,4-oxadiazol-2(3H)-one (**12**)

Chromatography: hexane to DCM. Pale yellow solid (75% yield) of mp 74–76 °C. ^{1}H NMR (500 MHz, $CDCl_3$) δ 7.88 (bs, 1H, NH), 7.25 (d, J = 8.0 Hz, 1H, H_7), 7.00 (d, J = 2.4 Hz, 1H, H_2), 6.99 (d, J = 2.5 Hz, 1H, H_4), 6.87 (dd, J = 8.8, 2.4 Hz, 1H, H_6), 3.87 (s, 3H, CH_3), 3.66 (d, J = 7.3 Hz, 2H, NCH_2), 3.12 (dd, J = 8.6, 6.7 Hz, 2H, H_α), 2.91 (dd, J = 8.4, 6.9 Hz, 2H, H_β), 2.68 (p, J = 7.7 Hz, 1H, $CH(CH_2)_2$), 2.06–1.96 (m, 2H, $CH(CH_2)_2$), 1.93–1.83 (m, 2H, $CH_2(CH_2)_2$), 1.81–1.69 (m, 2H, $CH(CH_2)_2$). ^{13}C NMR (126 MHz, $CDCl_3$) δ 155.7 ($C_{5'}$), 154.5 ($C_{2'}$), 154.3 (C_5), 131.5 (C_{7a}), 127.5 (C_{3a}), 122.5 (C_2), 100.3 (C_4), 56.1 (CH_3), 50.6 (NCH_2), 34.3 ($CH(CH_2)_2$), 27.6 (C_β), 25.7 ($CH(CH_2)_2$), 21.5 (C_α), 18.3 ($CH_2(CH_2)_2$). HPLC-MS (50:95- g.t.5 min) ^{t}R 2.35 min, m/z = 328.37 $[M+H]^+$, calcd. for $[C_{18}H_{21}N_3O_3+H]^+$ 328.38. HRMS $[ESI^+]$ m/z = 327.15892 $[M]^+$, calcd. for $[C_{18}H_{21}N_3O_3]^+$ 327.15829.

4.3.12. 3-(Cyclopentylmethyl)-5-[2-(5-methoxy-1H-indol-3-yl)ethyl]-1,3,4-oxadiazol-2(3H)-one (**13**)

Chromatography: hexane to DCM. White solid (72% yield) of mp 81–84 °C. ^{1}H NMR (500 MHz, $CDCl_3$) δ 7.88 (bs, 1H, NH), 7.25 (d, J = 8.8 Hz, 1H, H_7), 7.01 (d, J = 2.5 Hz, 1H, H_2), 6.99 (d, J = 2.4 Hz, 1H, H_4), 6.86 (dd, J = 8.8, 2.4 Hz, 1H, H_6), 3.87 (s, 3H, CH_3), 3.56 (d, J = 7.4 Hz, 2H, NCH_2), 3.13 (t, J = 7.6 Hz, 2H, H_α), 2.92 (t, J = 7.6 Hz, 2H, H_β), 2.29 (p, J = 7.6 Hz, 1H, $CH(CH_2)_2$), 1.70–1.59 (m, 4H, $CH(CH_2)_2$, H_d, H_c), 1.58–1.50 (m, 2H, $CH(CH_2)_2(CH_2)_2$), 1.27–1.16 (m, 2H, $CH(CH_2)_2$). ^{13}C NMR (126 MHz, $CDCl_3$) δ 155.7 ($C_{5'}$), 154.5 ($C_{2'}$), 154.3 (C_5), 131.5 (C_{7a}), 127.5 (C_{3a}), 122.5 (C_2), 113.7 (C_3), 112.7 (C_6), 112.1 (C_7), 100.3 (C_4), 56.1 (CH_3), 50.5 (NCH_2), 39.0 ($CH(CH_2)_2$), 30.1 ($CH(CH_2)_2$), 27.6 (C_β), 25.2 ($CH(CH_2)_2(CH_2)_2$), 21.6 (C_α). HPLC-MS (50:95- g.t.5 min) ^{t}R 3.14 min, m/z = 342.20 $[M+H]^+$, calcd. for $[C_{19}H_{23}N_3O_3+H]^+$ 342.41. HRMS $[ESI^+]$ m/z = 341.17482 $[M]^+$, calcd. for $[C_{19}H_{23}N_3O_3]^+$ 341.17394.

4.3.13. 3-Benzyl-5-[2-(5-methoxy-1H-indol-3-yl)ethyl]-1,3,4-oxadiazol-2(3H)-one (**14**)

Chromatography: DCM. White solid (57% yield) of mp 118–121 °C. ^{1}H NMR (500 MHz, $CDCl_3$) δ 7.85 (s, 1H, NH), 7.38–7.33 (m, 2H, Ph_o), 7.32–7.30 (m, 1H, Ph_p), 7.30–7.21 (m, 3H, Ph_m, H_7), 6.98 (d, J = 2.4 Hz, 1H, H_4), 6.94 (s, 1H, H_2), 6.87 (dd, J = 8.7, 2.4 Hz, 1H, H_6), 4.81 (s, 2H, NCH_2), 3.86 (s, 3H, CH_3), 3.11 (t, J = 7.6 Hz, 2H,

H_α), 2.90 (t, J = 7.6 Hz, 2H, H_β). ^{13}C NMR (126 MHz, $CDCl_3$) δ 156.1 ($C_{5'}$), 154.3 (C_5), 154.2 ($C_{2'}$), 135.1 (Ph_i), 131.4 (C_{7a}), 129.0 (Ph_o), 128.4 (Ph_p), 128.3 (Ph_m), 127.4 (C_{3a}), 122.5 (C_2), 113.6 (C_3), 112.7 (C_6), 112.1 (C_7), 100.2 (C_4), 56.0 (CH_3), 49.5 (NCH_2), 27.6 (C_β), 21.5 (C_α). HPLC-MS (30:95- g.t.5 min) ^{t}R 4.23 min, m/z = 350.26 $[M+H]^+$, calcd. for $[C_{20}H_{19}N_3O_3+H]^+$ 350.14. HRMS [ESI$^+$] m/z = 349.14257$[M]^+$, calcd. for $[C_{20}H_{19}N_3O_3]^+$ 349.14264.

4.3.14. 5-[2-(5-Methoxy-1H-indol-3-yl)ethyl]-3-(3-phenylpropyl)-1,3,4-oxadiazol-2(3H)-one (**15**)

Chromatography: hexane to hexane:DCM 8:2. Pale yellow oil (92% yield). ^{1}H NMR (500 MHz, $CDCl_3$) δ 7.85 (s, 1H, NH), 7.32–7.09 (m, 6H, H_7, Ph), 6.98 (bs, 2H, H_2, H_4), 6.85 (dd, J = 8.8, 2.5 Hz, 1H, H_6), 3.86 (s, 3H, CH_3), 3.68 (t, J = 7.0 Hz, 2H, NCH_2), 3.12 (dd, J = 8.6, 6.4 Hz, 2H, H_α), 2.91 (dd, J = 8.3, 6.4 Hz, 2H, H_β), 2.58 (t, J = 7.6 Hz, 2H, CH_2Ph), 2.00 (p, J = 7.2 Hz, 2H, $NCH_2\underline{CH_2}$). ^{13}C NMR (125 MHz, $CDCl_3$) δ 155.9 ($C_{5'}$), 154.3 (C_5), 154.2 ($C_{2'}$), 140.9 (Ph_i), 131.5 (C_{7a}), 128.6 (Ph), 128.5 (Ph), 126.3 (Ph_p), 122.5 (C_2), 113.7 (C_3), 112.7 (C_6), 112.1 (C_7), 100.3 (C_4), 56.1 (CH_3), 45.2 (NCH_2), 32.7 (CH_2Ph), 29.7 ($NCH_2\underline{C}H_2$), 27.6 (C_β), 21.5 (C_α). HPLC-MS (50:95- g.t.5 min) ^{t}R 3.42 min, m/z = 378.31$[M+H]^+$, calcd. for $[C_{22}H_{23}N_3O_3+H]^+$ 378.44. HRMS [ESI$^+$] m/z = 377.1737$[M]^+$, calcd. for $[C_{22}H_{23}N_3O_3]^+$ 377.17394.

4.3.15. 5-[2-(5-Methoxy-1H-indol-3-yl)ethyl]-N-methyl-1,3,4-oxadiazol-2-amine (**16**)

To a solution of **1** (150 mg, 0.58 mmol) in 5.8 mL of anhydrous DMF, TEA (162 μL, 1.16 mmol), BOP (282 mg, 0.64 mmol) and methyl amine (580 μL of a 2M solution in THF) were slowly added. The mixture was stirred at rt overnight and the solvent was removed under reduced pressure. The crude was extracted with EtOAc (3x10 mL) and washed with H_2O (10 mL) and brine (10 mL). The organic layer was dried over $MgSO_4$ and the solvent was evaporated. The residue was purified by flash chromatography (DCM to DCM:MeOH 9:1) and washed with hexane to afford derivative **16** (29 mg, 18% yield) as a white solid of mp 145–148 °C. ^{1}H NMR (500 MHz, DMSO-d_6) δ 10.65 (bs, 1H, NH_{indole}), 7.24 (t, J = 4.9 Hz, 1H, $N\underline{H}CH_3$), 7.21 (d, J = 8.9 Hz, 1H, H_7), 7.08 (d, J = 2.5 Hz, 1H, H_2), 6.93 (d, J = 2.5 Hz, 1H, H_4), 6.70 (dd, J = 8.7, 2.4 Hz, 1H, H_6), 3.75 (s, 3H, OCH_3), 2.99 (m, 4H, H_α, H_β), 2.75 (d, J = 4.9 Hz, 3H, $NHC\underline{H_3}$). ^{13}C NMR (126 MHz, DMSO-d_6) δ 164.0 ($C_{2'}$), 159.5 ($C_{5'}$), 153.0 (C_5), 131.3 (C_{7a}), 127.1 (C_{3a}), 123.2 (C_2), 112.4 (C_3), 112.0 (C_7), 111.2 (C_6), 99.8 (C_4), 55.3 (OCH_3), 29.0 ($NHCH_3$), 25.8 (C_β), 22.0 (C_α). HPLC-MS (15:95-g.t.5 min) ^{t}R 3.17 min, m/z = 273.34 $[M+H]^+$, calcd. for $[C_{14}H_{16}N_4O_2+H]^+$ 273.31. HRMS [ESI$^+$] m/z = 272.12816 $[M]^+$, calcd. for $[C_{14}H_{16}N_4O_2]^+$ 272.12733.

4.3.16. N-Ethyl-5-[2-(5-methoxy-1H-indol-3-yl)ethyl]-1,3,4-oxadiazol-2-amine (**17**)

Ethyl derivative **17** was synthesized from **1** following the same procedure as for **16**, but using ethyl amine. In this case, a column chromatography (DCM to DCM:MeOH 9:1) and a semi-preparative HPLC separation (20:80 g t. 60 min, isocratic gradient) were necessary to purified **17** (6 mg, 6% yield). ^{1}H NMR (500 MHz, DMSO-d_6) δ 10.65 (bs, 1H, NH_{indole}), 7.32 (t, J = 5.6 Hz, 1H, $N\underline{H}CH_2$), 7.21 (dd, J = 8.7, 0.5 Hz, 1H, H_7), 7.09 (d, J = 2.3 Hz, 1H, H_2), 6.94 (d, J = 2.4 Hz, 1H, H_4), 6.70 (dd, J = 8.7, 2.4 Hz, 1H, H_6), 3.75 (s, 3H, OCH_3), 3.15 (qd, J = 7.2, 5.6 Hz, 2H, $C\underline{H_2}CH_3$), 3.04–2.95 (m, 4H, 4H, H_α, H_β), 1.11 (t, J = 7.2 Hz, 3H, $CH_2C\underline{H_3}$). ^{13}C NMR (126 MHz, DMSO-d_6) δ 163.3 ($C_{2'}$), 159.3 ($C_{5'}$), 153.0 (C_5), 131.3 (C_{7a}), 127.2 (C_{3a}), 123.2 (C_2), 112.4 (C_3), 112.0 (C_7), 111.2 (C_6), 99.8 (C_4), 55.3 (OCH_3), 37.3 ($\underline{C}H_2CH_3$), 25.8 (C_β), 22.0 (C_α), 14.5 ($CH_2\underline{C}H_3$). HPLC-MS (15:95-g.t.5 min) ^{t}R 3.53 min, m/z = 287.11 $[M+H]^+$, calcd. for $[C_{19}H_{25}N_3O_3+H]^+$ 287.34. HRMS [ESI$^+$] m/z = 286.14359 $[M]^+$, calcd. for $[C_{15}H_{18}N_4O_2]^+$ 286.14298.

4.3.17. 5-[1-(5-Methoxy-1H-indol-3-yl)propan-2-yl]-1,3,4-oxadiazol-2(3H)-one (**21**)

Entitled compound was prepared in a multi-step synthesis starting from a mixture of 5-methoxy-1*H*-indole-3-carbaldehyde (**18**, 1.0 g, 5.7 mmol) and (carbethoxyethylidene) triphenylphosphorane (1.3 equiv) in DCM (50 mL) that was refluxed overnight. Solvent was evaporated under reduced pressure to give intermediate **19** [68] as a white solid of mp 116–117 °C (1.4 g, 95% yield) after a column chromatography (pure hexane to hexane: EtOAc 1:1). Then, the α,β-unsaturated ester **19** (500 mg, 1.93 mmol) in EtOH (20 mL) was treated with a catalytic amount of Pd–C (5%) under N_2 atmosphere. N_2 was displaced by H_2 and the flask was sealed up with a septum. A balloon with H_2 was connected with a needle to stir at rt overnight. Then, Pd–C was removed by filtration and the solvent was evaporated to dryness under reduced pressure, obtaining **20** [69] as a white solid (500 mg, > 99% yield), which was used without further purification. A mixture of ester **20** (360 mg, 1.38 mmol) and hydrazine hydrate in EtOH (15 mL) was heated to 150 °C for 45 min under MW irradiation. After the solvent was evaporated, DCM (10 mL) was added to the crude and the organic layer was washed with saturated aq. solution of $NaHCO_3$ (3x10 mL), brine (10 mL) and dried over $MgSO_4$. Solvent was filtered and evaporated under reduced pressure to obtain the corresponding hydrazide, which was not isolated but identified by its HPLC-MS data (15:95- g.t.5), ^{t}R 2.97 min, m/z = 248.17 $[M+H]^+$, calcd. for $[C_{13}H_{17}N_3O_2+H]^+$ 248.30. Intermediate hydrazide was reacted with CDI (1.2 equiv) in anhydrous DMF (10 mL/mmol) under MW-irradiation at 120 °C for 25 min. Solvent was removed and the residue was dissolved in EtOAc, washed with H_2O (3x10 mL) and brine (10 mL), dried over $MgSO_4$, filtered and evaporated to dryness under reduced pressure. Purification was made by column chromatography (hexane to hexane:EtOAc 1:1) obtaining **21** (180 mg, 48% yield) as a white solid of mp 90–93 °C. ^{1}H NMR (400 MHz, $CDCl_3$) δ 8.40 (bs, 1H, NHCO), 7.91 (bs, 1H, NH_{indole}), 7.25 (d, J = 9.0 Hz, 1H, H_7), 6.98 (d, J = 2.4 Hz, 1H, H_2), 6.97 (d, J = 2.4 Hz, 1H, H_4), 6.86 (dd, J = 8.8, 2.4 Hz, 1H, H_6), 3.87 (s, 3H, OCH_3), 3.19 (dd, J = 13.7, 6.7 Hz, 1H, H_α), 3.11 (h, J = 6.8 Hz, 1H, H_β), 2.94 (dd, J = 13.8, 7.0 Hz, 1H, H_α), 1.32 (d, J = 6.8 Hz, 3H, $CH_\beta C\underline{H_3}$). ^{13}C NMR (101 MHz, $CDCl_3$) δ 161.4 ($C_{5'}$), 155.0 ($C_{2'}$), 154.3 (C_5), 131.4 (C_{7a}), 127.8 (C_{3a}), 123.4 (C_2), 112.6 (C_6), 112.3 (C_3), 112.1 (C_7), 100.4 (C_4), 56.1 (OCH_3), 33.7 (C_β), 29.4 (C_α), 16.9 ($CH_\beta\underline{C}H_3$). HPLC-MS (40:95- g.t.10 min) ^{t}R 1.25 min, m/z = 274.22 $[M+H]^+$, calcd. for $[C_{14}H_{15}N_3O_3+H]^+$ 274.29. HRMS [ESI$^+$] m/z = 273.11073 $[M]^+$, calcd. for $[C_{14}H_{15}N_3O_3]^+$ 273.11134.

4.3.18. 5-[(E)-2-(5-Methoxy-1H-indol-3-yl)ethenyl]-1,3,4-oxadiazol-2(3H)-one (**23**)

Derivative **23** was prepared in a multi-step synthesis as explained below. To a solution of the commercial aldehyde **18** (500 mg, 2.8 mmol) in pyridine (20 mL), malonic acid (2 equiv) and piperidine (13 μL/mmol) were added and the mixture was stirred at 70 °C overnight under N_2 atmosphere. Solvent was evaporated under reduced pressure and EtOAc was added. The organic layer was washed with H_2O (3x10 mL) and 10% citric acid solution (10 mL), dried over $MgSO_4$, filtered, and evaporated to dryness, to give **22** (97% yield) as a white solid of mp 208–211 °C (bibl [70]. 197–200 °C). Then, to a suspension of the α,β-unsaturated acid **22** (500 mg, 2.30 mmol) and activated 4 Å molecular sieves in anhydrous ACN (40 mL) at rt under N_2 atmosphere, HOBt (1.2 equiv), EDC·HCl (1.2 equiv) and DMAP (0.12 equiv) were orderly added. The mixture was stirred for 3 h until the complete acid activation and then, $N_2H_4 \cdot H_2O$ (excess) was added. Once finished the reaction, H_2O was added, extracted with DCM and washed with saturated $NaHCO_3$ (aq). The organic layer was separated and evaporated under reduced pressure to obtain the corresponding *N*-

acylhydrazine, which was not isolated but identified by HPLC-MS (15:95- g.t.5), ^{t}R 1.99 min, *m/z* = 232.39 $[M+H]^+$, calcd. for $[C_{12}H_{13}N_3O_2+H]^+$ 232.26. Intermediate hydrazide (525 mg, 2.28 mmol) was reacted with CDI (1.2 equiv) in anhydrous DMF (20 mL) under MW-irradiation at 120 °C for 25 min. Solvent was removed and the residue was dissolved in EtOAc (10 mL), washed with H_2O (3x10 mL) and brine (10 mL), dried over $MgSO_4$, filtered and evaporated to dryness under reduced pressure. Purification was made by column chromatography (hexane to hexane:EtOAc 1:1) obtaining **23** (502 mg, 1.95 mmol, 85% yield) as a white solid of mp 206–209 °C. ^{1}H NMR (500 MHz, DMSO-*d*$_6$) δ 11.53 (bs, 1H, NH_{indole}), 7.85 (d, *J* = 2.8 Hz, 1H, H_2), 7.49 (d, *J* = 16.4 Hz, 1H, H_α), 7.34 (d, *J* = 2.7 Hz, 1H, H_4), 7.34 (d, *J* = 8.5 Hz, 1H, H_7), 6.82 (dd, *J* = 8.8, 2.3 Hz, 1H, H_6), 6.59 (d, *J* = 16.4 Hz, 1H, H_β), 3.82 (s, 3H, CH_3). ^{13}C NMR (126 MHz, DMSO-*d*$_6$) δ 155.4 ($C_{5'}$), 154.6 (C_5), 154.4 ($C_{2'}$), 132.0 (C_{7a}), 131.1 (C_α), 129.7 (C_2), 125.5 (C_{3a}), 112.9 (C_7), 112.3 (C_6), 111.9 (C_3), 103.9 (C_β), 101.5 (C_4) 55.5 (CH_3). HPLC-MS (15:95-g.t.10 min) ^{t}R 6.04 min, *m/z* = 258.32 $[M+H]^+$, calcd. for $[C_{13}H_{11}N_3O_3+H]^+$ 258.25. HRMS [ESI$^+$] *m/z* = 257.08107 $[M]^+$, calcd. for $[C_{13}H_{11}N_3O_3]^+$ 257.08004.

4.3.19. 5-[(E)-2-(5-Methoxy-1H-indol-3-yl)ethenyl]-3-(prop-2-yn-1-yl)-1,3,4-oxadiazol-2(3H)-one (**24**)

Alkylation of **23** (60 mg, 0.23 mmol) with propargyl bromide (1.2 equiv) in the presence of K_2CO_3 (1.2 equiv) under MW-irradiation at 120 °C for 10 min, using acetone (7 mL/mmol) as solvent, gave **24** (12 mg, 17% yield) as a white solid of mp 201–203 °C. Purification by semipreparative HPLC (gradient 35:40-g.t.30 min). ^{1}H NMR (400 MHz, DMSO-*d*$_6$) δ 11.59 (s, 1H, NH), 7.88 (d, *J* = 2.5 Hz, 1H, H_2), 7.56 (d, *J* = 16.4 Hz, 1H, H_α), 7.37 (d, *J* = 2.4 Hz, 1H, H_4), 7.35 (d, *J* = 8.8 Hz, 1H, H_7), 6.83 (dd, *J* = 8.7, 2.4 Hz, 1H, H_6), 6.63 (d, *J* = 16.4 Hz, 1H, H_β), 4.58 (d, *J* = 2.6 Hz, 2H, CH_2), 3.83 (s, 3H, CH_3), 3.45 (t, *J* = 2.5 Hz, 1H, ≡CH). ^{13}C NMR (101 MHz, DMSO-*d*$_6$) δ 154.7 (C_5), 154.3 ($C_{5'}$), 152.1 ($C_{2'}$), 132.3 (C_α), 132.1 (C_{7a}), 130.4 (C_2), 125.4 (C_{3a}), 113.0 (C_7), 112.5 (C_6), 111.9 (C_3), 102.9 (C_β), 101.6 (C_4), 77.3 (≡C), 76.0 (≡CH), 55.5 (CH_3), 35.2 (CH_2). HPLC-MS (15:95-g.t.10 min) ^{t}R 7.63 min, *m/z* = 296.25 $[M+H]^+$, calcd. for $[C_{16}H_{13}N_3O_3+H]^+$ 296.30. HRMS [ESI$^+$] *m/z* = 270.10827 $[M]^+$, calcd. for $[C_{16}H_{13}N_3O_3]^+$ 270.10044.

4.3.20. (2E)-3-(5-Methoxy-1H-indol-3-yl)-N-(prop-2-yn-1-yl) prop-2-enamide (**25**)

Under N_2 atmosphere, to a solution of the acid **22** (100 mg, 0.46 mmol) in anhydrous ACN (15 mL/mmol) in the presence of activated 4 Å molecular sieves, HOBt (1.2 equiv), EDC·HCl (1.2 equiv) and DMAP (0.12 equiv) were orderly added at rt. The mixture was stirred for 3 h and then, propargylamine (1.2 equiv) was added. Afterward, H_2O was added, extracted with DCM (3x10 mL) and washed with saturated $NaHCO_3$ aq (10 mL). The organic layer was separated, dried with $MgSO_4$ and solvent evaporated under reduced pressure. Residue was purified by column chromatography (hexane to hexane:EtOAc 1:1), obtaining **25** as an oil (60 mg, 0.23 mmol, 51% yield). ^{1}H NMR (500 MHz, DMSO-*d*$_6$) δ 11.44 (s, 1H, NH_{indole}), 8.29 (t, *J* = 5.5 Hz, 1H, NH_{amide}), 7.72 (d, *J* = 2.9 Hz, 1H, H_2), 7.62 (d, *J* = 15.8 Hz, 1H, H_α), 7.34 (d, *J* = 8.8 Hz, 1H, H_7), 7.34 (d, *J* = 1.9 Hz, 1H, H_4), 6.85 (dd, *J* = 8.7, 2.5 Hz, 1H, H_6), 6.53 (d, *J* = 15.8 Hz, 1H, H_β), 4.01 (dd, *J* = 5.5, 2.5 Hz, 2H, CH_2), 3.84 (s, 3H, CH_3), 3.16 (t, *J* = 2.6 Hz, 1H, ≡CH). ^{13}C NMR (126 MHz, DMSO-*d*$_6$) δ 166.1 (CO), 154.5 (C_5), 133.9 (C_α), 132.3 (C_{7a}), 131.0 (C_2), 125.3 (C_{3a}), 114.7 (C_β), 112.8 (C_7), 111.8 (C_6), 109.5 (C_3), 102.5 (C_4), 81.5 (≡C), 73.1 (≡CH), 55.5 (CH_3), 27.8 (CH_2). HPLC-MS (15:95- g.t.10 min) ^{t}R 5.80 min, *m/z* = 255.07 $[M+H]^+$, calcd. for $[C_{15}H_{14}N_2O_2+H]^+$ 255.29. HRMS [ESI$^+$] *m/z* = 254.10667 $[M]^+$, calcd. for $[C_{15}H_{14}N_2O_2]^+$ 254.10553.

4.3.21. (2E)-3-(5-Methoxy-1H-indol-3-yl)-N-(prop-2-en-1-yl) prop-2-enamide (**26**)

Similarly, to the synthesis of **25** but using allylamine, derivative **26** was obtained (72% yield) as a pale yellow solid of mp 124–126 °C. Chromatography: hexane to hexane:EtOAc 3:7. ^{1}H NMR (500 MHz, $CDCl_3$) δ 8.77 (s, 1H, NH_{indole}), 7.87 (d, *J* = 15.5 Hz, 1H, H_α), 7.40 (d, *J* = 2.8 Hz, 1H, H_2), 7.30 (d, *J* = 2.6 Hz, 1H, H_4), 7.30 (d, *J* = 8.7 Hz, 1H, H_7), 6.90 (dd, *J* = 8.9, 2.3 Hz, 1H, H_6), 6.35 (d, *J* = 15.6 Hz, 1H, H_β), 5.92 (ddt, *J* = 17.1, 10.1, 5.6 Hz, 1H, CH =), 5.72 (t, *J* = 6.4 Hz, 1H, CONH), 5.25 (dd, *J* = 17.2, 1.5 Hz, 1H, CH_{2trans} =), 5.17 (dd, *J* = 10.3, 1.5 Hz, 1H, CH_{2cis} =), 4.05 (tt, *J* = 5.8, 1.6 Hz, 2H, CH_2), 3.87 (s, 3H, CH_3). ^{13}C NMR (126 MHz, $CDCl_3$) δ 167.3 (CO), 155.3 (C_5), 135.1 (C_α), 134.6 (CH =), 132.2 (C_{7a}), 128.7 (C_2), 126.2 (C_{3a}), 116.6 (=CH_2), 115.2 (C_β), 113.3 (C_3), 112.9 (C_6), 112.6 (C_7), 102.8 (C_4), 56.2 (CH_3), 42.3 (CH_2). HPLC-MS (15:95- g.t.10 min) ^{t}R 6.12 min, *m/z* = 257.23 $[M+H]^+$, calcd. for $[C_{15}H_{16}N_2O_2+H]^+$ 257.31. HRMS [ESI$^+$] *m/z* = 256.12237 $[M]^+$, calcd. for $[C_{15}H_{16}N_2O_2]^+$ 256.12118.

4.3.22. 6-Methoxy-4-methyl-1,2-dihydronaphthalene (**28**)

To a solution of 7-methoxy-1-tetralone (200 mg, 1.13 mmol) in 5 mL of Et_2O, CH_3MgI (1.3 equiv) was added dropwise at rt. The mixture was stirred for 3 h, washed with a saturated solution of NH_4Cl and extracted with Et_2O (3x10 mL), obtaining the intermediate alcohol. Then, a 2 M HCl solution was added dropwise until pH 5 and the mixture was heated at 40 °C for 3 h. The layers were separated, and the organic layer was washed with a solution of $Na_2S_2O_3$, and brine; dried over $MgSO_4$, filtrated and the solvent was removed under reduced pressure. The crude was purified by flash chromatography in hexane, obtaining **28** [34] (191 mg, 1.10 mmol, 97% yield) as a colorless oil.

4.3.23. Oxidation reaction of **28** with selenium oxide

To compound **28** (238 mg, 1.37 mmol) in EtOH (5 mL), a solution of SeO_2 (5 equiv) in EtOH:H_2O (15 mL, 10:1) was added dropwise (35 min addition). The mixture was heated at reflux overnight and then, it was extracted with EtOAc (3x10 mL) and washed with a saturated solution of $NaHCO_3$ (10 mL) and brine (10 mL). The organic layer was dried over $MgSO_4$, filtered and concentrated under reduced pressure. The crude was purified by column chromatography (hexane to hexane:EtOAc 6:4) to afford 7-methoxynaphthalene-1-carbaldehyde (**30**) [35] as a colorless oil (8 mg, 20% yield) and 7-methoxy-3,4-dihydronaphthalene-1-carbaldehyde (**29**) (64 mg, 25% yield) as a brown oil. ^{1}H NMR (400 MHz, $CDCl_3$) δ 9.68 (s, 1H, COH), 7.87 (d, *J* = 2.7 Hz, 1H, H_8), 7.10 (d, *J* = 8.5 Hz, 1H, H_5), 7.04 (t, *J* = 4.7 Hz, 1H, H_2), 6.80 (dd, *J* = 8.3, 2.7 Hz, 1H, H_6), 3.83 (s, 3H, CH_3), 2.76 (t, *J* = 7.9 Hz, 2H, H_4), 2.61–2.54 (m, 2H, H_3). ^{13}C NMR (101 MHz, $CDCl_3$) δ 192.7 (CO), 158.4 (C_7), 153.7 (C_2), 138.0 (C_1), 130.3 (C_{8a}), 128.4 (C_5), 127.8 (C_{4a}), 114.2 (C_6), 111.4 (C_8), 55.5 (CH_3), 26.3 (C_4), 24.8 (C_3). HPLC-MS (50:95- g.t.10 min) ^{t}R 2.46 min, *m/z* = 189.39 $[M+H]^+$, calcd. for $[C_{12}H_{12}O_2+H]^+$ 189.23.

4.3.24. 9-Methoxy-2,4a,5,6-tetrahydro-3H-naphtho[2,1-b]pyran-3-one (**32**)

To a solution of aldehyde **29** (280 mg, 1.49 mmol) in pyridine (7 mL/mmol), malonic acid (2 equiv) and piperidine (13 μL/mmol) were added and the mixture was stirred at 70 °C overnight under N_2 atmosphere. Solvent was evaporated under reduced pressure and EtOAc (10 mL) was added. The organic layer was washed with H_2O (10 mL), 10% citric acid solution (10 mL), dried over $MgSO_4$, filtered, and evaporated to dryness, obtaining lactone **32** as a white solid of mp 96–98 °C (23% yield). ^{1}H NMR (500 MHz, $CDCl_3$) δ 7.10 (d, *J* = 2.7 Hz, 1H, H_{10}), 7.07 (d, *J* = 8.4 Hz, 1H, H_7), 6.81 (dd, *J* = 8.4, 2.6 Hz, 1H, H_8), 6.37 (dt, *J* = 5.6, 2.7 Hz, 1H, H_1), 5.15 (dtd, *J* = 13.7, 4.4, 1.6 Hz, 1H, H_{4a}), 3.82 (s, 3H, CH_3), 3.36 (ddd, *J* = 20.6, 5.9, 1.5 Hz,

1H, H_2), 3.21 (ddd, J = 20.7, 4.4, 2.8 Hz, 1H, H_2), 2.91–2.75 (m, 2H, H_6), 2.42 (dq, J = 12.4, 4.3 Hz, 1H, H_5), 1.99 (tddd, J = 12.2, 11.4, 5.0, 0.6 Hz, 1H, H_5). ^{13}C NMR (126 MHz, $CDCl_3$) δ 170.2 (C_3), 158.5 (C_9), 134.5 (C_{1b}), 131.8 (C_{10a}), 130.0 (C_7), 128.7 (C_{6a}), 114.8 (C_8), 114.7 (C_1), 108.0 (C_{10}), 77.7 (C_{4a}), 55.5 (CH_3), 31.8 (C_2), 29.6 (C_5), 26.9 (C_6). HPLC-MS (50:95- g.t.10 min) ^{t}R 1.75 min, m/z = 231.17 $[M+H]^+$, calcd. for $[C_{14}H_{14}O_3+H]^+$ 231.26.

*4.3.25. 5-[(E)-2-(7-Methoxy-3,4-dihydronaphthalen-1-yl)ethenyl]-1,3,4-oxadiazol-2(3H)-one (**33**)*

Lactone **32** (70 mg, 0.30 mmol) was treated with HOBt (1.2 equiv), EDC·HCl (1.2 equiv) and DMAP (0.12 equiv) in anhydrous ACN (15 mL) in the presence of activated 4 Å molecular sieves at rt for 3 h. Then, $N_2H_4{\cdot}H_2O$ (excess) was added to give the corresponding hydrazide, which was not isolated but identified by HPLC-MS. Intermediate hydrazide was treated with CDI (1.2 equiv) in anhydrous DMF (10 mL) under MW-irradiation at 120 °C for 25 min. Solvent was removed and the residue was dissolved in EtOAc, washed with H_2O and brine, dried over $MgSO_4$, filtered and evaporated to dryness under reduced pressure. Purification was made by column chromatography (hexane to hexane:EtOAc 3:7) obtaining **33** (15% yield) as a white solid of mp 133–136 °C. ^{1}H NMR (400 MHz, MeOD) δ 7.11 (d, J = 8.4 Hz, 1H, H_5), 7.09 (dd, J = 16.2, 1.2 Hz, 1H, H_α), 6.91 (d, J = 2.6 Hz, 1H, H_8), 6.75 (dd, J = 8.2, 2.6 Hz, 1H, H_6), 6.50 (d, J = 16.2 Hz, 1H, H_β), 6.45 (t, J = 4.8 Hz, 1H, H_2), 3.78 (s, 3H, CH_3), 2.66 (t, J = 7.7 Hz, 2H, H_4), 2.35–2.27 (m, 2H, H_3). ^{13}C NMR (126 MHz, $CDCl_3$) δ 158.5 (C_7), 155.6 ($C_{5'}$), 153.9 ($C_{2'}$), 137.5 (C_α), 134.7 (C_1), 133.7 (C_{8a}), 133.1 (C_2), 128.9 (C_{4a}), 128.8 (C_5), 112.4 (C_6), 111.3 (C_β), 110.7 (C_8), 55.6 (CH_3), 27.1 (C_4), 24.1 (C_3). HPLC-MS (50:95- g.t.10 min) ^{t}R 4.72 min, m/z = 271.10 $[M+H]^+$, calcd. for $[C_{15}H_{14}N_2O_3+H]^+$ 271.29. HRMS [ESI$^+$] m/z = 270.10827 $[M]^+$, calcd. for $[C_{15}H_{14}N_2O_3]^+$ 270.10044.

*4.3.26. Ethyl (2E)-3-(7-Methoxy-3,4-dihydronaphthalen-1-yl) prop-2-enoate (**35**)*

Under inert atmosphere, Tf_2O (0.6 mL, 3.31 mmol) and 2-chloropyridine (0.3 mL, 3.31 mmol) were added to a solution of commercial 7-methoxy-1-tetralone (507 mg, 2.88 mmol) in 7 mL of dry DCM at rt. After 2 h the reaction was finished and the solvent was evaporated to dryness. The crude was purified by flash chromatography on hexane, obtaining the triflate **34** [36] as colorless oil (697 mg, 78% yield). Intermediate **34** (120 mg, 0.39 mmol) was solved in 1 mL of anhydrous DMF under N_2 atmosphere and a solution of ethyl acrylate (93 μL, 0.86 mmol, 2.2 equiv), TEA (189 μL, 1.36 mmol, 3.5 equiv) and $Pd(PPh_3)_2Cl_2$ (6 mg, 2.2 mol %) in 0.5 mL of DMF was added. Reaction was heated under MW irradiation at 105 °C for 15 min. DMF was evaporated to dryness and the residue was extracted with ether (3x10 mL). Organic layer was washed with H_2O (3x10 mL), dried over $MgSO_4$ and filtered. Crude was purified by preparative TLC in hexane:EtOAc 8:2 to afford unsaturated ester **35** as a white solid of mp: 72–74 °C (46 mg, 50% yield). ^{1}H NMR (400 MHz, MeOD) δ 7.60 (d, J = 16.0 Hz, 1H, H_α), 7.12 (d, J = 8.3 Hz, 1H, H_5), 6.87 (d, J = 2.6 Hz, 1H, H_8), 6.77 (dd, J = 8.2, 2.7 Hz, 1H, H_6), 6.56 (t, J = 5.0 Hz, 1H, H_2), 6.26 (d, J = 15.9 Hz, 1H, H_β), 4.24 (q, J = 7.2 Hz, 2H, OCH_2), 3.78 (s, 3H, OCH_3), 2.66 (t, J = 7.8 Hz, 2H, H_4), 2.33 (td, J = 7.6, 4.7 Hz, 2H, H_3), 1.32 (t, J = 7.1 Hz, 3H, $CH_2\underline{CH_3}$). ^{13}C NMR (101 MHz, MeOD) δ 168.8 (CO), 159.9 (C_7), 144.7 (C_α), 135.7 (C_1), 135.1 (C_2), 134.8 (C_{8a}), 129.9 (C_{4a}), 129.6 (C_5), 120.0 (C_β), 113.3 (C_6), 111.4 (C_8), 61.7 (OCH_2), 55.8 (OCH_3), 27.9 (C_4), 25.0 (C_3), 14.6 ($CH_2\underline{CH_3}$). HPLC-MS (50:95- g.t.10 min) ^{t}R 5.38 min, m/z = 259.11 $[M+H]^+$, calcd. for $[C_{16}H_{18}O_3+H]^+$ 259.32.

*4.3.27. 6,7-Dimethoxy-3,4-dihydronaphthalen-1-yl trifluoromethanesulfonate (**37**)*

Tf_2O (1.1 equiv) and 2-chloropyridine (1.1 equiv) were added to a solution of commercial 6,7-dimethoxy-1-tetralone (550 mg, 2.67 mmol) in 10 mL of dry DCM at rt, under inert atmosphere. After 2 h of reaction, the solvent was evaporated and the crude was purified by flash chromatography (hexane to hexane:EtOAc 75:25), obtaining 301 mg (33% yield) of **37** as a colorless oil [71].

*4.3.28. 7-Methoxynaphthalen-1-yl trifluoromethanesulfonate (**38**)*

To a solution of **34** (165 mg, 0.53 mmol) in DCM (5 mL/mmol), a solution of 2,3-dichloro-5,6-dicyano-1,4-benzoquinone (DDQ, 1.2 equiv) in DCM (5 mL/mmol) was added. The mixture was stirred for 10 min and washed with a saturated solution of $NaHCO_3$ (3x10 mL) and brine (10 mL). Organic layer was dried over $MgSO_4$, filtrated and the solvent was removed under reduced pressure. The crude was purified by column chromatography (hexane), giving **38** as a colorless oil (142 mg, 88% yield) [72].

*4.3.29. 6,7-Dimethoxynaphthalen-1-yl trifluoromethanesulfonate (**39**)*

Similarly to the synthesis of **38** but using **37** as starting material, the 6,7-dimethoxynaphthalene derivative **39** [72] was obtained as a colorless oil (86% yield), after a column chromatography (hexane to hexane:EtOAc 9:1).

*4.3.30. Ethyl (2E)-3-(7-methoxynaphthalen-1-yl)prop-2-enoate (**40**)*

To a solution of triflate **38** (220 mg, 1.70 mmol) in anhydrous DMF (5 mL/mmol), 1,10-phenanthroline (5.5% mol), $Pd(OAc)_2$ (5.5% mol), TEA (1.2 equiv) and ethyl acrylate (5 equiv) were successively added. The reaction was heated under MW irradiation at 150 °C for 1 h. The solvent was evaporated and the product was purified by column chromatography (hexane to hexane:EtOAc 95:5), giving ester **40** [73] (390 mg, 1.52 mmol, 90% yield) as a white solid of mp 76–78 °C.

*4.3.31. Ethyl (2E)-3-(6,7-dimethoxynaphthalen-1-yl)prop-2-enoate (**41**)*

Similarly to the synthesis of **40**, but using the triflate derivative **39** as reactant, the α,β-unsaturated ester **41** was obtained in 81% yield as a white solid of mp 89–90 °C. Chromatography: hexane to hexane:EtOAc 85:15. ^{1}H NMR (400 MHz, $CDCl_3$) δ 8.44 (d, J = 15.7 Hz, 1H, H_α), 7.74 (d, J = 8.1 Hz, 1H, H_4), 7.62 (d, J = 7.4 Hz, 1H, H_2), 7.39 (s, 1H, H_8), 7.34 (t, J = 7.7 Hz, 1H, H_3), 7.14 (s, 1H, H_5), 6.52 (d, J = 15.7 Hz, 1H, H_β), 4.32 (q, J = 7.1 Hz, 2H, CH_2), 4.05 (s, 3H, CH_3OC_7), 4.01 (s, 3H, CH_3OC_6), 1.37 (t, J = 7.1 Hz, 3H, $CH_2\underline{CH_3}$). ^{13}C NMR (101 MHz, $CDCl_3$) δ 167.3 (CO), 150.4 (C_7), 149.7 (C_6), 142.1 (C_α), 130.4 (C_1), 129.9 (C_{4a}), 129.0 (C_4), 127.6 (C_{8a}), 124.1 (C_3), 123.6 (C_2), 120.5 (C_β), 107.1 (C_5), 102.4 (C_8), 60.7 (CH_2), 56.2 ($\underline{CH_3}OC_7$), 56.0 ($\underline{CH_3}OC_6$), 14.5 ($CH_2\underline{CH_3}$). HPLC-MS (50:95- g.t.10 min) ^{t}R 3.50 min, m/z = 287.27 $[M+H]^+$, calcd. for $[C_{17}H_{18}O_4+H]^+$ 287.33.

*4.3.32. (2E)-3-(7-Methoxynaphthalen-1-yl)prop-2-enoic acid (**42**)*

LiOH (1.3 equiv) was added to a solution of **40** (100 mg, 0.39 mmol) in THF:H_2O 1:1 (10 mL) and the mixture was stirred at rt overnight. The solution was adjusted to pH = 1 by addition of 1 M HCl. The product was precipitated, washed with H_2O until neutral pH, centrifuging to avoid losing product, and lyophilized to remove water traces to obtain acid **42** [73] (889 mg, 0.39 mmol, >99% yield) as a white solid of mp 212–215 °C.

*4.3.33. (2E)-3-(6,7-Dimethoxynaphthalen-1-yl)prop-2-enoic acid (**43**)*

In the same way to the synthesis of **42**, from ester **41** (150 mg, 0.52 mmol) acid **43** was obtained in quantitative yield (134 mg, 0.52 mmol), as a white solid of mp 220–222 °C. ^{1}H NMR (500 MHz, MeOD) δ 8.45 (d, J = 15.7 Hz, 1H, H_α), 7.84 (d, J = 8.1 Hz, 1H, H_4), 7.75

(d, J = 7.0 Hz, 1H, H_2), 7.53 (s, 1H, H_8), 7.38 (t, J = 7.9 Hz, 1H, H_3), 7.36 (s, 1H, H_5), 6.57 (d, J = 15.7 Hz, 1H, H_β), 4.02 (s, 3H, CH_3OC_7), 3.96 (s, 3H, CH_3OC_6). ^{13}C NMR (126 MHz, MeOD) δ 167.8 (CO_2H), 151.6 (C_7), 151.0 (C_6), 142.6 (C_α), 131.0 (C_1), 130.9 (C_{4a}), 129.8 (C_4), 128.3 (C_{8a}), 124.6 (C_3), 124.1 (C_2), 121.2 (C_β), 108.1 (C_5), 103.0 (C_8), 56.0 ($\underline{C}H_3OC_7$), 55.9 ($\underline{C}H_3OC_6$). HPLC-MS (50:95- g.t.10 min) ^{t}R 1.62 min, it does not ionize.

4.3.34. 5-[(E)-2-(7-Methoxynaphthalen-1-yl)ethenyl]-1,3,4-oxadiazol-2(3H)-one (**44**)

Acid **42** (230 mg, 1.01 mmol) was transformed into the corresponding hydrazide by treatment with HOBt (1.2 equiv), EDC·HCl (1.2 equiv) and DMAP (0.12 equiv) in anhydrous ACN (10 mL) at rt for 3 h and then, with $N_2H_4 \cdot H_2O$. The corresponding acylhydrazine was not isolated, but identified by HPLC-MS (50:95- g.t.10 min and 2:30- g.t.10 min), m/z = 243.11 $[M+H]^+$, calcd. for $[C_{14}H_{14}N_2O_2+H]^+$ 243.28. Intermediate hydrazide was treated with CDI (1.2 equiv) in anhydrous DMF (10 mL/mmol) under MW-irradiation at 130 °C for 25 min. Solvent was removed and the residue was dissolved in EtOAc (10 mL), washed with H_2O (3x10 mL) and brine (10 mL), dried over $MgSO_4$, filtered and evaporated to dryness under reduced pressure. Purification was made by column chromatography (hexane to hexane:EtOAc 6:4) obtaining **44** (245 mg, 91% yield) as a white solid of mp 207–208 °C. ^{1}H NMR (500 MHz, MeOD) δ 8.10 (d, J = 16.1 Hz, 1H, H_α), 7.84 (d, J = 8.4 Hz, 1H, H_4), 7.82 (d, J = 9.0 Hz, 2H, H_5, H_2), 7.45 (d, J = 2.5 Hz, 1H, H_8), 7.37 (dd, J = 8.0, 7.4 Hz, 1H, H_3), 7.20 (dd, J = 9.0, 2.4 Hz, 1H, H_6), 6.83 (d, J = 16.1 Hz, 1H, H_β), 3.98 (s, 3H, CH_3). ^{13}C NMR (126 MHz, MeOD) δ 160.0 (C_7), 156.6 ($C_{5'}$), 135.4 (C_α), 133.9 (C_{8a}), 132.1 (C_1), 131.4 (C_5), 131.0 (C_4), 130.8 (C_{4a}), 126.1 (C_2), 124.3 (C_3), 119.9 (C_6), 113.5 (C_β), 102.5 (C_8), 55.9 (CH_3). HPLC-MS (50:95- g.t.10 min) ^{t}R 1.83 min, m/z = 269.16 $[M+H]^+$, calcd. for $[C_{15}H_{12}N_2O_3+H]^+$ 269.27. HRMS $[ESI^+]$ m/z = 268.08547 $[M]^+$, calcd. for $[C_{15}H_{12}N_2O_3]^+$ 268.08479.

4.3.35. 5-[(E)-2-(6,7-Dimethoxynaphthalen-1-yl)ethenyl]-1,3,4-oxadiazol-2(3H)-one (**45**)

Similarly to the synthesis of **44**, acid **43** (100 mg, 0.39 mmol) was first transformed into the corresponding hydrazide that was identified by HPLC-MS (2:30- g.t.10 min), m/z = 273.11 $[M+H]^+$, calcd. for $[C_{15}H_{16}N_2O_3+H]^+$ 273.30. This intermediate hydrazide was then reacted with CDI to obtain the oxadiazolone **45** (99 mg, 85% yield) as a yellow pale solid of mp 232–234 °C. Chromatography: hexane to hexane:EtOAc 6:4. ^{1}H NMR (400 MHz, DMSO-d_6) δ 8.04 (d, J = 16.1 Hz, 1H, H_α), 7.82 (d, J = 8.1 Hz, 1H, H_4), 7.78 (d, J = 7.3 Hz, 1H, H_2), 7.46 (s, 1H, H_8), 7.41–7.32 (m, 2H, H_5, H_3), 6.93 (d, J = 16.1 Hz, 1H, H_β), 3.97 (s, 3H, C_7OCH_3), 3.90 (s, 3H, C_6OCH_3). ^{13}C NMR (101 MHz, DMSO-d_6) δ 154.4 ($C_{5'}$), 154.2 ($C_{2'}$), 149.9 (C_7), 149.3 (C_6), 133.7 (C_α), 130.1 (C_1), 129.4 (C_{4a}), 128.4 (C_4), 126.6 (C_{8a}), 123.8 (C_3), 122.7 (C_2), 112.6 (C_β), 107.2 (C_5), 102.2 (C_8), 55.6 ($C_7O\underline{C}H_3$), 55.4 ($C_6O\underline{C}H_3$). HPLC-MS (50:95- g.t.10 min) ^{t}R 1.22 min, m/z = 299.18 $[M+H]^+$, calcd. for $[C_{16}H_{14}N_2O_4+H]^+$ 299.30. HRMS $[ESI^+]$ m/z = 298.09568 $[M]^+$, calcd. for $[C_{16}H_{14}N_2O_4]^+$ 298.09536.

4.4. Pharmacology

4.4.1. Assays for human MT_1R and MT_2R subtypes

These experiments were performed at Eurofins-CEREP (France), using hMT$_1$R and hMT$_2$R stably transfected in Chinese hamster ovary cells (catalog refs. 1538 and 1687, respectively) [37,38]. In the case of hMT$_1$R cell membrane homogenates (about 80 μg protein) are incubated for 240 min at 22 °C with 0.01 nM [^{125}I]iodomelatonin in the absence or presence of the test compound in a buffer containing 50 mM Tris-HCl (pH 7.4), 5 mM $MgCl_2$ and 0.1% BSA. For hMT$_2$R cell membrane homogenates (6 μg protein) are incubated for 120 min at 37 °C with 0.05 nM [^{125}I]iodomelatonin in the absence or presence of the test compound in a buffer containing 50 mM Tris-HCl (pH 7.4) and 5 mM $MgCl_2$.

In both cases, nonspecific binding is determined in the presence of 1 μM melatonin. Following incubation, the samples are filtered rapidly under vacuum through glass fibre filters (GF/B, Packard) presoaked with 0.3% PEI and rinsed several times with ice-cold 50 mM Tris-HCl using a 96-sample cell harvester (Unifilter, Packard). The filters are dried then counted for radioactivity in a scintillation counter (Topcount, Packard) using a scintillation cocktail (Microscint 0, Packard).

4.4.2. Binding assays in quinone reductase-2

Evaluation of the affinity of compounds for QR2 in the hamster brain was performed by a radioligand binding assay (Eurofins-CEREP, France, catalog ref. 0088) [39]. Membrane homogenates of brain (750 μg protein) are incubated for 60 min at 4 °C with 0.1 nM [^{125}I]iodomelatonin in the absence or presence of the test compound in a buffer containing 50 mM Tris-HCl (pH 7.4) and 4 mM $CaCl_2$. Nonspecific binding is determined in the presence of 30 μM melatonin. Following incubation, the samples are filtered rapidly under vacuum through glass fiber filters (Filtermat B, Wallac) presoaked with 0.5% PEI (pH 7.4) and rinsed several times with an ice-cold buffer containing 50 mM Tris-HCl and 2 M NaCl using a 48-sample cell harvester (Mach II, Tomtec). The filters are dried then counted for radioactivity in a scintillation counter (Betaplate 1204, Wallac) using a solid scintillator (Meltilex B/HS, Wallac).

4.4.3. Methodology and expression of the results of binding assays in hMT_1R, hMT_2R and QR2

Radioligand displacements were measured at a fixed concentration of compound in each receptor subtype in 3 independent experiments. Then, compounds displaying a radioligand displacement above 80% were re-evaluated using a range of 5 different concentrations in 3 independent experiments, to determine the binding constants (K_i). The standard reference compound was melatonin, which was tested in each experiment at several concentrations to obtain a competition curve from which its IC_{50} was calculated.

The IC_{50} values (concentration causing a half-maximal inhibition of control specific binding) and Hill coefficients (nH) were determined by non-linear regression analysis of the competition curves generated with mean replicate values using Hill equation curve fitting

$$Y = D + [(A-D) / [1+(C/IC_{50})^{nH}]$$

where Y = specific binding, A = left asymptote of the curve, D = right asymptote of the curve, C = compound concentration, and nH = slope factor.

The inhibition constants (K_i) were calculated using the Cheng Prusoff equation

$$K_i = IC_{50} / (1 + L/K_D)$$

where L = concentration of radioligand in the assay, and K_D = affinity of the radioligand for the receptor. A scatchart plot is used to determine the K_D. In all cases, K_is are expressed as the mean ± SEM of three independent experiments.

4.4.4. Functional assay at human MT_2R

Evaluation of the agonist activity of **44** at hMT$_2$R expressed in transfected CHO cells was performed by measuring its effects on cAMP modulation using the HTRF detection method (Eurofins-CEREP, France, catalog ref. G028-2092) [38]. The cells were suspended in HBSS buffer (Invitrogen) complemented with 20 mM

HEPES (pH 7.4) and 500 μM IBMX, then distributed in microplates at a density of 7.10^3 cells/well in the presence of either of the following: HBSS (basal control), the reference agonist at 10 nM (stimulated control) or various concentrations (EC_{50} determination), or the test compound. Thereafter, the adenylyl cyclase activator NKH 477 is added at a final concentration of 5 μM. Following 10 min incubation at 37 °C, the cells are lysed and the fluorescence acceptor (D2-labelled cAMP) and fluorescence donor (anti-cAMP antibody labelled with europium cryptate) are added. After 60 min at room temperature, the fluorescence transfer is measured at λex = 337 nm and λem = 620 and 665 nm using a microplate reader (Envison, PerkinElmer). The cAMP concentration is determined by dividing the signal measured at 665 nm by that measured at 620 nm (ratio).

The EC_{50} value (concentration producing a half-maximal response) was determined by non-linear regression analysis of the concentration-response curves generated with mean replicate values of three independent experiments using Hill equation curve fitting

$$Y = D+\{(A-D) / [1+(C/EC_{50})^{nH}]\}$$

where Y = response, A = left asymptote of the curve, D = right asymptote of the curve, C = compound concentration, and nH = slope factor.

The standard reference agonist is melatonin, which was tested in each experiment at several concentrations to generate a concentration-response curve from which its EC_{50} value was calculated.

4.4.5. Oxygen radical absorbance capacity assay (ORAC)

Antioxidant activities were measured using the ORAC method [43], in a Polarstar Galaxy plate reader (BMG Labtechnologies GmbH, Offenburg, Germany) with 485-P excitation and 520-P emission filters. The equipment was controlled by the Fluorostar Galaxy software (version 4.11-0) for fluorescence measurement. 2,2′-Azobis-(amidinopropane) dihydrochloride (AAPH), (±)-6-hydroxy-2,5,7,8-tetramethylchromane-2-carboxylic acid (trolox) and fluorescein (FL) were purchased from Sigma-Aldrich. The reaction was carried out in 75 mM phosphate buffer (pH 7.4) and the final reaction mixture was 200 μL. Antioxidant (20 μL) and FL (120 μL; 70 mM, final concentration) solutions were placed in a black 96-well microplate (96F untreat, Nunc). The mixture was pre-incubated for 15 min at 37 °C and then, AAPH solution (60 μL, 12 mM, final concentration) was added rapidly using a multichannel pipette. The microplate was immediately placed in the reader and the fluorescence recorded every minute for 80 min. The microplate was automatically shaken prior each reading. Samples were measured at eight different concentrations (0.1–1 μM). A blank (FL + AAPH in phosphate buffer) instead of the sample solution and eight calibration solutions using trolox (1–8 μM) were also carried out in each assay. All the reaction mixtures were prepared in duplicate, and at least three independent assays were performed for each sample. Raw data were exported from the Fluostar Galaxy Software to an Excel sheet for further calculations. Antioxidant curves (fluorescence *vs.* time) were first normalized to the curve of the blank corresponding to the same assay, and the area under the fluorescence decay curve (AUC) was calculated. The net AUC corresponding to a sample was calculated by subtracting the AUC corresponding to the blank. Regression equations between net AUC and antioxidant concentration were calculated for all the samples, measured in three independent experiments. ORAC values were expressed as trolox equivalents by using the standard curve calculated for each assay, where the ORAC value of trolox was taken as 1.0.

4.4.6. NRF2 induction by luciferase activity in AREc32 cells

AREc32 cells were kindly provided by Prof. Roland Wolf (University of Dundee, UK) [48]. AREc32 cells were cultured in DMEM with glutamax and high glucose, supplemented with 1% penicillin-streptomycin (10,000 units), geneticin (0.8 mg mL^{-1}) and 10% FBS, at 37 °C in a 5% CO_2 air atmosphere. AREc32 cells were sub-cultured in 96-well white plates at 2×10^4 cells/well density. Cells were incubated with increasing concentrations of tested compounds in duplicate for 24 h. Luciferase expression was assayed with the Luciferase Assay System by luminescence in an Orion II microplate luminometer (Berthold, Germany). Luciferase activity increase was normalized to basal conditions considered as 1. CD (concentration that duplicates the luciferase activity) values are expressed as the mean ± SEM of four independent experiments in duplicate.

4.4.7. Expression of KEAP1

4.4.7.1. pET15b-6xHis-Kelch domain construction. The human Kelch domain fragment from vector pcDNA3.1-KEAP1-HA [74] was subcloned in pET15b-6xHIis using the following oligonucleotides that introduce an NdeI restriction site at both ends (Forward**:** 5′-TCGACATATGCAGGCAGTGCCCTGCCGCCGC-3′) and BamHI (Reverse**:** 5′-TGACGGATCCTTAGGTGACGGCCACACCCAC-3′).

4.4.7.2. Expression of recombinant 6xHis-Kelch domain. The pET15b-6xHIis-Kelch expression vector was used to express the Kelch domain of KEAP1 as a 6xHis-fusion protein in the BL21-DE3 strain of *Escherichia coli* cultivated overnight at 37 °C in LB medium. Expression was induced at an optical density $A_{550} = 0.4$ by adding isopropyl-1-thio-β-D-galactopyranoside (IPTG) to a final concentration of 0.5 mM. After 3 h at 37 °C temperature, cells were lysed, and 6xHIS-fusion protein was purified using the ProBond Purification System (Invitrogen) as described by the manufacturer.

4.4.8. Surface plasmon resonance (SPR) assays

SPR experiments were performed at 20 °C with a Biacore X-100 apparatus (Biacore, GE) in PBS-T with 1 mM DTT and 2% de DMSO (running buffer) at 25 °C. The KEAP1 Kelch domain protein was immobilized on a CM5 sensor chip (Biacore, GE) following standard amine coupling method [75]. The carboxymethyl dextran surface of the flow cell 2 was activated with a 7-min injection of a 1:1 ratio of 0.4 M EDC and 0.1 M NHS. The protein was coupled to the surface with a 7-min injection at 100 μg/mL in 10 mM sodium acetate, pH 5.0. The unreacted *N*-hydroxysuccinimide esters were quenched by a 7-min injection of 0.1 M ethanolamine-HCl (pH 8.0). The level of immobilization was 7000 RUs. Flow cell 1 treated as a flow cell 2 (amine coupling procedure) without protein was used as a reference. Prior to use 10 mM stock solutions of compounds were diluted several times until 100 μM final concentration in the running buffer. Typically, a series of different compounds was injected onto the sensor chip a flow rate of 45 μL/min for a period of 1 min followed by a dissociation period of 1 min. After the dissociation process an extra-wash treatment was made over the flow cells with a 50% DMSO solution. No regeneration was needed. Sensograms data were double-referenced and solvent corrected using the Biaevaluation X-100 software (Biacore, GE).

4.4.9. Inhibition of human monoamine oxidases (hMAO-A and hMAO-B)

MAO inhibition measurements were evaluated following the general procedure previously described [76]. Briefly, test drugs and adequate amounts of recombinant *h*MAO-A or *h*MAO-B (Sigma-Aldrich, Spain) required and adjusted to oxidize 165 pmol of p-tyramine/min in the control group, were incubated for 15 min at 37 °C in a flat-black-bottom 96-well microtest plate (BD Biosciences, Franklin Lakes, NJ) placed in the dark fluorimeter

chamber. The reaction was started by adding 200 mM Amplex Red reagent (Molecular Probes, Inc., Eugene, OR), 1 U/mL horseradish peroxidase, and 1 mM *p*-tyramine. Then, the production of resorufin was quantified at 37 °C in a multidetection microplate fluorescence reader (FLX800, Bio-Tek Instruments, Inc., Winooski, VT) based on the fluorescence generated (excitation, 545 nm; emission, 590 nm). The specific fluorescence emission was calculated after subtraction of the background activity, which was determined from wells containing all components except the *h*MAO isoforms, which were replaced by a sodium phosphate buffer solution. IC_{50} values were the mean ± SD of three independent experiments performed in triplicate.

4.4.10. Inhibition of human lipoxygenase-5 (hLOX-5)

The fluorescence-based enzyme method developed by Pufahl et al. was followed [77], in 96-well microtiter plates. The assay solution consists of Tris buffer (50 mM, pH 7.5), ethylenediaminetetraacetic acid (EDTA, 2 mM), $CaCl_2$ (2 mM), arachidonic acid (AA, 3 μM), ATP (10 μM), 2′,7′-dichlorodihydrofluorescein diacetate (H_2DCFDA, 10 μM), *h*LOX-5 (100 mU/well), bovine glutathione peroxidase (GPx, 25 mU/well) and reduced glutathione (GSH, 1 mM). Compounds to be tested were added to the test solution prior to AA and ATP, and pre-incubated for a period of 10 min at room temperature. Then, the AA and ATP substrates were added; the enzymatic reaction allowed to progress for 20 min and ended by the addition of 40 μL of acetonitrile. The fluorescence measurements (excitation: 485 nm; emission: 520 nm) were performed on a FLUOstar OPTIMA (BMG LABTECH, Offenburg, Germany). IC_{50} is defined as the concentration of compound that inhibits enzymatic activity by 50% over the control of untreated enzyme. Data were the mean ± SD of three independent experiments performed in triplicate.

4.4.11. In vitro blood–brain barrier permeation assay (PAMPA-BBB)

Prediction of the brain penetration was evaluated using a parallel artificial membrane permeation assay (PAMPA-BBB), in a similar manner as previously described [27,29,78–80]. Pipetting was performed with a semi-automatic pipettor (CyBi®-SELMA) and UV reading with a microplate spectrophotometer (Multiskan Spectrum, Thermo Electron Co.). Commercial drugs, phosphate buffered saline solution at pH 7.4 (PBS), and dodecane were purchased from Sigma, Aldrich, Acros, and Fluka. Millex filter units (PVDF membrane, diameter 25 mm, pore size 0.45 μm) were acquired from Millipore. The porcine brain lipid (PBL) was obtained from Avanti Polar Lipids. The donor microplate was a 96-well filter plate (PVDF membrane, pore size 0.45 μm) and the acceptor microplate was an indented 96-well plate, both from Millipore. The acceptor 96-well microplate was filled with 200 μL of PBS: ethanol (70:30) and the filter surface of the donor microplate was impregnated with 5 μL of porcine brain lipid (PBL) in dodecane (20 mg mL^{-1}). Compounds were dissolved in PBS: ethanol (70:30) at 100 μg mL^{-1}, filtered through a Millex filter, and then added to the donor wells (200 μL). The donor filter plate was carefully put on the acceptor plate to form a sandwich, which was left undisturbed for 120 min at 25 °C. After incubation, the donor plate is carefully removed and the concentration of compounds in the acceptor wells was determined by UV–Vis spectroscopy. Every sample is analysed at five wavelengths, in four wells and at least in three independent runs, and the results are given as the mean ± standard deviation. In each experiment, 11 quality control standards of known BBB permeability were included to validate and normalize the analysis set.

4.4.12. Neurogenic assays

Ten three-month-old male C57BL/6 mice were used throughout this study. All experimental procedures were previously approved by the Ethics Committee for Animal Experimentation of the CSIC in accordance with the European Communities Council, directive 2010/63/EEC and National regulations, normative 53/2013. Special care was taken to minimize animal suffering. Neural stem cells (NSCs) were isolated from the SGZ of the hippocampal dentate gyrus and prepared following previously published methods [58,81]. The isolated NSCs were seeded into 12-well dishes at a density of ~40,000 cells per cm2 in DMEM/F12 (1:1) containing N2 medium. NSCs were grown as free-floating cells under proliferative conditions (10 ng/mL epidermal growth factor + 10 ng/mL fibroblast growth factor) allowing the formation of neural stem cells-enriched growing spheres also called neurospheres (NS). After 7 days, with all NS having the same stage and size, cultures were treated daily for 7 days with vehicle or 10 μM of compound **6** (10). Now, NS were adhered onto 100 μg mL^{-1} poly-L-lysine-coated coverslips and treated for 3 additional days under differentiation conditions (medium containing 1% fetal bovine serum and without exogenous growth factors) [82]. Once neurospheres were differentiated (72 h), coverslips were processed as previously described[41] and used for immunofluorescence analysis. Then the expression of neuronal markers was analysed. The following antibodies linked to neurogenesis were used: β-III-tubulin polyclonal antibody (TuJ clone; Abcam), a protein expressed at early stages of neurogenesis and a monoclonal microtubule-associated protein type 2 (MAP-2) antibody, a classical marker of late neuronal maturation. To visualize primary antibodies Alexa-fluor-labelled secondary antibodies (Molecular probes) were used. Nuclei were stained with DAPI. Fluorescent representative images from four independent experiments were acquired in a LSM710 laser scanning spectral confocal microscope (Zeiss). Confocal microscope settings were adjusted to produce the optimum signal to noise ratio.

4.4.13. In silico model building of ligands and proteins

The molecular graphics program PyMOL [83] was employed in the construction of the initial molecular models, trajectory visualization and 3D figure generation. *Ab initio* geometry optimization of the derivatives studied was achieved using a 6-31G* basis set and the Hartree-Fock method, as implemented in the Gaussian 09 program [84]. The *SCRF = (Solvent = Water)* option was used to place the solute in a cavity within the solvent reaction field and mimic hydration effects. For melatonin, 2-iodomelatonin and resveratrol, the optimized geometries were also written in Crystallographic Information File (CIF) format [85] using eLBOW [86] for re-refinement of several human quinone reductase II (QR2) X-ray crystal structures retrieved from the Protein Data Bank (entries 2QWX, 2QX8 [87], and 1SG0 [60]) against structure factor amplitudes using Phenix [88,89] and Coot [90]. Six macrocycles were used in each refinement round and concerted motions of atomic groups were taken into account by means of the translation-libration-screw (TLS) model [91]. PDB entries 6ME3 [62] and 6ME6 [63] containing the XFEL structures of chimeric MT_1 and MT_2 receptor constructs, respectively, in complex with 2-phenylmelatonin were used as templates to model the complexes of the studied compounds with the wild-type human receptors with the aid of the Swiss-Model server [92,93]. Consequently, our MT_1 and MT_2 receptor models (UniProt [94] identifiers P48039 and P49286, respectively) contained the original truncations at both termini but had all the introduced point mutations replaced by the natural amino acids and a short added sequence bridging the ICL3 gap (residues 219–227 and 232–240 in MT_1 and MT_2 receptors, respectively). The conserved disulfide bridge between $C100^{3.25}$ and $C177^{ECL2}$ in MT_1 and between $C113^{3.25}$ and $C190^{ECL2}$ in MT_2 were explicitly defined.

Atom-centered charges for all ligands were calculated on the 6-

31G*-optimized geometries with the *sqm* program [95] in AmberTools17 and the default AM1-BCC option [96], so as to reproduce the molecular electrostatic potential in a way consistent with the *ff14SB* force field parameter set [97] in AMBER 16 (http://ambermd.org).

4.4.14. Molecular docking

The protein in the X-ray crystal structure of KEAP1 Kelch Domain was prepared with the Protein Preparation procedure as implemented in Maestro. All hydrogens were added and the charge states of titratable amino acids were defined using the PROTKA procedure, followed by H-bond optimization and constrained relaxation to 0.2 rmsd tolerance. The resulting structures were used to generate docking grids and perform docking studies with compounds **23** and **24** using GLIDE [98]. The ligands were prepared with the LigPrep module using the parameters of OPLS3 Force Field. Generation of possible tautomers was done with Epik routine in Maestro at pH range of 7 ± 2. All the modelling was done with Maestro 11.5 Release 2018-1 (Schrodinger LLC).

4.4.15. Molecular dynamics simulations

The complexes of **44** with MT_1R and MT_2R were embedded in a lipid bilayer made up of 240 1,2-dioleoyl-*sn*-glycero-3-phosphocholine (DOPC) and 21 cholesterol molecules with the aid of the web-based CHARMM-GUI Membrane Builder graphical user interface [99]. The system size along the Z axis was determined by specifying a 10 Å thickness of 150 mM NaCl aqueous solution on each side of the membrane. The AMBER *ff14SB* [97] and *lipid14* [100] force fields were used for protein and lipids, respectively.

For each complex studied, all hydrogens and water molecules were first reoriented in the electric field of the solute and then all protein residues, ligands and waters were relaxed by performing 25 000 steps of steepest descent followed by 25 000 steps of conjugate gradient energy minimization. The resulting geometry-optimized coordinate sets were then heated up to 300 K using the Langevin thermostat; thereafter the temperature was maintained at 300 K whereas the system's dimensions and density were equilibrated at a constant pressure of 1 atm by means of an anisotropic Berendsen weak-coupling barostat, essentially as described [100]. The uMD simulations were run for 200 ns using the *pmemd.cuda* code [101], as implemented in AMBER16, running on single Nvidia® GPUs. The coupling constants for the temperature and pressure baths were 1.0 and 0.2 ps, respectively. The application of SHAKE to all bonds allowed an integration time step of 2 fs to be used. A cutoff distance of 9 Å was selected for the nonbonded interactions and the list of nonbonded pairs was updated every 25 steps. Periodic boundary conditions were applied and electrostatic interactions were represented using the smooth particle-mesh Ewald method [102] with a grid spacing of 1 Å. Trajectory snapshots were saved every 0.1 ns for further analysis. Besides, a simulated annealing procedure [103] was followed every 5 ns to cool the system down from 300 to 273 K over a 1-ns period. Thereafter the geometries of these "frozen" complexes were optimized by carrying out an energy minimization until the root-mean-square of the Cartesian elements of the gradient was less than 0.01 kcal mol^{-1} $Å^{-1}$. A similar procedure was used to simulate the fully solvated complexes of human QR2 with compounds using our refined structure from PDB entry 1SG0; in these cases, however, we found it necessary to add distance restraints (100 kcal mol^{-1} $Å^{-2}$) to the Zn^{2+} coordination sphere and weak positional restraints (1 kcal mol^{-1} $Å^{-2}$) to the Ca trace of the protein. The highly converged ensemble of 40 low-energy configurations thus obtained for each complex is expected to represent more accurately the global energy minimum than isolated trajectory frames [104,105].

4.4.16. Potentiometric pK_a determination

Titrations were carried out at 25 °C in 0.15 M KCl solution (aq) in a SiriusT3 equipment (Sirius Analytical Instruments Ltd, East Sussex, Britain) equipped with an Ag/AgCl double junction reference pH electrode, a Peltier temperature system and a turbidity sensor. Standardized 0.5 M KOH and 0.5 M HCl were used as titration reagents. KOH solution was standardized by potassium phthalate. The pK_a value is the mean of 3 titrations ± SD [106].

Declaration of competing interest

The authors declare that they have no known competing financial interests or personal relationships that could have appeared to influence the work reported in this paper.

Acknowledgments

The authors gratefully acknowledge the following financial supports: Spanish Ministry of Science, Innovation and Universities; Spanish Research Agency; and European Regional Development Funds (grants RTI2018-093955-B-C21 and SAF2015-64948-C2-1-R to M.I.R.-F.; RTI2018-095793-B-I00 to M.G.L., SAF2015-64629-C2-2-R to F.G.), General Council for Research and Innovation of the Community of Madrid and European Structural Funds (grant B2017/BMD-3827 — NRF24ADCM), Health Institute Carlos III (Miguel Servet II Program CP16/00014 and grant PI17/01700 to R.L.). CH-A and P.M. thank their PhD fellowships from Spanish Ministry of Education (MEC, PhD grant FPU16/01704 and mobility grant FPUEST17/00233 to CH-A and FPU13/03737 to P.M.).

Appendix A. Supplementary data

Supplementary data to this article can be found online at https://doi.org/10.1016/j.ejmech.2020.112090.

References

[1] D.M. Holtzman, J.C. Morris, A.M. Goate, Alzheimer's disease: the challenge of the second century, Sci. Transl. Med. 3 (2011), 77sr71-77sr71.
[2] J. Hroudova, N. Singh, Z. Fisar, K.K. Ghosh, Progress in drug development for Alzheimer's disease: an overview in relation to mitochondrial energy metabolism, Eur. J. Med. Chem. 121 (2016) 774–784.
[3] M. Zabel, A. Nackenoff, W.M. Kirsch, F.E. Harrison, G. Perry, M. Schrag, Markers of oxidative damage to lipids, nucleic acids and proteins and antioxidant enzymes activities in Alzheimer's disease brain: a meta-analysis in human pathological specimens, Free Radic. Biol. Med. 115 (2018) 351–360.
[4] C. Fernández-Moriano, E. González-Burgos, M.P. Gómez-Serranillos, Mitochondria-targeted protective compounds in Parkinson's and Alzheimer's diseases, Oxid. Med. Cell. Long. 2015 (2015).
[5] A. Cuadrado, G. Manda, A. Hassan, M.J. Alcaraz, C. Barbas, A. Daiber, P. Ghezzi, R. León, M.G. López, B. Oliva, M. Pajares, A.I. Rojo, N. Robledinos-Antón, A.M. Valverde, E. Guney, H.H.H.W. Schmidt, Transcription factor NRF2 as a therapeutic target for chronic diseases: a systems medicine approach, Pharmacol. Rev. 70 (2018) 348–383.
[6] G.J. McBean, M.G. López, F.K. Wallner, Redox-based therapeutics in neurodegenerative disease, Br. J. Pharmacol. 174 (2017) 1750–1770.
[7] J.A. Johnson, D.A. Johnson, A.D. Kraft, M.J. Calkins, R.J. Jakel, M.R. Vargas, P.C. Chen, The Nrf2-ARE pathway: an indicator and modulator of oxidative stress in neurodegeneration, Ann. N. Y. Acad. Sci. 1147 (2008) 61–69.
[8] R. Vianello, M. Repič, J. Mavri, How are biogenic amines metabolized by monoamine oxidases? Eur. J. Org Chem. 2012 (2012) 7057–7065.
[9] S. Schedin-Weiss, M. Inoue, L. Hromadkova, Y. Teranishi, N.G. Yamamoto, B. Wiehager, N. Bogdanovic, B. Winblad, A. Sandebring-Matton, S. Frykman, Monoamine oxidase B is elevated in Alzheimer disease neurons, is associated with γ-secretase and regulates neuronal amyloid β-peptide levels, Alzheimer's Res. Ther. 9 (2017) 57.
[10] M.T. Heneka, M.J. Carson, J. El Khoury, G.E. Landreth, F. Brosseron, D.L. Feinstein, A.H. Jacobs, T. Wyss-Coray, J. Vitorica, R.M. Ransohoff, Neuroinflammation in Alzheimer's disease, Lancet Neurol. 14 (2015) 388–405.
[11] O. Rådmark, O. Werz, D. Steinhilber, B. Samuelsson, 5-Lipoxygenase: regulation of expression and enzyme activity, Trends Biochem. Sci. 32 (2007) 332–341.
[12] M.D. Ikonomovic, E.E. Abrahamson, T. Uz, H. Manev, S.T. DeKosky, Increased

5-lipoxygenase immunoreactivity in the hippocampus of patients with Alzheimer's disease, J. Histochem. Cytochem. 56 (2008) 1065–1073.
[13] P.F. Giannopoulos, Y.B. Joshi, D. Praticò, Novel lipid signaling pathways in Alzheimer's disease pathogenesis, Biochem. Pharmacol. 88 (2014) 560–564.
[14] O. Firuzi, J. Zhuo, C.M. Chinnici, T. Wisniewski, D. Praticò, 5-Lipoxygenase gene disruption reduces amyloid-β pathology in a mouse model of Alzheimer's disease, Faseb. J. 22 (2008) 1169–1178.
[15] D. Acuña-Castroviejo, I. Rahim, C. Acuña-Fernandez, M. Fernandez-Ortiz, J. Solera-Marin, R.K.A. Sayed, M.E. Diaz-Casado, I. Rusanova, L.C. Lopez, G. Escames, Melatonin, clock genes and mitochondria in sepsis, Cell. Mol. Life Sci. 74 (2017) 3965–3987.
[16] O. Nosjean, M. Ferro, F. Cogé, P. Beauverger, J.-M. Henlin, F. Lefoulon, J.-L. Fauchère, P. Delagrange, E. Canet, J.A. Boutin, Identification of the melatonin-binding site MT 3 as the quinone reductase 2, J. Biol. Chem. 275 (2000) 31311–31317.
[17] R. Jockers, P. Delagrange, M.L. Dubocovich, R.P. Markus, N. Renault, G. Tosini, E. Cecon, D.P. Zlotos, Update on melatonin receptors: IUPHAR Review 20, Br. J. Pharmacol. 173 (2016) 2702–2725.
[18] L.-E. Cassagnes, P. Perio, G. Ferry, N. Moulharat, M. Antoine, R. Gayon, J.A. Boutin, F. Nepveu, K. Reybier, In cellulo monitoring of quinone reductase activity and reactive oxygen species production during the redox cycling of 1, 2 and 1, 4 quinones, Free Radic. Biol. Med. 89 (2015) 126–134.
[19] T. Hashimoto, M. Nakai, Increased hippocampal quinone reductase 2 in Alzheimer's disease, Neurosci. Lett. 502 (2011) 10–12.
[20] L.-E. Cassagnes, M. Chhour, P. Pério, J. Sudor, R. Gayon, G. Ferry, J.A. Boutin, F. Nepveu, K. Reybier, Oxidative stress and neurodegeneration: the possible contribution of quinone reductase 2, Free Radic. Biol. Med. 120 (2018) 56–61.
[21] J.A. Boutin, Quinone reductase 2 as a promising target of melatonin therapeutic actions, Expert Opin. Ther. Targets 20 (2016) 303–317.
[22] M. Boldrini, C.A. Fulmore, A.N. Tartt, L.R. Simeon, I. Pavlova, V. Poposka, G.B. Rosoklija, A. Stankov, V. Arango, A.J. Dwork, R. Hen, J.J. Mann, Human hippocampal neurogenesis persists throughout aging, Cell Stem Cell 22 (2018) 589–599, e585.
[23] S.F. Sorrells, M.F. Paredes, A. Cebrian-Silla, K. Sandoval, D. Qi, K.W. Kelley, D. James, S. Mayer, J. Chang, K.I. Auguste, E.F. Chang, A.J. Gutierrez, A.R. Kriegstein, G.W. Mathern, M.C. Oldham, E.J. Huang, J.M. Garcia-Verdugo, Z. Yang, A. Alvarez-Buylla, Human hippocampal neurogenesis drops sharply in children to undetectable levels in adults, Nature 555 (2018) 377–381.
[24] G. Kempermann, F.H. Gage, L. Aigner, H. Song, M.A. Curtis, S. Thuret, H.G. Kuhn, S. Jessberger, P.W. Frankland, H.A. Cameron, E. Gould, R. Hen, D.N. Abrous, N. Toni, A.F. Schinder, X. Zhao, P.J. Lucassen, J. Frisen, Human adult neurogenesis: evidence and remaining questions, Cell Stem Cell 23 (2018) 25–30.
[25] C. Herrera-Arozamena, O. Martí-Marí, M. Estrada, M. de la Fuente Revenga, M.I. Rodríguez-Franco, Recent advances in neurogenic small molecules as innovative treatments for neurodegenerative diseases, Molecules 21 (2016) 1165–1185.
[26] G. Ramírez-Rodríguez, N.M. Vega-Rivera, G. Benítez-King, M. Castro-García, L. Ortiz-López, Melatonin supplementation delays the decline of adult hippocampal neurogenesis during normal aging of mice, Neurosci. Lett. 530 (2012) 53–58.
[27] B. López-Iglesias, C. Pérez, J.A. Morales-García, S. Alonso-Gil, A. Pérez-Castillo, A. Romero, M.G. López, M. Villarroya, S. Conde, M.I. Rodríguez-Franco, New melatonin-*N*,*N*-dibenzyl(*N*-methyl)amine hybrids: potent neurogenic agents with antioxidant, cholinergic, and neuroprotective properties as innovative drugs for Alzheimer's disease, J. Med. Chem. 57 (2014) 3773–3785.
[28] M. de la Fuente Revenga, C. Pérez, J.A. Morales-García, S. Alonso-Gil, A. Pérez-Castillo, D.H. Caignard, M. Yáñez, A.M. Gamo, M.I. Rodríguez-Franco, Neurogenic potential assessment and pharmacological characterization of 6-methoxy-1,2,3,4-tetrahydro-beta-carboline (pinoline) and melatonin-pinoline hybrids, ACS Chem. Neurosci. 6 (2015) 800–810.
[29] M. de la Fuente Revenga, N. Fernández-Sáez, C. Herrera-Arozamena, J.A. Morales-García, S. Alonso-Gil, A. Pérez-Castillo, D.H. Caignard, S. Rivara, M.I. Rodríguez-Franco, Novel *N*-acetyl bioisosteres of melatonin: melatonergic receptor pharmacology, physicochemical studies, and phenotypic assessment of their neurogenic potential, J. Med. Chem. 58 (2015) 4998–5014.
[30] J.A. Morales-García, M. de la Fuente Revenga, S. Alonso-Gil, M.I. Rodríguez-Franco, A. Feilding, A. Perez-Castillo, J. Riba, The alkaloids of *Banisteriopsis caapi*, the plant source of the Amazonian hallucinogen Ayahuasca, stimulate adult neurogenesis *in vitro*, Sci. Rep. 7 (2017) 5309.
[31] M.I. Rodríguez-Franco, M. de la Fuente Revenga, C. Pérez, A. Pérez-Castillo, J.A. Morales-García, S. Alonso-Gil, J. Figueiró, E. Carro, Neurogenic Compounds Comprising Melatonin and the Efficacy Thereof in in Vivo Experiments for Use in the Treatment of Diseases of the Nervous System, in.
[32] J. Figueiró-Silva, D. Antequera, C. Pascual, M. de la Fuente Revenga, H. Volt, D. Acuña-Castroviejo, M.I. Rodríguez-Franco, E. Carro, The melatonin analog IQM316 may inducea dult hippocampal neurogenesis and preserve recognition memories in mice, Cell Transplant. 27 (2018) 423–437.
[33] R.H. Swerdlow, Alzheimer's disease pathologic cascades: who comes first, what drives what, Neurotox. Res. 22 (2012) 182–194.
[34] M.C. Carreño, Á. Enríquez, S. García-Cerrada, M.J. Sanz-Cuesta, A. Urbano, F. Maseras, A. Nonell-Canals, Towards configurationally stable [4]helicenes: enantioselective synthesis of 12-substituted 7,8-dihydro[4]helicene quinones, Chem. Eur J. 14 (2008) 603–620.
[35] R.S. Garigipati, G. Seibel, R.J. Mayer, B. Bolognese, M. McCord, L.A. Marshall, J.L. Adams, Novel frameworks for trifluoromethyl ketone and phosphonate tsa inhibitors of type II PLA2, Bioorg. Med. Chem. Lett 7 (1997) 1421–1426.
[36] D.L. Cain, C. McLaughlin, J.J. Molloy, C. Carpenter-Warren, N.A. Anderson, A.J.B. Watson, A cascade Suzuki–Miyaura/Diels–Alder protocol: exploring the bifunctional utility of vinyl bpin, Synlett 30 (2019) 787–791.
[37] P.A. Witt-Enderby, M.L. Dubocovich, Characterization and regulation of the human ML1A melatonin receptor stably expressed in Chinese hamster ovary cells, Mol. Pharmacol. 50 (1996) 166–174.
[38] I.J. Beresford, C. Browning, S.J. Starkey, J. Brown, S.M. Foord, J. Coughlan, P.C. North, M.L. Dubocovich, R.M. Hagan, GR196429: a nonindolic agonist at high-affinity melatonin receptors, J. Pharmacol. Exp. Therapeut. 285 (1998) 1239–1245.
[39] D.S. Pickering, L.P. Niles, Pharmacological characterization of melatonin binding sites in Syrian hamster hypothalamus, Eur. J. Pharmacol. 175 (1990) 71–77.
[40] I. Gameiro, P. Michalska, G. Tenti, Á. Cores, I. Buendia, A.I. Rojo, N.D. Georgakopoulos, J.M. Hernández-Guijo, M.T. Ramos, G. Wells, Discovery of the first dual GSK3β inhibitor/Nrf2 inducer. A new multitarget therapeutic strategy for Alzheimer's disease, Sci. Rep. 7 (2017) 45701.
[41] P. Depreux, D. Lesieur, H.A. Mansour, P. Morgan, H.E. Howell, P. Renard, D.-H. Caignard, B. Pfeiffer, P. Delagrange, Synthesis and structure-activity relationships of novel naphthalenic and bioisosteric related amidic derivatives as melatonin receptor ligands, J. Med. Chem. 37 (1994) 3231–3239.
[42] L. Einhorn, K. Krapfenbauer, HTRF: a technology tailored for biomarker determination-novel analytical detection system suitable for detection of specific autoimmune antibodies as biomarkers in nanogram level in different body fluids, EPMA J. 6 (2015) 23.
[43] A. Dávalos, C. Gómez-Cordovés, B. Bartolomé, Extending applicability of the oxygen radical absorbance capacity (ORAC-fluorescein) assay, J. Agric. Food Chem. 52 (2004) 48–54.
[44] L. Monjas, M.P. Arce, R. León, J. Egea, C. Pérez, M. Villarroya, M.G. López, C. Gil, S. Conde, M.I. Rodríguez-Franco, Enzymatic and solid-phase synthesis of new donepezil-based L- and D-glutamic acid derivatives and their pharmacological evaluation in models related to Alzheimer's disease and cerebral ischemia, Eur. J. Med. Chem. 130 (2017) 60–72.
[45] M. Estrada Valencia, C. Herrera-Arozamena, L. de Andrés, C. Pérez, J.A. Morales-García, A. Pérez-Castillo, E. Ramos, A. Romero, D. Viña, M. Yáñez, E. Laurini, S. Pricl, M.I. Rodríguez-Franco, Neurogenic and neuroprotective donepezil-flavonoid hybrids with sigma-1 affinity and inhibition of key enzymes in Alzheimer's disease, Eur. J. Med. Chem. 156 (2018) 534–553.
[46] M. Estrada-Valencia, C. Herrera-Arozamena, C. Pérez, D. Viña, J.A. Morales-García, A. Pérez-Castillo, E. Ramos, A. Romero, E. Laurini, S. Pricl, M.I. Rodríguez-Franco, New flavonoid – *N*,*N*-dibenzyl(*N*-methyl)amine hybrids: multi-target-directed agents for Alzheimer's disease endowed with neurogenic properties, J. Enzym. Inhib. Med. Chem. 34 (2019) 712–727.
[47] E. Sofic, Z. Rimpapa, Z. Kundurovic, A. Sapcanin, I. Tahirovic, A. Rustembegovic, G. Cao, Antioxidant capacity of the neurohormone melatonin, J. Neural. Transm. 112 (2005) 349–358.
[48] X.J. Wang, J.D. Hayes, C.R. Wolf, Generation of a stable antioxidant response element–driven reporter gene cell line and its use to show redox-dependent activation of Nrf2 by cancer chemotherapeutic agents, Canc. Res. 66 (2006) 10983–10994.
[49] L. Wang, T. Lewis, Y.L. Zhang, C. Khodier, S. Magesh, L. Chen, D. Inoyama, Y. Chen, J. Zhen, L. Hu, L.J. Beamer, P.W. Faloon, S. Dandapani, J.R. Perez, B. Munoz, M. Palmer, S. Schreiber, The identification and characterization of non-reactive inhibitor of Keap1-Nrf2 interaction through HTS using a fluorescence polarization assay, in: Probe Reports from the NIH Molecular Libraries Program, Bethesda (MD), 2010.
[50] M.J. Matos, F. Rodríguez-Enríquez, S. Vilar, L. Santana, E. Uriarte, G. Hripcsak, M. Estrada, M.I. Rodríguez-Franco, D. Viña, Potent and selective MAO-B inhibitory activity: amino-versus nitro-3-arylcoumarin derivatives, Bioorg. Med. Chem. Lett 25 (2015) 642–648.
[51] R.A. Pufahl, T.P. Kasten, R. Hills, J.K. Gierse, B.A. Reitz, R.A. Weinberg, J.L. Masferrer, Development of a fluorescence-based enzyme assay of human 5-lipoxygenase, Anal. Biochem. 364 (2007) 204–212.
[52] L. Di, E.H. Kerns, K. Fan, O.J. McConnell, G.T. Carter, High throughput artificial membrane permeability assay for blood–brain barrier, Eur. J. Med. Chem. 38 (2003) 223–232.
[53] M. Estrada, C. Pérez, E. Soriano, E. Laurini, M. Romano, S. Pricl, J.A. Morales-García, A. Pérez-Castillo, M.I. Rodríguez-Franco, New neurogenic lipoic-based hybrids as innovative Alzheimer's drugs with sigma-1 agonism and beta-secretase inhibition, Future Med. Chem. 8 (2016) 1191–1207.
[54] M. Estrada, C. Herrera-Arozamena, C. Pérez, D. Viña, A. Romero, J.A. Morales-García, A. Pérez-Castillo, M.I. Rodríguez-Franco, New cinnamic - *N*-benzylpiperidine and cinnamic - *N*,*N*-dibenzyl(*N*-methyl)amine hybrids as Alzheimer-directed multitarget drugs with antioxidant, cholinergic, neuroprotective and neurogenic properties, Eur. J. Med. Chem. 121 (2016) 376–386.
[55] T. Sterling, J.J. Irwin, ZINC 15–ligand discovery for everyone, J. Chem. Inf. Model. 55 (2015) 2324–2337.
[56] J.J. Irwin, D. Duan, H. Torosyan, A.K. Doak, K.T. Ziebart, T. Sterling, G. Tumanian, B.K. Shoichet, An aggregation advisor for ligand discovery, J. Med. Chem. 58 (2015) 7076–7087.

[57] A. Daina, O. Michielin, V. Zoete, SwissADME: a free web tool to evaluate pharmacokinetics, drug-likeness and medicinal chemistry friendliness of small molecules, Sci. Rep. 7 (2017) 42717.

[58] J.A. Morales-Garcia, S. Alonso-Gil, C. Gil, A. Martinez, A. Santos, A. Perez-Castillo, Phosphodiesterase 7 inhibition induces dopaminergic neurogenesis in hemiparkinsonian rats, Stem Cells Transl. Med. 4 (2015) 564–575.

[59] G. Kempermann, S. Jessberger, B. Steiner, G. Kronenberg, Milestones of neuronal development in the adult hippocampus, Trends Neurosci. 27 (2004) 447–452.

[60] L. Buryanovskyy, Y. Fu, M. Boyd, Y. Ma, T.C. Hsieh, J.M. Wu, Z. Zhang, Crystal structure of quinone reductase 2 in complex with resveratrol, Biochemistry 43 (2004) 11417–11426.

[61] S.D. Pegan, M. Sturdy, G. Ferry, P. Delagrange, J.A. Boutin, A.D. Mesecar, X-ray structural studies of quinone reductase 2 nanomolar range inhibitors, Protein Sci. 20 (2011) 1182–1195.

[62] B. Stauch, L.C. Johansson, J.D. McCorvy, N. Patel, G.W. Han, X.P. Huang, C. Gati, A. Batyuk, S.T. Slocum, A. Ishchenko, W. Brehm, T.A. White, N. Michaelian, C. Madsen, L. Zhu, T.D. Grant, J.M. Grandner, A. Shiriaeva, R.H.J. Olsen, A.R. Tribo, S. Yous, R.C. Stevens, U. Weierstall, V. Katritch, B.L. Roth, W. Liu, V. Cherezov, Structural basis of ligand recognition at the human MT_1 melatonin receptor, Nature 569 (2019) 284–288.

[63] L.C. Johansson, B. Stauch, J.D. McCorvy, G.W. Han, N. Patel, X.P. Huang, A. Batyuk, C. Gati, S.T. Slocum, C. Li, J.M. Grandner, S. Hao, R.H.J. Olsen, A.R. Tribo, S. Zaare, L. Zhu, N.A. Zatsepin, U. Weierstall, S. Yous, R.C. Stevens, W. Liu, B.L. Roth, V. Katritch, V. Cherezov, XFEL structures of the human MT_2 melatonin receptor reveal the basis of subtype selectivity, Nature 569 (2019) 289–292.

[64] S.C. Lo, X. Li, M.T. Henzl, L.J. Beamer, M. Hannink, Structure of the Keap1:Nrf2 interface provides mechanistic insight into Nrf2 signaling, EMBO J. 25 (2006) 3605–3617.

[65] W.C. Still, A. Tempczyk, R.C. Hawley, T. Hendrickson, Semianalytical treatment of solvation for molecular mechanics and dynamics, J. Am. Chem. Soc. 112 (1990) 6127–6129.

[66] M.F. Sanner, A.J. Olson, J.C. Spehner, Reduced surface: an efficient way to compute molecular surfaces, Biopolymers 38 (1996) 305–320.

[67] W. Humphrey, A. Dalke, K. Schulten, VMD: visual molecular dynamics, J. Mol. Graph. 14 (33–38) (1996) 27–38.

[68] G. Jin, S. Lee, M. Choi, S. Son, G.W. Kim, J.W. Oh, C. Lee, K. Lee, Chemical genetics-based discovery of indole derivatives as HCV NS5B polymerase inhibitors, Eur. J. Med. Chem. 75 (2014) 413–425.

[69] I. Takase, T. Hiramura, T. Kato, T. Suzuki, K. Onda, J. Hirosumi, Process for Preparation of Indoline Derivatives, in: WO 2007069633 A1 20070621, 2007.

[70] A.J. Greenberg, R. Ketcham, Determination of urinary indolic metabolites, J. Pharmaceut. Sci. 67 (1978) 478–480.

[71] A. Arcadi, S. Cacchi, G. Fabrizi, L. Moro, Palladium-catalyzed cyclocarbonylation of o-ethynylphenols and vinyl triflates to form 3-alkylidene-2-coumaranones, Eur. J. Org Chem. 1999 (1999) 1137–1141.

[72] A.N. Hulme, S.S. Henry, A.I. Meyers, Asymmetric synthesis of the key intermediates leading to (-)-aphanorphine and (-)-eptazocine, J. Org. Chem. 60 (1995) 1265–1270.

[73] L. Morellato, M. Lefas-Le Gall, M. Langlois, D.H. Caignard, P. Renard, P. Delagrange, M. Mathe-Allainmat, Synthesis of new N-(arylcyclopropyl) acetamides and N-(arylvinyl)acetamides as conformationally-restricted ligands for melatonin receptors, Bioorg. Med. Chem. Lett 23 (2013) 430–434.

[74] P. Rada, A.I. Rojo, S. Chowdhry, M. McMahon, J.D. Hayes, A. Cuadrado, SCF/{beta}-TrCP promotes glycogen synthase kinase 3-dependent degradation of the Nrf2 transcription factor in a Keap1-independent manner, Mol. Cell Biol. 31 (2011) 1121–1133.

[75] B. Johnsson, S. Lofas, G. Lindquist, Immobilization of proteins to a carboxymethyldextran-modified gold surface for biospecific interaction analysis in surface plasmon resonance sensors, Anal. Biochem. 198 (1991) 268–277.

[76] M.J. Matos, F. Rodríguez-Enríquez, F. Borges, L. Santana, E. Uriarte, M. Estrada, M.I. Rodríguez-Franco, R. Laguna, D. Viña, 3-Amidocoumarins as potential multifunctional agents against neurodegenerative diseases, ChemMedChem 10 (2015) 2071–2079.

[77] R.A. Pufahl, T.P. Kasten, R. Hills, J.K. Gierse, B.A. Reitz, R.A. Weinberg, J.L. Masferrer, Development of a fluorescence-based enzyme assay of human 5-lipoxygenase, Anal. Biochem. 364 (2007) 204–212.

[78] M.I. Rodríguez-Franco, M.I. Fernández-Bachiller, C. Pérez, B. Hernández-Ledesma, B. Bartolomé, Novel tacrine-melatonin hybrids as dual-acting drugs for Alzheimer disease, with improved acetylcholinesterase inhibitory and antioxidant properties, J. Med. Chem. 49 (2006) 459–462.

[79] M.I. Fernández-Bachiller, C. Pérez, L. Monjas, J. Rademann, M.I. Rodríguez-Franco, New tacrine–4-oxo-4*H*-chromene hybrids as multifunctional agents for the treatment of Alzheimer's disease, with cholinergic, antioxidant, and beta-amyloid-reducing properties, J. Med. Chem. 55 (2012) 1303–1317.

[80] J. Reis, F. Cagide, M. Estrada Valencia, J. Teixeira, D. Bagetta, C. Pérez, E. Uriarte, P.J. Oliveira, F. Ortuso, S. Alcaro, M.I. Rodríguez-Franco, F. Borges, Multi-target-directed ligands for Alzheimer's disease: discovery of chromone-based monoamine oxidase/cholinesterase inhibitors, Eur. J. Med. Chem. 158 (2018) 781–800.

[81] J.A. Morales-García, R. Luna-Medina, C. Alfaro-Cervello, M. Cortés-Canteli, A. Santos, J.M. García-Verdugo, A. Pérez-Castillo, Peroxisome proliferator-activated receptor gamma ligands regulate neural stem cell proliferation and differentiation *in vitro* and *in vivo*, Glia 59 (2011) 293–307.

[82] J.A. Morales-García, R. Luna-Medina, S. Alonso-Gil, M. Sanz-Sancristóbal, V. Palomo, C. Gil, A. Santos, A. Martínez, A. Pérez-Castillo, Glycogen synthase kinase 3 inhibition promotes adult hippocampal neurogenesis *in vitro* and *in vivo*, ACS Chem. Neurosci. 3 (2012) 963–971.

[83] W.L. DeLano, in: The PyMOL Molecular Graphics System, Schrödinger, LLC., 2013.

[84] M.J. Frisch, G.W. Trucks, H.B. Schlegel, G.E. Scuseria, M.A. Robb, J.R. Cheeseman, G. Scalmani, V. Barone, B. Mennucci, G.A. Petersson, H. Nakatsuji, M. Caricato, X. Li, H.P. Hratchian, A.F. Izmaylov, J. Bloino, G. Zheng, J.L. Sonnenberg, M. Hada, M. Ehara, K. Toyota, R. Fukuda, J. Hasegawa, M. Ishida, T. Nakajima, Y. Honda, O. Kitao, H. Nakai, T. Vreven, J.A. Montgomery Jr., J.E. Peralta, F. Ogliaro, M.J. Bearpark, J. Heyd, E.N. Brothers, K.N. Kudin, V.N. Staroverov, R. Kobayashi, J. Normand, K. Raghavachari, A.P. Rendell, J.C. Burant, S.S. Iyengar, J. Tomasi, M. Cossi, N. Rega, N.J. Millam, M. Klene, J.E. Knox, J.B. Cross, V. Bakken, C. Adamo, J. Jaramillo, R. Gomperts, R.E. Stratmann, O. Yazyev, A.J. Austin, R. Cammi, C. Pomelli, J.W. Ochterski, R.L. Martin, K. Morokuma, V.G. Zakrzewski, G.A. Voth, P. Salvador, J.J. Dannenberg, S. Dapprich, A.D. Daniels, Ö. Farkas, J.B. Foresman, J.V. Ortiz, J. Cioslowski, D.J. Fox, in: Gaussian 09, Gaussian, Inc., Wallingford, CT, USA, 2009.

[85] I.D. Brown, B. McMahon, CIF: the computer language of crystallography, Acta Crystallogr. B 58 (2002) 317–324.

[86] N.W. Moriarty, R.W. Grosse-Kunstleve, P.D. Adams, Electronic Ligand Builder and Optimization Workbench (eLBOW): a tool for ligand coordinate and restraint generation, Acta Crystallogr. D Biol. Crystallogr. 65 (2009) 1074–1080.

[87] B. Calamini, B.D. Santarsiero, J.A. Boutin, A.D. Mesecar, Kinetic, thermodynamic and X-ray structural insights into the interaction of melatonin and analogues with quinone reductase 2, Biochem. J. 413 (2008) 81–91.

[88] P.D. Adams, P.V. Afonine, G. Bunkoczi, V.B. Chen, I.W. Davis, N. Echols, J.J. Headd, L.W. Hung, G.J. Kapral, R.W. Grosse-Kunstleve, A.J. McCoy, N.W. Moriarty, R. Oeffner, R.J. Read, D.C. Richardson, J.S. Richardson, T.C. Terwilliger, P.H. Zwart, PHENIX: a comprehensive Python-based system for macromolecular structure solution, Acta Crystallogr. D Biol. Crystallogr. 66 (2010) 213–221.

[89] P.D. Adams, P.V. Afonine, G. Bunkoczi, V.B. Chen, N. Echols, J.J. Headd, L.W. Hung, S. Jain, G.J. Kapral, R.W. Grosse Kunstleve, A.J. McCoy, N.W. Moriarty, R.D. Oeffner, R.J. Read, D.C. Richardson, J.S. Richardson, T.C. Terwilliger, P.H. Zwart, The Phenix software for automated determination of macromolecular structures, Methods 55 (2011) 94–106.

[90] P. Emsley, B. Lohkamp, W.G. Scott, K. Cowtan, Features and development of Coot, Acta Crystallogr. D Biol. Crystallogr. 66 (2010) 486–501.

[91] A. Urzhumtsev, P.V. Afonine, A.H. Van Benschoten, J.S. Fraser, P.D. Adams, From deep TLS validation to ensembles of atomic models built from elemental motions, Acta Crystallogr. D Biol. Crystallogr. 71 (2015) 1668–1683.

[92] S. Bienert, A. Waterhouse, T.A. de Beer, G. Tauriello, G. Studer, L. Bordoli, T. Schwede, The SWISS-MODEL Repository-new features and functionality, Nucleic Acids Res. 45 (2017) D313–D319.

[93] M. Biasini, S. Bienert, A. Waterhouse, K. Arnold, G. Studer, T. Schmidt, F. Kiefer, T. Gallo Cassarino, M. Bertoni, L. Bordoli, T. Schwede, SWISS-MODEL: modelling protein tertiary and quaternary structure using evolutionary information, Nucleic Acids Res. 42 (2014) W252–W258.

[94] T. UniProt Consortium, UniProt: the universal protein knowledgebase, Nucleic Acids Res. 46 (2018) 2699.

[95] R.C. Walker, M.F. Crowley, D.A. Case, The implementation of a fast and accurate QM/MM potential method in AMBER, J. Comput. Chem. 29 (2008) 1019–1031.

[96] A. Jakalian, D.B. Jack, C.I. Bayly, Fast, efficient generation of high-quality atomic charges. AM1-BCC model: II. Parameterization and validation, J. Comput. Chem. 23 (2002) 1623–1641.

[97] J.A. Maier, C. Martinez, K. Kasavajhala, L. Wickstrom, K.E. Hauser, C. Simmerling, ff14SB: improving the accuracy of protein side chain and backbone parameters from ff99SB, J. Chem. Theor. Comput. 11 (2015) 3696–3713.

[98] R.A. Friesner, R.B. Murphy, M.P. Repasky, L.L. Frye, J.R. Greenwood, T.A. Halgren, P.C. Sanschagrin, D.T. Mainz, Extra precision glide: docking and scoring incorporating a model of hydrophobic enclosure for protein-ligand complexes, J. Med. Chem. 49 (2006) 6177–6196.

[99] E.L. Wu, X. Cheng, S. Jo, H. Rui, K.C. Song, E.M. Davila-Contreras, Y. Qi, J. Lee, V. Monje-Galvan, R.M. Venable, J.B. Klauda, W. Im, CHARMM-GUI *Membrane Builder* toward realistic biological membrane simulations, J. Comput. Chem. 35 (2014) 1997–2004.

[100] C.J. Dickson, B.D. Madej, A.A. Skjevik, R.M. Betz, K. Teigen, I.R. Gould, R.C. Walker, Lipid14: the AMBER lipid force field, J. Chem. Theor. Comput. 10 (2014) 865–879.

[101] R. Salomon-Ferrer, A.W. Götz, D. Poole, S. Le Grand, R.C. Walker, Routine microsecond molecular dynamics simulations with AMBER on GPUs. 2. Explicit solvent Particle Mesh Ewald, J. Chem. Theor. Comput. 9 (2013) 3878–3888.

[102] T. Darden, D. York, L. Pedersen, Particle mesh Ewald: an N·log(N) method for Ewald sums in large systems, J. Chem. Phys. 98 (1993) 10089–10092.

[103] A.T. Brunger, P.D. Adams, Molecular dynamics applied to X-ray structure refinement, Acc. Chem. Res. 35 (2002) 404–412.

[104] A. Salgado, E. Tatunashvili, A. Gogolashvili, B. Chankvetadze, F. Gago, Structural rationale for the chiral separation and migration order reversal of clenpenterol enantiomers in capillary electrophoresis using two different β-cyclodextrins, Phys. Chem. Chem. Phys. 19 (2017) 27935–27939.

[105] P.A. Sánchez-Murcia, A. Cortés-Cabrera, F. Gago, Structural rationale for the cross-resistance of tumor cells bearing the A399V variant of elongation factor eEF1A1 to the structurally unrelated didemnin B, ternatin, nannocystin A and ansatrienin B, J. Comput. Aided Mol. Des. 31 (2017) 915–928.

[106] B.A. Caine, C. Dardonville, P.L. Popelier, Prediction of aqueous p*K*a values for guanidine-containing compounds using *ab initio* gas-phase equilibrium bond lengths, ACS Omega 3 (2018) 3835–3850.